Universidad de Sevilla
Escuela Técnica Superior de Ingeniería

Doctoral Thesis

Aircraft Trajectory Optimization Using Parametric Optimization Theory

Thesis submitted to Dpto. de Ingeniería Mecánica y de los Materiales,
for the doctoral degree at
Universidad de Sevilla

Author: Alfonso Valenzuela Romero
Supervisor: Prof. Damián Rivas Rivas, Dr.
Dpto. Ingeniería Aeroespacial y Mecánica de Fluidos
Tutor: Miguel Pérez-Saborid Sánchez-Pastor, Dr.
Dpto. Ingeniería Aeroespacial y Mecánica de Fluidos

Sevilla, November, 2012

Contents

This page intentionally left blank

List of Figures

List of Tables

This page intentionally left blank

Abstract

In this thesis, a study of the optimization of aircraft trajectories using parametric optimization theory is presented. To that end, an approach based on the use of predefined trajectory patterns and parametric optimization is proposed. The trajectory patterns are in fact flight intents, formed by flight segments which model procedures commonly flown by airlines, following air-traffic-control rules. The patterns allow to describe the trajectory by a small number of parameters, whose values, continuous or discrete, can be chosen to optimize a given property of the trajectory. A mixed-integer nonlinear programming (MINLP) problem is formulated to obtain the optimum values.

Firstly, the approach is used to solve the general problem of minimum direct-operating-cost cruise (unsteady, with variable mass, and without any constraint on speed or altitude) with given range. The trajectory pattern considered in this application is formed by segments at constant Mach number and constant altitude, restricted to take discrete values: Mach numbers multiple of 0.01, and altitudes defined by flight levels. The unrestricted problem in which the Mach numbers and the altitudes are continuous variables is also considered. The optimized procedures define not only the optimum values of speed and altitude for the different cruise segments, but also the optimum lengths of each segment. The main objective of this application is to analyze how the optimized procedures change when the Mach numbers and the altitudes are restricted to take discrete values. The effects of the cost index, of the initial aircraft weight and of an average horizontal wind in the optimized procedures are also analyzed.

Next, the problem of minimum-fuel cruise at constant altitude with fixed range and fixed arrival time is solved and the optimized procedures obtained using the proposed approach are compared with known optimal laws obtained using singular optimal control theory. The trajectory pattern considered in this application is similar to the previous one, formed by segments at constant Mach number restricted to take discrete values. The comparison shows that the optimized procedures approximate very well the optimal laws and give results that are very close to the optimal values.

Following, the approach is applied to a set of aircraft, taking into account the losses of separation that may arise among them. An algorithm for conflict resolution (CR) is presented, in which conflict-free trajectories are optimized. The optimality criterium is defined so that the deviation from the intended (preferred) trajectories in the lateral profile is minimized. This problem is solved in two phases: one in which a first valid solution is found by means of a random search, and another one in which this first valid solution is optimized. The resolution trajectory patterns take into account changes of the nominal waypoints (vectoring) and changes of the aircraft speeds. The algorithm is applied to the case of multiple conflicts

among commercial transport aircraft in converging traffic in the terminal area. Different scenarios are considered, which include locked aircraft, that is, aircraft whose trajectories are known and fixed. The cost of the global resolution process is assessed, in terms of extra distance travelled, extra flight time and extra fuel consumed for each aircraft.

Finally, the previous CR algorithm is extended to solve the problem of optimizing conflict-free trajectories that meet scheduled times of arrival (STA). In this application, the resolution process has three steps: avoidance, which generates conflict-free trajectories that meet the given sequence of arrival (which is a hard constraint of the problem); recovery, in which the resolution trajectories are modified to meet the STA (which is a primary objective); and, optimization, to minimize a combination of costs (secondary objective). Two algorithms are presented: one in which the optimization step is applied globally (to all aircraft) after the other two steps are performed for all aircraft, and another one in which the optimization step is applied locally to each aircraft after the other two steps are performed for the given aircraft; this second algorithm is efficient when the scenario is very demanding (in which the global optimization is not effective). Results are presented for two scenarios, one with a traffic of 30 aircraft in an hour, all of the same wake-turbulence category, and another one with 35 aircraft in an hour and with aircraft of different categories.

In all cases, a kinetic trajectory predictor (nonlinear point-mass model with variable mass) is used, which is accurate, flexible and transparent, and provides the high-fidelity prediction required in all the applications.

Foreword

This PhD thesis was written under the supervision of Professor Damián Rivas, from University of Seville. The work presented in this document is the result of original research carried out by myself, in collaboration with others, while enrolled in the Department of Aerospace Engineering and Fluid Mechanics. Some of this work was previously published in the following papers:

1. A. Valenzuela and D. Rivas. "Conflict Detection and Resolution in Converging Air Traffic". AIAA paper 2009-7022, pp. 1–13, 2009.

2. A. Valenzuela, D. Rivas and A. Franco. "Cruise Optimization Using Trajectory Patterns". AIAA paper 2010-9140, pp. 1–11, 2010.

3. A. Valenzuela and D. Rivas. "Conflict Resolution in Converging Air Traffic Using Trajectory Patterns". *Journal of Guidance, Control, and Dynamics*, vol. 34, no. 4, pp. 1172–1189, 2011.

4. A. Valenzuela and D. Rivas. "Optimization of Aircraft Cruise Procedures Using Predefined Trajectory Patterns". Submitted for publication to *Journal of Aircraft*, 2012.

The journal paper "Conflict Resolution in Converging Air Traffic Using Trajectory Patterns" has been awarded by Fundación Aena the 17th edition of Premio Luis Azcárraga (2012). This yearly prize recognizes a singular contribution in the field of air transport and navigation.

The extension of the conflict resolution algorithm presented in this paper to solve the problem of generation and optimization of conflict-free trajectories with scheduled times of arrival, presented in Chapter 6, was funded by the Spanish Comisión para el Desarrollo Tecnológico e Industrial (CDTI), through the Project ATLANTIDA/Cenit 2007-2010. As a result of this work, The Boeing Company has filed a European patent application under the name "Conflict Detection and Resolution Using Predicted Aircraft Trajectories" with reference number 12382209.0 - 1232.

This page intentionally left blank

Acknowledgements

I owe a tremendous debt of gratitude to my advisor, Dr. Damián Rivas, for his guidance, corrections, advices, and patience throughout all these years. Furthermore, I am thankful to Damián for being not only a supervisor but also a good friend. This thesis would not have been possible without him.

I would also like to thank Antonio Franco for the hours shared in the office, for helping me with useful discussions which led to new ways of solving the problems. Special thanks to the rest of the Aerospace Engineering Group: Carlos Antúnez, Antonio Corrales, Sergio Esteban, Francisco Gavilán and Rafael Vázquez, for their invaluable help and friendship.

Thanks to all the people of the Department of Aerospace Engineering and Fluid Mechanics, particularly to Miguel Pérez-Saborid for accepting being the tutor of this thesis.

Thanks to all my friends. I do not cite any name because I might omit someone. Thanks for their constant presence, care and instant moral support.

Most importantly, I thank my parents and my brother and sister for their continuous support and patience. Sharing my entire life with them has made it possible for me to be here. This thesis is dedicated to them.

Alfonso Valenzuela Romero

This page intentionally left blank

1 Introduction

1.1 Motivation

The air-transport sector is a key component of the economy of all the States of the World, since it allows to maintain or stimulate the economic growth and to assist in the supply of services to the different communities. From its beginning it has undergone a nearly continuous growth. For example, in the United States, from 1990 to 2010, the number of aircraft handled by the air-traffic centers increased a 8.1%[1] (which takes into account the effect of the present economic crisis; until 2005, last year before the crisis, the increase was 26.6%), and the forecast for 2030 is another increment in the air traffic of 61.5% with respect to the levels of 2010 [FAA 11]. In Europe, the forecast for 2030 is an increment of 1.8 times the traffic of 2009, reaching a total of 16.9 million of flights per year [EURO 10].

In the decade of 1980, ICAO (*International Civil Aviation Organization*) considered that the air navigation system was limiting the growth of aviation and improvements in the safety, efficiency and regularity of flights. In 1983, ICAO established the special committee FANS (*Future Air Navigation Systems*), charged with generating recommendations for the development of the future air navigation for a period of 95 years. The concept proposed by this committee was named CNS/ATM (*Communications, Navigation, and Surveillance / Air Traffic Management*) and was approved in 1991 by ICAO. In 1996, it was determined that the CNS/ATM systems were mature enough and that it was necessary to create a world plan where all the developments and possible technical solutions were included. For this purpose, the revised document *Global Air Navigation Plan* [ICAO 07b] was generated, a strategic document that serves as a guide in the implementation of the CNS/ATM systems.

In the following years, some States and all the regions belonging to ICAO launched programs orientated to improve the aeronautical operations through the utilization of the CNS/ATM technologies. For example, in 2003, the United States Congress established the JPDO (*Joint Planning and Development Office*) to plan and coordinate the development of NextGen (*Next Generation Air Transportation System*[2]). In 2004, Europe started the definition phase of the SESAR (*Single European Sky ATM Research*[3]) program, founded by the European Commission and Eurocontrol (*European Organization for the Safety of Air Navigation*). The complete implementation of NextGen and SESAR is foreseen for the year 2030.

Among others, one of the actions included in all these programs is the introduction

[1] Source: FAA Air Traffic Activity System (ATADS), `http://aspm.faa.gov/opsnet/sys/Center.asp`

[2] `http://www.faa.gov/nextgen`

[3] `http://www.sesarju.eu`

of automatic systems based on the TBO (*Trajectory-Based Operations*) concept. In these systems the present and future aircraft position is known and shared, so that the aircraft are handled by their trajectories. The trajectories can then be modified if they do not meet some requirements, can be accepted if they do, and they are transmitted to the involved agents. It is expected that these systems based on the TBO concept will improve the detection and resolution of conflicts between aircraft, providing an automatic generation of conflict-free trajectories and offering a way of adaptation to the always changing necessities of the traffic. As a result, the aircraft will be able to fly optimal trajectories which will reduce the cost of the airlines and will allow an optimal management of the airspace.

The importance of the aircraft trajectory in the CNS/ATM systems has stimulated many different projects in the last years that try to improve its prediction, optimization and management. For example, the following projects can be highlighted: the database BADA [Nuic 09] (*Base of Aircraft DAta*) created by Eurocontrol, which models the aircraft performance and the global trajectory from liftoff to touchdown (the last available version, version 3.10, models 339 different aircraft); the CTAS[4] program (*Center-TRACON Automation System*) developed by NASA, provides automation tools that generate advisories to the air-traffic controllers for planning and controlling arrival air traffic; the AIRE[5] program (*Atlantic Interoperability Initiative to Reduce Emissions*) in collaboration between SESAR and FAA (*Federal Aviation Administration*), which expects to reduce the fuel consumption in hundreds of kilograms per flight [AIRE 12] through the optimization of the aircraft trajectories in all the flight phases; and the network HALA![6] (*Higher Automation Levels in ATM*) established within the framework of SESAR, whose projects try to increase the automation in the transmission and generation of trajectories.

The participation of Spain in the modernization of the air navigation systems is mainly carried out by its participation in SESAR, but also national projects are promoted as, for example, the projects CENIT ATLANTIDA[7] (*Aplicación de Tecnologías Líder a Aeronaves No Tripuladas para la Investigación y Desarrollo en ATM*) and CENIT SINTONIA (*SIstemas No Tripulados Orientados al Nulo Impacto Ambiental*). The former develops innovative concepts for the automation in air-traffic management, testing them in high-fidelity simulations and in experiments based on the use of UAVs (*Unmanned Air Vehicles*); while the latter tries to increase the efficiency and to reduce the environmental impact of UAVs through the introduction of improvements in the whole life cycle, including the generation of optimal trajectories.

Since 2005, the Department of Aerospace Engineering and Fluid Mechanics has conducted research in the fields of trajectory prediction and optimization. In this context, the Aerospace Engineering Group has participated in the following projects: IMPACT (*Advanced Multi-Purpose Infrastructure for Trajectory Computation*), funded by Boeing Research and Technology Europe, for the development of trajectory calculators; CENIT ATLANTIDA, for the development of conflict resolution algorithms in arrival air traffic in the terminal maneuvering area; CENIT SINTONIA, for the development of an automatic optimal-trajectory generator for UAVs; and, presently, the group is the scientific leader of the ComplexWorld

[4] `http://www.aviationsystemsdivision.arc.nasa.gov/research/foundations`
[5] `http://www.sesarju.eu/environment/aire`
[6] `http://www.hala-sesar.net`
[7] `http://www.atlantida-project.org`

network established within the framework of SESAR, for the understanding and modeling of the behavior and evolution of the air-traffic management system.

The thesis presented in this document deals with the optimization of aircraft trajectories. In the next section, the main objective of the thesis is described.

1.2 Objective

The objective of this thesis is to study the optimization of aircraft trajectories using parametric optimization theory, both to a single aircraft and to a set of aircraft. To that end, an original approach based on the use of predefined *trajectory patterns* and parametric optimization is presented. The trajectory patterns are parameterizations of the *flight intents*, that model the aircraft trajectories actually flown. In these parameterizations, the aircraft trajectory is described by *flight segments*, and the segments are defined by a small number of parameters, on which the optimization is performed.

To carry out the study, three different applications are analyzed. Firstly, the approach is applied to one single aircraft. Cruise procedures commonly flown by airlines are optimized, and the effects of considering discrete parameters as defined by the current air-traffic regulation, of the cost index, of the initial weight, and of horizontal winds are analyzed. When possible, the trajectories are compared with known optimal laws obtained with the theory of singular optimal control. Secondly, the optimization approach is applied to a set of aircraft, taking into account the losses of separation that may arise among them. This traffic problem leads to the development of a conflict resolution (CR) algorithm in which conflict-free trajectories are generated and optimized. The case of arrival air traffic is considered, which is one of the most demanding scenarios since all the aircraft share a common resource: the runway. Finally, it is applied to the optimization of conflict-free trajectories that meet given scheduled times of arrival. This last problem is an extension of the previous one in which the resolution process of the optimization problem is modified to handle time constraints and a large number of aircraft.

As it will be shown throughout the document, the proposed optimization approach has the following advantages: 1) it allows to optimize any property or combination of properties derived from the trajectory (e.g., fuel consumption, flight time, range, etc.); 2) it allows to generate trajectories based on flight procedures easily performed by the aircraft; 3) it allows to readily incorporate any kind of restriction on the trajectory; and 4) the optimization is performed on a small number of parameters.

The model adopted to describe the aircraft motion is a general nonlinear point-mass kinetic model, commonly used for trajectory prediction, in which realistic aerodynamic and engine models are used. The assumptions considered to obtain the equations of motion are appropriate for subsonic, transport aircraft. Regarding the trajectory patterns, the flight procedures and regulations proposed by ICAO (for example, those described in Docs. 8168 [ICAO 06] and 4444 [ICAO 07a]) and commonly used by airlines are considered, such as segments at constant speed and constant altitude, standard arrivals, speed limitations, idle descents, etc.

1.3 Outline

The structure of this document is as follows. Next, in Chapter 2, a review of the state of the art in parametric optimization, trajectory parameterization, trajectory optimization, and conflict resolution is presented, the elements on which the thesis is based. Once the review is performed, the general problem of trajectory optimization using trajectory patterns is formulated in Chapter 3. In Chapter 4, the formulated optimization problem is used to analyze the optimization of the cruise trajectory of one single aircraft. After this analysis, the optimization of trajectories of several aircraft in converging traffic while keeping separation among them is addressed in Chapter 5, and the extension of this problem to consider given scheduled times of arrival is performed in Chapter 6. Finally, the conclusions obtained from the applications are presented in Chapter 7, and the future work is presented in Chapter 8.

The math notation and acronyms used throughout this document can be found in Appendixes A and B, respectively. A summary of the procedure followed in this thesis to compute the trajectories is given in Appendix C, and the supplementary models (Earth and aircraft models) used throughout the document are described in Appendix D. The key performance indicators developed to evaluate the performance of the algorithms described in Chapter 6 are defined in Appendix E, and the nominal traffic considered in this same chapter and the obtained resolution trajectories are presented in Appendix F.

2 Literature Review

Parametric optimization plays a key role in this thesis. For this reason, in Section 2.1 an overview of resolution techniques that are suitable to solve the optimization problem that appears in this work is presented. In Chapter 3, once the mathematical problem is formulated, the most appropriate optimization algorithm will be chosen according to the characteristics of the problem.

This thesis is also based on the parameterization of trajectories. Parameterized trajectories have already been used in different contexts as, for example, in the standardization of flight procedures. In Section 2.2, the applications on which they have been considered and the associated parameterizations are reviewed.

The applications considered in this thesis are the optimization of the cruise trajectory of one single aircraft and of a set of several aircraft taking into account the losses of separation among them, which leads to the conflict detection and resolution problem. In Section 2.3, a summary of works on the optimization of one single aircraft trajectory is presented. They will serve as a basis to establish which problems are of interest in the field of aviation and, if possible, to determine if the obtained results are correct. In Section 2.4 different strategies considered to solve the conflict resolution problem are reviewed, with particular attention to the resolution maneuvers considered and to the methods used to generate the conflict-free trajectories.

2.1 Parametric Optimization

Optimization problems can be classified in several ways. According to Ref. [Bieg 04], one possible classification can be made attending to the nature of the *decision variables*. In this sense, one can have *parametric optimization problems* (in which each variable can only take a single value from a given set), *optimal control problems* (which usually correspond to dynamic systems in which the decision variables are functions of, for example, time), or *stochastic optimization problems* (in which the variables are defined by probability functions). Each type of problem is solved by appropriate resolution techniques, see, for example, Refs. [Flet 87] and [Brys 75]. The basis of some of these techniques is to obtain an approximated solution of the original problem by means of the resolution of auxiliary problems of another type. For example, optimal control problems can be solved as parametric optimization problems if the continuous variables are discretized, and also stochastic problems can be solved through the resolution of numerous parametric problems. In this thesis, since the trajectories are defined by parametric variables, stochastic and optimal control problems are not considered.

In a general manner, a parametric optimization problem can be stated as follows:

$$\begin{aligned} &\text{minimize} && J(\mathbf{x}) && \mathbf{x} \in \mathbb{R}^n \\ &\text{subject to} && \mathbf{f}(\mathbf{x}) = 0 \\ & && \mathbf{g}(\mathbf{x}) \leq 0 \end{aligned} \tag{2.1}$$

where $\mathbf{x}$ is an n-dimensional vector that collects the *decision variables*, $J(\mathbf{x})$ is termed the *objective function*, $\mathbf{f}(\mathbf{x})$ the *equality constraints*, and $\mathbf{g}(\mathbf{x})$ the *inequality constraints*.

Depending on the nature of the decision variables, the objective function, and the constraints one has different optimization problems. They can be classified in several ways, as shown in Ref. [Rao 96]:

- Linear, quadratic, geometric or nonlinear programming[1] problems, depending on the nature of the expressions for the objective function and the constraints. The nonlinear programming (NLP) problem is the most general optimization problem and all other problems can be considered as special cases of the NLP problem.
- Constrained or unconstrained optimization problems, depending on whether or not constraints exist in the problem.
- Integer- or real-valued programming problems, depending on the values permitted for the decision variables. If some variables are integer whereas others are real, the problem is then called a mixed-integer programming problem.
- Separable or non-separable programming problems, depending on whether or not both the objective and constraint functions can be expressed as the sum of several single-variable functions.
- Single- and multi-objective programming problems, depending on the number of objective functions to be minimized.

As it will be shown in Chapter 3, in general, in the case of aircraft trajectory optimization using trajectory patterns, the optimization problem is nonlinear, constrained, mixed integer, non separable, and single objective. Next, a review of techniques to solve this kind of problems is presented (since all of them are applicable to non-separable and single-objective problems, these two characteristics are not treated separately).

2.1.1 Nonlinear-Optimization Techniques

Nonlinear-optimization techniques can be divided into two groups, *direct search methods* and *gradient methods*, depending on whether or not they require the computation of derivatives (this classification is found, for example, in Refs. [Rao 96, Garc 95]). The direct search methods, also known as zeroth-order methods, only require the function values. Since they do not make use of derivatives they can be easily applied to problems in which the objective function or the decision variables are discontinuous, e.g. integer values. Popular algorithms

[1] The term *'programming'* is synonymous with optimization and was originally used to mean *'optimization'* in the sense of optimal planning (see Ref. [Flet 87]).

are Powell's method [Powe 64], simulated annealing [Kirk 83], and evolutionary algorithms such as particle swarm optimization [Kenn 95] and genetic algorithms [Holl 92].

On the other side, gradient methods require, in addition to the function values, the first and in some cases the second derivatives of the objective function (they are known as first- and second-order methods, respectively). Since more information about the function being minimized is used (through the use of derivatives), gradient methods are generally more efficient than direct search techniques. The basic philosophy of most of the gradient methods is, starting from an initial trial point, to produce a sequence of improved approximations to the optimum by determining a direction of search and then finding an appropriate steplength for movement along that direction. The differences among the methods lie in the way they define the search direction and the steplength. Usually, the former is defined using the derivatives of the objective function and the latter is obtained after a one-dimensional optimization along the search direction. Representative algorithms are Fletcher-Reeves method [Flet 64] (first-order) and Newton's method (second order). Of special importance are quasi-Newton methods, a derivation of the Newton's method in which the inverse of the Hessian matrix is approximated by a symmetric positive definite matrix, which is updated at each iteration and which only requires the first derivatives of the objective function. The most common update is the Broyden-Fletcher-Goldfarb-Shanno (BFGS) formula [Broy 70a, Broy 70b, Flet 70, Gold 70, Shan 70]) which gives better performance than other methods (specially in large or difficult problems) and is considered as the most preferable quasi-Newton method [Flet 87].

2.1.2 Constrained-Optimization Techniques

Constrained-optimization techniques can be classified into two broad categories (see Ref. [Rao 96]): *indirect methods*, which solve the constrained problem as a sequence of unconstrained minimization problems, and *direct methods*, which handle the constraints in an explicit manner. Typical indirect methods are: superiority of feasible points methods [Deb 00] (this method is only applicable to algorithms that generate a population of candidate points, usually evolutionary algorithms: it sorts the candidate points according to the value of the objective function and the constraints violation), penalty methods [Cour 43] (the constrained problem is solved by a series of unconstrained problems whose solutions ideally converge to the solution of the original problem; the unconstrained problems are formed by combining the objective function and a measure of the violation of the constraints, penalized by means of *penalty parameters*), and augmented Lagrangian multiplier methods [Hest 69] (similar to the penalty methods but incorporating the Lagrange multipliers to the objective function).

Representative direct methods are: quadratic programming methods (which deal with the minimization of quadratic functions subject to linear constraints), the generalized reduced gradient (GRG) method (which solves nonlinear programming problems with nonlinear constraints), and sequential quadratic programming (SQP) methods [Han 77] (analogous to the Newton's method for unconstrained problems). Although most of the direct methods are only able to handle equality constraints, the inequality constraints can be incorporated using the *active set method*: the inequality constraints that hold with equality are handled as equality constraints while the rest are temporarily disregarded. The problem subject to equality and inequality constraints can be then solved as a sequence of equality constrained subproblems.

References [Flet 87, Gill 89, Schi 85] agree that SQP and SQP-related methods are widely considered as the most effective general methods today for solving nonlinear-programming problems on small- and medium-scale problems. However, in large problems they do not exploit any sparsity and, therefore, this fact limits the size of problem that can be handled effectively.

2.1.3 Mixed-Integer Optimization Techniques

The most common methods to solve mixed-integer programming problems are: branch and bound, outer-approximation, generalized Benders decomposition, and extended cutting plane.

The branch and bound methods propose a tree search in the space of the integer variables, and at each node of the tree an auxiliary optimization problem where all the variables are continuous is solved [Daki 65]. According to Ref. [Bieg 04], these methods are generally only attractive if the auxiliary subproblems are relatively inexpensive to solve, or when only few of them need to be solved.

Outer-approximation [Flet 94] and generalized Benders decomposition methods [Flip 93] are similar among them. Both approaches solve the mixed-integer nonlinear programming problem by alternating between an NLP subproblem (obtained from the original problem by fixing the integer variables) and relaxations of a mixed-integer linear programming master problem. The difference between both methods lies in the derivation of the master problem.

The extended cutting plane [West 95] generates a non-decreasing sequence of lower bounds by solving a sequence of mixed-integer linear programming problems, in which each problem adds as a constraint a linearization of the most violated constraint evaluated at the previous suboptimal point.

2.2 Trajectory Parameterization

The parameterization of trajectories consists in describing, without ambiguity, the trajectories in terms of a set of parameters. In aviation this description appears naturally because the aircraft trajectories are discretized in flight procedures, and the procedures are usually described in terms of, for example, speeds, altitudes, angles, or waypoints coordinates (see, for instance, the operational procedures described in ICAO Doc. 8168 [ICAO 06]). Following, examples of parameterizations of trajectories are presented.

Parameterized trajectories have already been used in trajectory optimization. Vormer et al. [Vorm 06] represent the flight paths as sets of straight and curved segments, which are described by lengths, radii, path angles and accelerations. Wu and Zhao [Wu 09] define the trajectory by a series of flight segments specified by a set of flight objectives, such as speeds, altitudes or throttle settings. Torres et al. [Torr 11] parameterize the trajectory through two sets of variables that describe the evolution of the aircraft speed and thrust.

Predefined trajectory patterns to treat CR problems have been used by different authors. Menon et al. [Meno 99] parameterize the trajectories in terms of four-dimensional waypoints, and approximate the trajectories by piecewise-linear paths. Vilaplana [Vila 02] defines a lateral shift maneuver, as a sequence of straight lines connected by inside turns, to solve en-route conflicts. Vivona et al. [Vivo 06] consider a conflict resolution algorithm based

on predefined maneuver patterns (lateral offset, direct intercept path, path stretch, waypoint migration and cruise step climb/descent), designed to execute different types of user-accepted path modifications. Coppenbarger et al. [Copp 04] describe the En route Descent Advisor (EDA), a CTAS tool that solves the meet-time problem, where the cruise and descent speeds are used as parameters, and a simple "dog-leg" maneuver is considered for lateral routing (path stretching to absorb large delays).

In other contexts, Gill and Maddock [Gill 97] use predefined strategies to meet time and altitude constraints within PHARE (*Program for Harmonized ATC Research in Europe*), Slattery and Zhao [Slat 97] use predefined profile types (fast, nominal and slow) to synthesize cruise-descent trajectories for air traffic automation, in BADA [Nuic 04] standard airline procedures are parameterized to provide means of simulating standard aircraft operation, Jackson et al. [Jack 99] consider nominal descent profiles (formed by 5 segments) to study the sensitivity of trajectory prediction, and Barrer [Barr 99] considers predefined patterns called path objects as a means to standardize flight procedures.

2.3 Trajectory Optimization

The development of numerical methods for trajectory optimization started in the 1950s with the development of the digital computer, which provided the tool for solving these new problems. Due to the high complexity in the formulation and the resolution of the problems, the first works started with simplified models of the aircraft, disregarding some terms in the equations of motion and considering simple aerodynamic and propulsive models. Once these problems were solved and more computational capacity was available, more complex models with more terms were considered.

Works on trajectory optimization can be classified attending to, for example:

- The flight phase which is optimized. It can be climb, cruise, or descent phases, separately, or the global trajectory (from takeoff to touchdown).
- The considered model for the aircraft motion. Usually, the aircraft is considered as a point mass and the equations of motion are obtained by the application of equilibrium of forces, which is quite adequate for trajectory analysis. Depending on the simplifications made to these equations and the propulsive and aerodynamic models considered, the optimal solution may exist or not, as shown by Schultz and Zagalsky [Schu 72].
- The property of the trajectory which is optimized. In principle, any property derived from the trajectory can be optimized, for example, range, fuel consumption, flight time, or a combination of fuel and time costs. Nowadays, other aspects such as greenhouse gases or noise emissions are taken into account.

The optimization of the cruise flight has been extensively treated in the literature, with different flight constraints and performance indices; see, for instance, the study of Menon [Meno 89], in which both speed and altitude are allowed to vary, and the many references therein. Other example is the work of Pargett and Ardema [Parg 07], who analyze the problem of range maximization in cruise at constant altitude as a singular optimal control problem. The same problem is also analyzed using different approaches by Miele [Miel 62]

and Torenbeek [Tore 97], who consider the case of quasi-steady flight. In Ref. [Parg 07], the singular arc that defines the optimal path is studied; in this study, a simple aircraft model defined by a parabolic drag polar of constant coefficients is considered and only one value of cruise altitude. Rivas and Valenzuela [Riva 09] generalize this analysis considering a general drag polar, so that compressibility effects are taken into account. Franco and Rivas [Fran 11] also apply singular optimal control theory to solve the minimum-cost cruise at constant altitude including wind effects.

Maximum-range glide between two given points (given initial and final speeds and altitudes, V_i, h_i and V_f, h_f) has been analyzed by different authors using different procedures. For instance, Miele [Miel 55] analyzes the problem using a method based on Green's theorem, using the limiting constraint $h_f \leq h \leq h_i$; the solution is formed by a central pattern and two decelerations at constant altitude (h_i and h_f). Bryson et al. [Brys 69] present an analysis using the energy-state approximation, with speed as control variable; the solution is formed by a central path and, depending on the initial and final conditions, by zoom climbs or zoom dives with constant energy. More recently, Shapira and Ben-Asher [Shap 04, Shap 05] use singular perturbation theory, considering two and three timescales, and obtain the inner and outer solutions using optimal control theory; the inner (boundary layer) solution is characterized by an increase in altitude, a decrease in speed, and large values of flight-path angle; the outer (slow) solution is a steady-state glide; these analyses are made for the simple incompressible case of a parabolic drag polar of constant coefficients. Franco et al. [Fran 12] optimize the unpowered descent using singular optimal control theory and considering compressible aerodynamics, obtaining a speed law which is very close to constant calibrated air speed.

The minimum time-to-climb and minimum fuel-to-climb problems have been formulated as optimal control problems by Bryson and Denham [Brys 62], Calise [Cali 77], and Ardema [Arde 76], who obtained numerical results using a steepest-ascent method, singular perturbation techniques, and matched asymptotic expansions, respectively. More recently, Dai and Crochran [Dai 09] solved the same problems with the restriction that the trajectory must lie inside an airspace defined by a rectangular prism which leads to an increase in flight time and fuel consumption. In other contexts, Prats et al. [Prat 11] and Torres et al. [Torr 11] formulate multi-objective optimization problems to minimize noise in different areas or pollutants emissions of the departure procedures.

Regarding global trajectories, minimum-DOC (Direct Operating Cost, a sum of fuel and time costs) problems have been studied by Barman and Erzberger [Barm 76], Erzberger and Lee [Erzb 80], Sorensen and Waters [Sore 81], and Burrows [Burr 83]; they consider steady cruise, and take the aircraft mass as constant. Burrows [Burr 82] does not consider constant mass, but he assumes that the cruise segment takes place in the stratosphere. Bilimoria et al. [Bili 85] and Chakravarty [Chak 85] analyze the minimum-DOC, steady cruise as the outer solution of a singular perturbation approach, where the aircraft mass is taken as constant.

However, most of the optimal trajectories obtained using optimization theory do not follow air-traffic-control (ATC) rules; an example is the cruise climb, which in practice is approximated by a stepped cruise climb.

The following works do take into account ATC rules. Betts and Cramer [Bett 95] apply the direct transcription technique, which combines nonlinear optimization with a discretization of

the trajectory dynamics, to the optimal design of trajectories (for several performance indices) subject to realistic constraints that represent the trajectory phases of a mission profile. Soler et al. [Sole 10] relax some of the constraints imposed in Ref. [Bett 95] to give more room for planning more efficient trajectories, formulating a single optimal control problem which is also solved as a nonlinear optimization problem. Wu and Zhao [Wu 09] optimize current flight procedures, formulating a parametric optimization problem to minimize flight time and fuel consumption; they also quantify the deviation from actual trajectories due to modeling errors and/or flight conditions.

2.4 Conflict Resolution

In the literature one can find different approaches to model the conflict resolution problem. Menon et al. [Meno 99] parameterize the actual trajectories in terms of 4D (space and time) trajectory waypoints, and formulate an optimization problem. Frazzoli et al. [Fraz 01] formulate the CR problem as a nonconvex quadratic programming problem, which is approximated by convex semidefinite programming. Hu et al. [Hu 02] formulate an optimal CR problem by defining an energy cost function for the joint maneuver, which must be conflict free; in the multiple-aircraft case, the original constrained optimization problem is approximated by a finite-dimensional convex optimization problem with linear constraints. Clements [Clem 02] formulates an optimal control problem, and computes optimal resolution maneuvers for conflicts between two aircraft; the avoidance maneuvers are flown at constant speed. Paielli [Paie 03] presents an iterative algorithm that searches for a combination of speed and heading maneuvers that resolves the conflict; the algorithm is applied to the case of conflicts between two aircraft. Raghunathan et al. [Ragh 04] also formulate an optimal control problem, which is discretized into a nonlinear programming problem; they address the issue of flyability of the generated trajectories. Vivona et al. [Vivo 06] use a genetic algorithm, as part of the CR method, to select and optimize a resolution maneuver from a set of predefined maneuver patterns (lateral offset, direct intercept path, path stretch, waypoint migration and cruise step climb/descent), designed to execute different types of user-acepted path modification. Bilimoria and Lee [Bili 02] consider the CR problem with the additional constraint of a fixed arrival time at a downstream waypoint; the resolution approach is divided into two general maneuvers: avoidance and recovery. All these works analyze en-route conflicts; Menon et al. [Meno 99] and Hu et al. [Hu 02] consider altitude changes in the resolution of the conflicts, whereas the rest of the works cited solve horizontal problems. Isaacson and Robinson [Isaa 01] present a knowledge-based CR algorithm for terminal areas, used in CTAS tools, which models the resolution tactics used by controllers. Other CR modeling methods can be found in the review performed by Kuchar and Yang [Kuch 00].

The CR algorithm must rely on a trajectory predictor, which can be of different levels of complexity. On one side, one has the case of kinematic trajectory modeling (see, for instance, Bilimoria [Bili 00a]), in which speed and heading changes are modeled as instantaneous maneuvers. On the other side, one has the general case of nonlinear point-mass kinetic trajectory modeling (see, for instance, Menon et al. [Meno 99]), in which the maneuver dynamics is taken into account. Paielli [Paie 03], however, presents an intermediate approach, in which speed and heading changes are modeled by simple maneuvers; this model improves

over those in which speed and heading changes are instantaneous, but lacks the accuracy of general nonlinear point-mass dynamic models.

3 Aircraft Trajectory Optimization Based on Trajectory Patterns

In this thesis, the optimization of aircraft trajectories is analyzed. The trajectories are modelled by predefined patterns, which are, in fact, flight intents that model both the vertical profile (altitude, speed, engine rating,...) and the lateral profile (route, turns,...), and are formed by flight segments commonly flown by airlines according to ATC regulations. These patterns allow to describe the trajectory in terms of a small number of parameters, some of which are fixed whereas the others are free. The set of free parameters is used to optimize the trajectory.

Next, the equations of aircraft motion, an example of a trajectory pattern and the formulated parametric optimization problem are described.

3.1 Equations of Motion

The model adopted to describe the aircraft motion is that of a point mass with three degrees of freedom, commonly used for trajectory prediction (see Ref. [Slat 97]); the equations describe the movement of the aircraft center of mass, considered as a mass-varying body. The scalar equations of motion are formulated based on the following general assumptions: spherical and non-rotating Earth, rigid and symmetric aircraft, symmetric flight, and thrust parallel to the aircraft aerodynamic velocity. These assumptions are appropriate for subsonic, transport aircraft. If a generic wind is considered, the scalar equations of motion are:

$$\begin{aligned}
m\frac{\mathrm{d}V}{\mathrm{d}t} &= T - D(V,h,L) - mg\sin\gamma + m\dot{w}_V \\
mV\cos\gamma\frac{\mathrm{d}\chi}{\mathrm{d}t} &= L\sin\mu + m\dot{w}_\chi \\
mV\frac{\mathrm{d}\gamma}{\mathrm{d}t} &= L\cos\mu - mg\cos\gamma + m\dot{w}_\gamma \\
\frac{\mathrm{d}m}{\mathrm{d}t} &= -c(V,h)T \\
(R_E+h)\frac{\mathrm{d}\varphi}{\mathrm{d}t} &= V\cos\gamma\cos\chi + w_1 \\
(R_E+h)\cos\varphi\frac{\mathrm{d}\lambda}{\mathrm{d}t} &= V\cos\gamma\sin\chi + w_2 \\
\frac{\mathrm{d}h}{\mathrm{d}t} &= V\sin\gamma - w_3
\end{aligned} \tag{3.1}$$

where V, χ, γ are the aerodynamic velocity modulus, heading and path angles; m the aircraft mass; φ, λ the geodetic latitude and longitude; h the altitude; μ, the bank angle; g the gravity acceleration; R_E the Earth radius; t the time; T, L, D the thrust, the lift and the aerodynamic drag; and c the specific fuel consumption. w_1, w_2, w_3 are the wind components in the local-axes system (north, east and down); and $\dot{w}_V$, $\dot{w}_\chi$, $\dot{w}_\gamma$ are wind accelerations given by (see Ref. [Jack 99])

$$\begin{aligned} \dot{w}_V &= -\dot{w}_1 \cos\gamma \cos\chi - \dot{w}_2 \cos\gamma \sin\chi + \dot{w}_3 \sin\gamma \\ \dot{w}_\chi &= \dot{w}_1 \sin\chi - \dot{w}_2 \cos\chi \\ \dot{w}_\gamma &= \dot{w}_1 \sin\gamma \cos\chi + \dot{w}_2 \sin\gamma \sin\chi + \dot{w}_3 \cos\gamma \end{aligned} \tag{3.2}$$

In this formulation V, χ, γ, m, φ, λ, and h are state variables; T, L and μ are control variables; and t is an independent variable.

On each application considered in this thesis the equations of motion are particularized attending to the characteristics of the problems being solved.

A flight segment is defined by three flight constraints (for example, to fly at constant altitude, constant speed, and constant heading angle), which together with Eqs. (3.1) form a system of differential algebraic equations (DAE); in general, they have the form

$$G_i(V, \chi, \gamma, m, \varphi, \lambda, h, T, L, \mu, t) = 0, \quad i = 1, 2, 3 \tag{3.3}$$

The constraints must be compatible and physically meaningful, that is, they must indeed close the mathematical problem. In Ref. [Lope 07] one can find a complete description of the different flight constraints that are meaningful in the ATM context (they call *instructions* the flight constraints, and *operation* the set formed by them). The flight constraints considered in this thesis are described in Appendix C.

The resolution of the DAE systems for the different flight segments is based on the reduction of the system of equations to a system of ordinary differential equations (ODE) through the explicit utilization of the flight constraints. A summary of this procedure, for the flight segments considered in this thesis, is also given in Appendix C. The ODE systems are then solved using MATLAB's *ode45* [Sham 97] (based on an explicit Runge Kutta formula) if the segment is at constant altitude, or *ode15s* (based on the numerical differentiation formulas, NDFs) if the segment is a climb/descent segment, which has shown a better performance in this type of segments.

The computation of each flight segment starts with the corresponding initial conditions, which must be compatible with the flight constraints, and ends when the appropriate stopping condition is reached (for instance, reaching a given altitude, or a given Mach number). The initial conditions of the first segment are given data. For any other segment, the initial conditions are the final conditions of the previous segment, except for those variables that can be discontinuous. For example, as it will be seen below, the path angle may be discontinuous since pull-ups or push-downs are not considered. In climb/descent segments, the initial value of γ is estimated using an approximation of the normal-force equation obtained after neglecting the term $\dfrac{\mathrm{d}\gamma}{\mathrm{d}t}$. The stopping conditions are described in Appendix C.

Additionally, to compute the flight segments, some supplementary models are needed: Earth, aerodynamic and propulsion models. The models considered in this thesis are described in Appendix D.

3.2 Trajectory Patterns

A trajectory pattern is a parameterization of the flight intent, which models the aircraft trajectories actually flown. It is described as a sequence of flight segments defined by a small number of parameters. Depending on the application, some of these parameters can be fixed (they are set to a given value), while the rest are free (they can take any value).

The definition of the pattern can introduce some constraints in the parameters in order to, for example, ensure the existence of some flight segments or to meet some conditions at certain points. Next, an example of a trajectory pattern where constraints appear is analyzed. The vertical profile (altitudes and speeds as a function of the horizontal distance, r) and the horizontal profile (the geodetic coordinates along the trajectory) of this pattern are represented in Fig. 3.1. Arrows in this figure indicate the stopping condition for the corresponding flight segment.

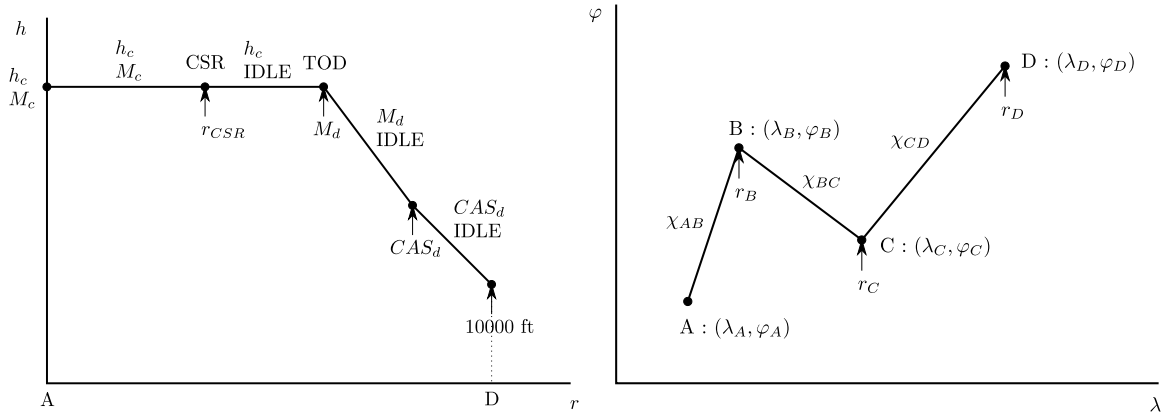

(a) Vertical profile.

(b) Horizontal profile.

Figure 3.1: Example of trajectory pattern.

The pattern is described next. It starts at the geodetic coordinates of the waypoint A (λ_A, φ_A), at cruise altitude h_c and at cruise Mach number M_c. The first segment is to fly at constant altitude and constant speed until a distance r_{CSR} is covered, which determines the CSR (Cruise Speed Reduction) point. This point is the beginning of the last segment of the cruise phase, which is a deceleration at cruise altitude and idle engine rating that ends when the descent Mach M_d is reached. At this new point, named Top of Descent (TOD), the aircraft starts a descent at constant Mach (M_d) and idle rating until the calibrated air speed (CAS) of descent is reached, CAS_d. Finally, the aircraft continues descending at idle and constant CAS (CAS_d) until 10000 ft, which must be reached at the waypoint D.

Note that, to be able to capture the stopping condition of covering a horizontal distance along the Earth surface, the equation

$$\frac{\mathrm{d}r}{\mathrm{d}t} = \frac{R_E}{R_E + h}\sqrt{(V\cos\gamma\sin\chi + w_\lambda)^2 + (V\cos\gamma\cos\chi + w_\varphi)^2} \tag{3.4}$$

must be integrated together with Eqs. (3.1).

In the horizontal profile, the aircraft starts at waypoint A and with heading χ_{AB}, towards waypoint B. Once the distance between A and B, r_B, is covered, an instantaneous turn is

performed and a new heading, χ_{BC}, is imposed to reach C. This process is repeated until all the waypoints are visited.

In the vertical profile of this pattern (and in all patterns defined in this document) pull-ups, push-downs and transients in the engine due to rating changes are not considered. These transition maneuvers are usually performed very fast by the aircraft and their effects in the global properties of the trajectory are very small. Not considering these segments usually yields to a faster computation of the trajectory without penalty in the results. Analogously, in the horizontal profile, changes in the bank angle are considered to be instantaneous, and, depending on the application, also turns. As a consequence the heading angle χ, path angle γ, bank angle μ, lift L and thrust T can be discontinuous variables in the junction of the segments.

The total number of parameters of the example pattern is 13: 8 geodetic coordinates (λ and φ of the 4 waypoints), 3 speeds (M_c, M_d and CAS_d), 1 altitude (h_c), and 1 distance (r_{CSR}). As stated before, some of these parameters can be fixed (for example, the coordinates of the waypoints and the cruise altitude), while the rest are free (for example, the speeds and the distance).

In this example, the fixed and free parameters must satisfy the following constraints:

1. M_d must be lower or equal to M_c (because in the segment after the CSR point the engine is set to idle and the altitude is constant, and therefore the aircraft cannot accelerate);

2. the altitude at which the transition between M_d and CAS_d is performed must lie between h_c and 10000 ft (because the trajectory must end at 10000 ft and CAS_d);

3. the altitude at which the aircraft flies over waypoint D must be 10000 ft (because the trajectory must end at 10000 ft at waypoint D; notice that this equality constraint can be used to eliminate one parameter).

In this thesis, a different trajectory pattern is proposed for each application. All patterns considered are formed by flight segments which comply with usual ATC procedures, namely, segments with constant speed and constant altitude, segments with a given engine rating and constant Mach or CAS (for descent/climb segments), segments with a given engine rating and constant altitude (for decelerating/accelerating segments), and segments with constant speed and constant path angle (for final approach segments).

3.3 Optimization Problem

Once the free parameters of the trajectory are defined, they are collected in a vector $\mathbf{x}$. Some parameters can be continuous variables whereas other parameters can be restricted to take discrete values. For example, according to ICAO Doc. 4444 (Ref. [ICAO 07a]) speed adjustments at or above flight level 250 should be expressed in multiples of 0.01 Mach, below flight level 250 in multiples of 10 kt, and the vertical separation between aircraft is achieved requiring aircraft to operate at different flight levels.

The set of free parameters is used to optimize a given property or combination of properties that can be derived from the computation of the trajectory. For example, it can be

fuel consumption, distance to a given point, noise emissions (which would require a model that depends on the state and/or control variables), or a combination of fuel and time costs. Multi-objective optimization is not considered in this thesis.

In general, the optimization problem can be formulated as a mixed-integer nonlinear programming (MINLP) problem:

$$\begin{array}{ll} \text{minimize} & J(\mathbf{x}) \\ \text{subject to} & \mathbf{f}(\mathbf{x}) = \mathbf{0} \\ & \mathbf{g}(\mathbf{x}) \leq \mathbf{0} \\ & \mathbf{x} \in X, \qquad x_i \text{ discrete } \forall i \in I \end{array} \tag{3.5}$$

where x_i is the i-th component of the vector $\mathbf{x}$, X is the feasible region of the continuous problem, and I defines the set of discrete variables. The equality and inequality constraints and the feasible region depend on the problem being solved and the considered trajectory pattern.

Different techniques can be used to solve MINLP problems, as reviewed in Section 2.1. In this thesis, because of the low dimensionality of the discrete variables, a branch and bound method is used, as described by Fletcher [Flet 87]. To solve the auxiliary optimization problems where all the variables are continuous MATLAB's *fmincon* is used, a SQP method, which was found to be the most efficient method to solve nonlinear programming problems on small- and medium-scale problems.

Next, in Chapter 4, the trajectory of one single aircraft is optimized in cruise flight. Afterwards, in Chapter 5, the vector of parameters $\mathbf{x}$ is extended to collect the parameters of several aircraft simultaneously and the constraints include the separation among aircraft, leading to the problem of CR. Finally, in Chapter 6, many aircraft are handled together and time constraints are added to the CR problem; these constraints are used to define a strategy to obtain a sub-optimum of the optimization problem.

This page intentionally left blank

4 Cruise Optimization

Trajectory optimization is an important subject in air traffic management, which aims at defining optimized flight procedures that lead to energy-efficient flights. According to the AIRE initiative [AIRE 12], flight procedures currently flown by aircraft can be optimized to save hundreds of kilograms of CO_2 per flight. Most of these savings can be obtained optimizing only the cruise procedures, both the lateral and the vertical profiles.

In this chapter, the proposed approach is applied to optimize the cruise flight of one aircraft in the vertical plane. Firstly, in Section 4.1, cruise procedures are optimized to solve the problem of minimum direct-operating-cost cruise with given range. The objective of this application is to analyze how the optimized procedures change when some parameters are restricted to take discrete values. Next, in Section 4.2, the problem of minimum-fuel cruise at constant altitude with fixed range and fixed arrival time is solved. In this application, the objective is to analyze the optimized procedures when they are subject to the additional equality constraint of fixed arrival time. These results are compared with known optimal solutions obtained using the theory of singular optimal control.

In all cases, results are presented for a model of a Boeing 767-300ER, with compressible aerodynamics and general fuel consumption and thrust models, which is described in Appendix D.

4.1 Minimum-DOC Cruise

In practice, the airlines consider a cost index (CI) and define the direct operating cost (DOC) as the combined cost of fuel consumed and flight time, weighted by the CI. Their goal is to minimize the DOC. In this section we address the problem of optimizing the cruise procedures commonly flown by airlines, complying with ATC rules, which are formed by segments at constant Mach number and constant altitude, restricted to take discrete values: Mach numbers multiple of 0.01 and altitudes given by flight levels. For comparison and for completeness, the unrestricted problem in which the speeds and altitudes are continuous variables is also considered. The main objective of the work is to analyze how the optimized procedures change when the altitudes and speeds are restricted to take discrete values. The results show that these changes are important.

This optimization approach based on trajectory patterns, which is somewhat similar to the approach used by Wu and Zhao [Wu 09], is used to solve the general problem of minimum-DOC cruise (unsteady, with variable mass, and without any constraint on speed or altitude) with given range and in the presence of an average horizontal wind. The results show

that the optimized procedures are cruise climbs (in fact, stepped cruise climbs, according to the trajectory pattern) with roughly constant Mach numbers, for all values of the CI. The optimized procedures define not only the optimum values of speed and altitude for the different cruise segments, but also, and more importantly, the optimum distances to be flown on each of the cruise segments that form the trajectory pattern. A heuristic rule to define the number of cruise segments as a function of the given cruise range is provided. The effects of the CI, of the initial aircraft weight and of an average horizontal wind on the optimized procedures are analyzed, in particular, the influence on the optimal values of Mach numbers, altitudes and lengths of the different cruise segments, as well as the influence on the minimum cost.

4.1.1 Problem Formulation

In this section, the optimization approach is used to solve the general unsteady problem of minimum-DOC cruise, without any constraint on speed or altitude. The main objective is to solve the problem in the case of restricted procedures, in order to comply with ATC rules. In the following, the equations of motion that describe the aircraft movement in a vertical plane with average horizontal winds, the trajectory pattern that models the cruise flight and the parametric optimization problem are described. The results are presented in Section 4.1.2.

4.1.1.1 Equations of motion

If the Eqs. (3.1) and (3.4) are particularized for flight in a vertical plane, flat Earth, and altitude-dependent constant horizontal winds contained in the flight plane, then they reduce to:

$$\begin{aligned} m\frac{\mathrm{d}V}{\mathrm{d}t} &= T - D(V,h,L) - mg\sin\gamma - mV\frac{\mathrm{d}w}{\mathrm{d}h}\sin\gamma\cos\gamma \\ mV\frac{\mathrm{d}\gamma}{\mathrm{d}t} &= L - mg\cos\gamma + mV\frac{\mathrm{d}w}{\mathrm{d}h}\sin^2\gamma \\ \frac{\mathrm{d}m}{\mathrm{d}t} &= -c(V,h)T \\ \frac{\mathrm{d}h}{\mathrm{d}t} &= V\sin\gamma \\ \frac{\mathrm{d}r}{\mathrm{d}t} &= V\cos\gamma + w(h) \end{aligned} \tag{4.1}$$

where w is the wind speed. In this equations, only two control variables appear, T and L.

4.1.1.2 Trajectory pattern

To model the cruise flight in a vertical plane, a trajectory pattern formed by n steps is considered, whose vertical profile is shown in Fig. 4.1.

Initially, the pattern starts from the initial altitude h_i and initial Mach number M_i. Then, each step j, $j = 1, \ldots, n$, is formed by three flight segments. The first one is a transition segment, a descent/climb at constant Mach, M_{j-1}, and with idle/maximum cruise engine rating (ER) ending at h_j. The second one is also a transition segment, a deceleration/acceleration at constant altitude, h_j, and with idle/maximum cruise engine rating, ending at M_j. The

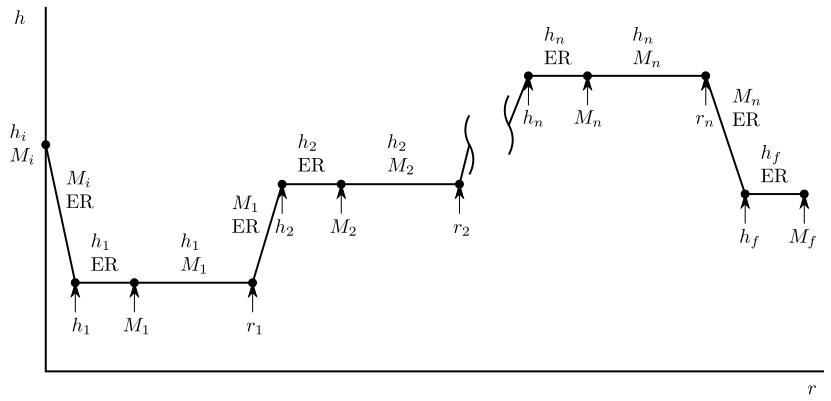

Figure 4.1: Trajectory pattern for cruise optimization.

third one is a segment at constant Mach, M_j, and constant altitude, h_j, which ends when a distance r_j is flown. Finally, because the cruise flight has to end at the final conditions h_f and M_f, two more transition segments, as those just described, complete the pattern.

Each step j is defined by 3 parameters: altitude h_j, Mach number M_j, and distance r_j. The initial and final altitudes, h_i and h_f, and the initial and final Mach numbers, M_i and M_f, are also parameters of the trajectory pattern. Thus, the total number of parameters of the pattern is $3n + 4$.

4.1.1.3 Optimization problem

The objective in this section is to minimize the direct operating cost in a cruise flight whith fixed range, r_A. The DOC is a combination of fuel and time costs, $DOC = m_F + CI\, t_f$ (measured in kg), where m_F is the mass of fuel consumption, t_f the flight time, and CI the cost index, a parameter that measures the relative importance of each cost (the case $CI = 0$ corresponds to minimum fuel).

In this application, the range to be flown is $r_A = 8000$ km, the CI ranges from 0 to 3 kg/s, and the initial and final altitudes and speeds are fixed, $h_i = h_f = 30000$ ft and $M_i = M_f = 0.79$. Because the initial and final conditions are given, the free parameters are the distances, speeds, and altitudes, r_j, M_j, and h_j. Thus, in this application, the total number of free parameters is $3n$.

Some of the parameters can be continuous variables whereas other parameters can be restricted to take discrete values. According to ICAO Doc. 4444 (Ref. [ICAO 07a]) speed adjustments at or above flight level 250 should be expressed in multiples of 0.01 Mach, and the vertical separation between aircraft is achieved requiring aircraft to operate at different flight levels.

The optimization problem is then formulated as a mixed-integer nonlinear programming (MINLP) problem:

$$\begin{array}{lll} \text{minimize} & m_F(\mathbf{x}) + CI\, t_f(\mathbf{x}) & \\ \text{subject to} & r_f(\mathbf{x}) - r_A = 0 & \\ & \mathbf{x} \in X, \qquad\qquad x_i \text{ discrete } \forall i \in I & \end{array} \tag{4.2}$$

where r_f is the total flown distance, function of the free parameters.

The feasible region is given by $r_j \in [0, r_A]$, $M_j \in [0.68, 0.86]$, and $h_j \in [24000, 38000]$ ft. The selection of the number of steps of the trajectory pattern is addressed below.

Two different types of problems are analyzed: one in which all the parameters are continuous variables, and another one in which some parameters are discrete variables (Mach numbers and altitudes). They define what we call unrestricted and restricted procedures, respectively.

Each optimization problem solved by the SQP method requires an initial point to start. In this work, it is considered that initially all the segments at constant speed and constant altitude have the same length, $r_j = r_A/n$, and the Mach numbers and altitudes are randomly generated within the feasible region.

Selection of the number of steps

In the optimization approach used in this application, the number of steps n is given, that is, the number of parameters on which the optimization is performed is fixed and known. An appropriate value must be selected. In Fig. 4.2 the increment in minimum DOC for different values of n is represented as a function of the CI for the case of unrestricted procedures, with no wind ($w = 0$) and for an initial aircraft weight of $W_i = 1600$ kN. Each curve corresponds to the increment $\Delta DOC = (DOC)_{n=k} - (DOC)_{n=k+1}$ for $k = 1, 2, 3$. One can see that increasing from $n = 3$ to 4 leads to a quite small savings: lower than 12.8 kg (value that corresponds to $CI = 3$ kg/s). Therefore, the value $n = 3$ is selected for the simulation presented below.

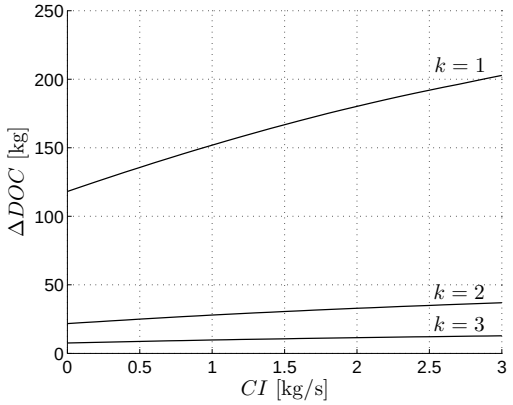

Figure 4.2: Differences in DOC vs CI for different values of n: $(DOC)_{n=k} - (DOC)_{n=k+1}$ ($r_A = 8000$ km, $W_i = 1600$ kN).

It must be noted that the value of n to be chosen clearly depends on the range to be flown. The increment in minimum DOC for different values of n is represented as a function of the range in Fig. 4.3, for $CI = 1$ kg/s, $w = 0$ and, to obtain realistic results, an initial aircraft weight that takes into account the variation of fuel load with range in the form $W_i[\text{kN}] = 1600 + (r_A[\text{km}] - 8000) \cdot 0.05$, that is, a linear decrease of 50 kN per 1000 km of range reduction. To choose the value of n, one can fix a maximum value of savings when

n increases from k to $k+1$, for example 15 kg. The values of range that correspond to $\Delta DOC = 15$ kg in Fig. 4.3 are $r_A = 3701$, 6499 and 9241 km for $k = 1$, 2 and 3, that is, there is a savings smaller than 15 kg for $r_A < 3701$ km when n increases from 1 to 2, for $r_A < 6499$ km when n increases from 2 to 3, and for $r_A < 9241$ km when n increases from 3 to 4. Therefore, the following heuristic rule can be obtained:

- for small ranges, $r_A < 3000$ km: $n = 1$;
- for medium ranges, $3000 < r_A < 6000$ km: $n = 2$;
- for large ranges, $6000 < r_A < 9000$ km: $n = 3$;
- for very large ranges, $r_A > 9000$ km: $n = 4$.

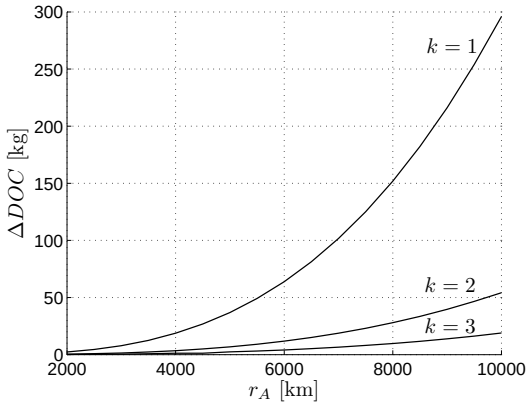

Figure 4.3: Differences in DOC vs r_A for different values of n: $(DOC)_{n=k} - (DOC)_{n=k+1}$ ($CI = 1$ kg/s).

4.1.2 Results

In this section optimization results are presented for the two cases of unrestricted and restricted procedures. In the restricted case, the Mach numbers are multiples of 0.01 and the altitudes are even flight levels (that is, FL240, FL260, FL280, and so on). In the following, the procedures are optimized and the effect of the CI on the optimum values of Mach numbers, flight levels and distances to be flown in each cruise segment is analyzed, in the case that there is no wind ($w = 0$), and for $W_i = 1600$ kN. The effects of the initial aircraft weight and of an average horizontal wind on the optimized procedures are analyzed, for a given CI, in Sections 4.1.2.3 and 4.1.2.4, respectively.

4.1.2.1 Optimized procedures

The optimized unrestricted procedures are shown in Fig. 4.4 for different values of the CI. It can be seen in Fig. 4.4a that the altitudes decrease as the CI increases; this same behaviour was found, for example, by Barman and Erzberger [Barm 76] for short-haul aircraft with

constant mass. Note that, for all values of the CI, the three steps have very similar lengths, so that the altitude changes are performed approximately at the same points. In Fig. 4.4b one has that the Mach number increases as the CI increases and its variation along the whole trajectory is very small.

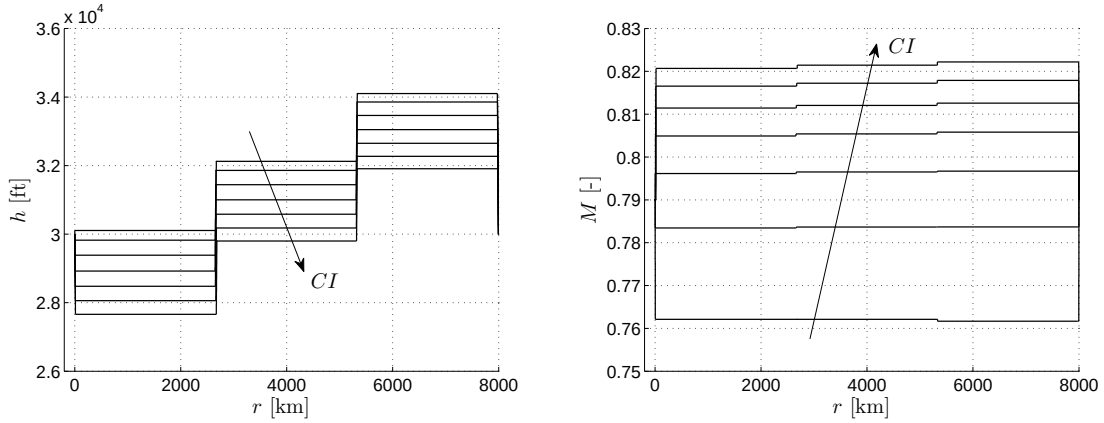

(a) Altitude profile.

(b) Speed profile.

Figure 4.4: Optimized unrestricted procedures, $CI = 0, 0.5, 1, 1.5, 2, 2.5, 3$ kg/s.

The altitude and speed profiles of the optimized restricted procedures are shown in Fig. 4.5 for different values of the CI. Unlike in the unrestricted case, the three steps have now quite different lengths, so that the altitude changes are performed at different points, depending on the value of the CI. Note that for large values of the CI the optimum flight levels drop one level. Regarding the speeds, in most cases the solution is to fly at constant Mach number during the whole trajectory; however, in some cases, two values are used, with a difference of just 0.01 (for instance, for $CI = 1.5$ kg/s, one has $M_1 = M_2 = 0.80$ and $M_3 = 0.81$).

These results indicate that the optimized procedures are always cruise climbs (in fact, stepped cruise climbs, according to the trajectory pattern) with roughly constant Mach numbers, for all values of the CI.

It is well known that for the quasi-steady minimum-fuel problem with small path angle approximation the optimal trajectories are cruise climbs with constant lift coefficient and constant Mach number. In Ref. [Riva 10] this optimum Mach number is computed for the aircraft model considered in this work, being $M^* = 0.7621$. The three Mach numbers of the optimized unrestricted procedure for $CI = 0$ are very close to this value, namely, 0.7621, 0.7621 and 0.7617, whereas in the optimized restricted procedure the three of them turn out to be 0.76, also very close to M^*. This good comparison serves as a reference to support the optimization results obtained in this section.

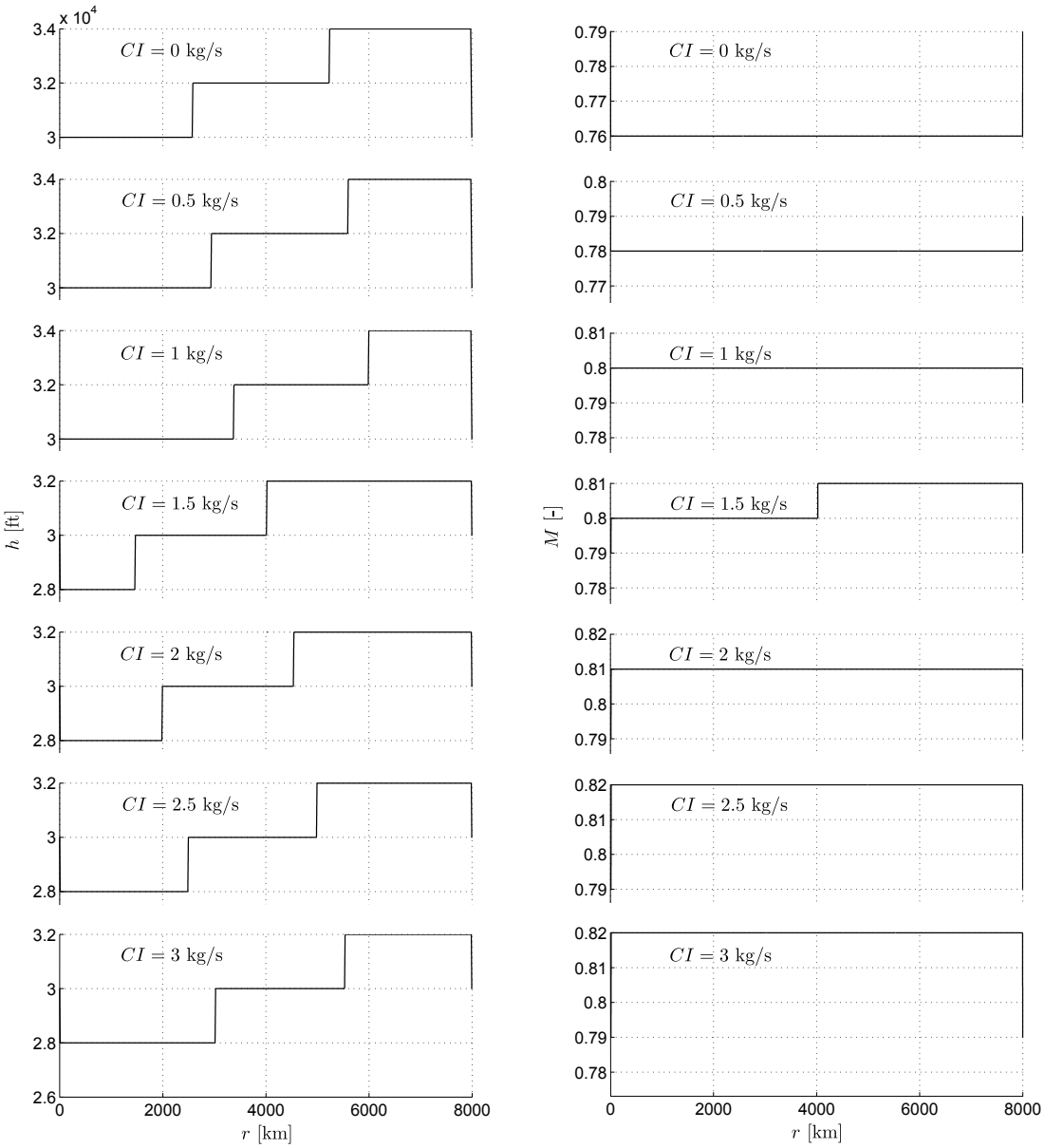

(a) Altitude profile.

(b) Speed profile.

Figure 4.5: Optimized restricted procedures, $CI = 0, 0.5, 1, 1.5, 2, 2.5, 3$ kg/s.

The evolution of the free parameters h_j, M_j, and r_j as a function of the CI is depicted in Fig. 4.6, for both the restricted and the unrestricted procedures. In the unrestricted case, the general trend is to have lower altitudes and larger Mach numbers as the CI increases (as already seen in Fig. 4.4): the three altitudes h_j decrease, keeping a roughly constant difference among them, and the three Mach numbers M_j increase, being very close to each other (with a maximum difference of just 0.0015 for $CI = 3$ kg/s).

In the restricted case, for values of the CI ranging from 0 to approximately 1.4 kg/s, the flight levels used in the optimized restricted procedure are FL300, FL320 and FL340, but beyond that point all the altitudes drop one level (as already mentioned) and then

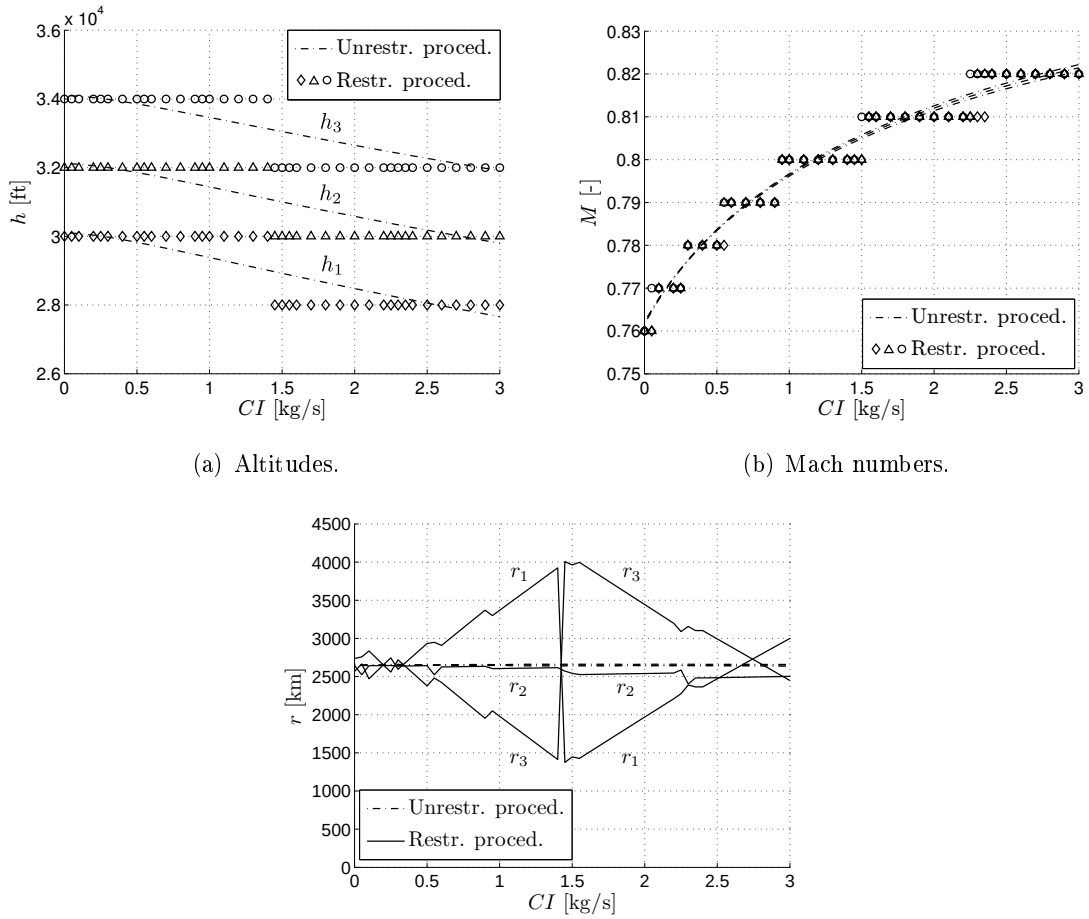

(a) Altitudes.

(b) Mach numbers.

(c) Distances.

Figure 4.6: Evolution of the free parameters vs CI.

the optimum flight levels are FL280, FL300 and FL320. Also, one has that only one or two speeds are used in the restricted procedure for each value of the CI, satisfying $M_1 \leq M_2 \leq M_3$ with a maximum difference of just 0.01. (Note that the key to the symbols in Fig. 4.6 is as follows: diamond, triangle and circle correspond to the first, second and third cruise segments, respectively.)

The distances r_j are shown in Fig. 4.6c. It can be seen that in the unrestricted procedure the three distances are almost independent of the CI and very close to each other, as it was observed in Fig. 4.4a. However, in the restricted procedure, they are quite different, with r_1 increasing and r_3 decreasing as the CI increases, and r_2 almost independent of the CI. Note that r_1 and r_3 present large jumps of about 2500 km at $CI \approx 1.4$ kg/s, which are caused by the change in the flight levels shown in Fig. 4.6a. As an example, for $CI = 1.3$ kg/s, in the unrestricted case one has (r_1, r_2, r_3)=(2639,2652,2661) km, whereas in the restricted case one has (r_1, r_2, r_3)=(3785,2614,1556) km, and for $CI = 1.7$ kg/s, the distances are (2640,2649,2662) km in the unrestricted case, and (1608,2531,3812) km in the restricted case. These jumps in the distances between the restricted and the unrestricted procedures are analyzed in detail in Section 4.1.2.2. The restricted distances also present some little

jumps which match with the speed changes observed in Fig. 4.6b.

The evolution of some global properties as a function of the CI is shown in Fig. 4.7: as expected, the flight time decreases and the fuel consumption and the DOC increase as the CI increases. Clearly, larger values of the CI require smaller values of t_f, which in turn require larger values of M_j with associated larger values of m_F and DOC. As a quantitative reference, in the unrestricted procedures, for an increase of CI from 0 to 3 kg/s, m_F increases in 2968 kg, t_f decreases in 47.56 min, and the minimum DOC increases in 9.93×10^4 kg.

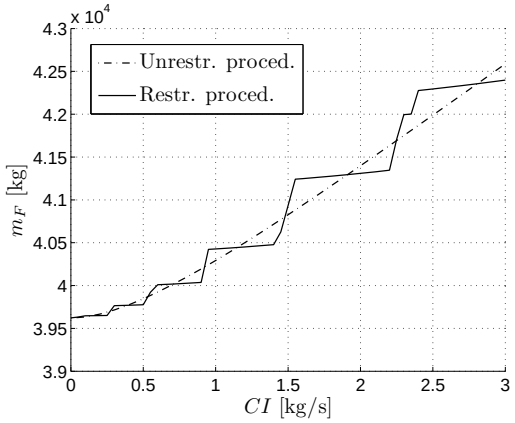

(a) Fuel consumption.

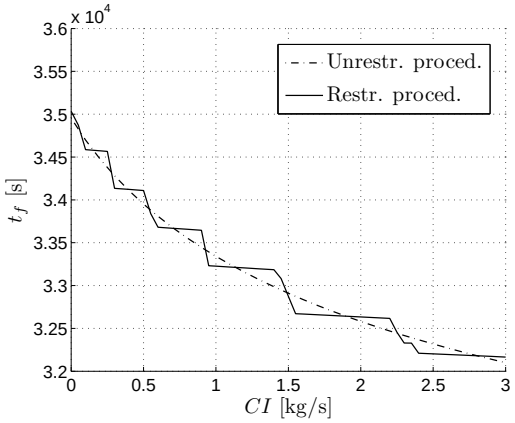

(b) Flight time.

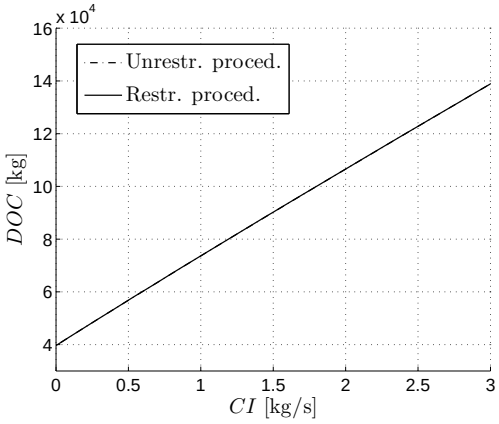

(c) Direct operating cost.

Figure 4.7: Evolution of global properties vs CI.

As it happens with the distances, the fuel consumption and the flight time show some little jumps that match with the altitude and speed changes observed in Fig. 4.6. However, because of the larger scale, the DOC presents a smooth evolution (Fig. 4.7c) and it is hard to distinguish between the restricted and the unrestricted procedures. The maximum difference found in the DOC between both procedures is as small as 54.1 kg (0.06% of the total).

The analysis of how the optimized procedures change when the altitudes and speeds are restricted to take discrete values is one of the main objectives of this application. As we have just seen, these changes are important (Fig. 4.6), although the influence on the cost is very small (Fig. 4.7c).

4.1.2.2 Minimum-DOC cruise with given flight levels

In this section, the results for the optimum distances r_j shown in Fig. 4.6c are analyzed. To carry out this analysis, a modified version of the minimum-DOC problem is solved. In this modified problem, the altitudes h_j are fixed to given flight levels, whereas the distances r_j and the Mach numbers M_j are the free parameters. Hence, the restricted procedure consists now in having just the Mach numbers take discrete values. In Fig. 4.8a it is shown the evolution of the distances as a function of the CI when the altitudes h_j are fixed to FL300, FL320 and FL340 (the same flight levels obtained for low values of the CI, as seen in Fig. 4.6a). In this figure, it can be seen that the differences in the distances between the restricted and the unrestricted procedures are very small, contrary to what was observed in Fig. 4.6c. Therefore, it can be said that, in the minimum-DOC cruise problem, the altitudes play a key role in the selection of the optimum distances r_j: when the altitudes are free parameters and continuous variables, then the distances are very similar among them and independent of the CI, but when the altitudes are fixed to given values, then the distances are quite different among them and greatly affected by the CI. In fact, it is observed in Fig 4.8a that for high values of the CI the distance r_3 goes to zero, which means that the associated step disappears and, therefore, flying at FL340 is not optimal.

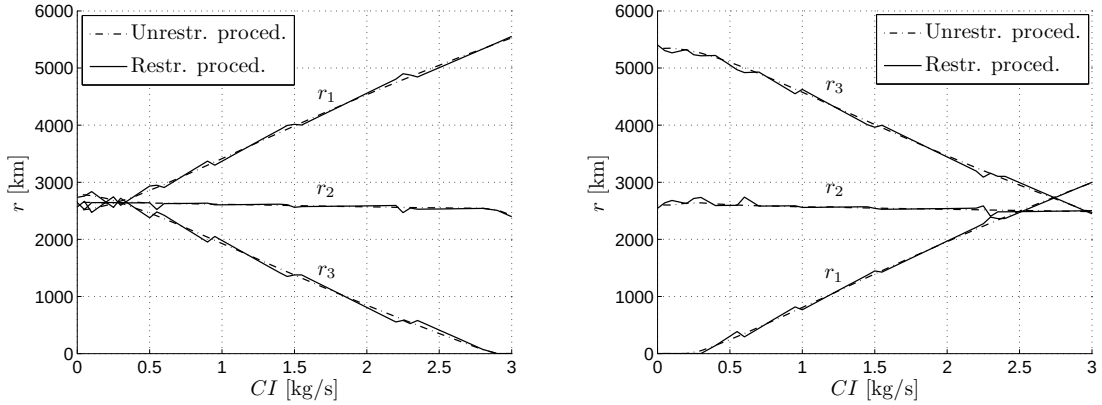

(a) h_1 =30000 ft, h_2 =32000 ft, and h_3 =34000 ft. (b) h_1 =28000 ft, h_2 =30000 ft, and h_3 =32000 ft.

Figure 4.8: Evolution of r_j vs CI when h_j are fixed parameters.

A similar behavior is found in Fig. 4.8b, where the altitudes are fixed to FL280, FL300 and FL320 (the flight levels obtained for high values of the CI, as seen in Fig. 4.6a). Again, the differences between the restricted and the unrestricted procedures are very small, and note that for small values of the CI the step associated to r_1 now disappears.

In both cases, r_1 increases and r_3 decreases as the CI increases, and r_2 is almost independent of the CI, but in the case starting at FL300 r_1 is larger than r_3, and conversely r_3 is larger than r_1 in the case starting at FL280.

The results obtained for this modified problem are now used to explain the change in flight levels shown in Fig. 4.6a and the associated steep change in the distances observed in Fig. 4.6c. The difference in cost, ΔDOC, between the lower-altitude procedure where the altitudes are fixed to FL280, FL300, and FL320, and the higher-altitude procedure where

the altitudes are fixed to FL300, FL320, and FL340 is represented in Fig. 4.9. It can be seen that when the CI ranges from 0 to approximately 1.4 kg/s the cost of the restricted procedure that starts at FL300 is lower, but beyond $CI \approx 1.4$ kg/s, the situation is reversed and then the cost is higher. These results show why in the problem where the altitudes are allowed to take discrete values the optimizer jumps from one solution to the other at $CI \approx$1.4 kg/s, producing that steep change in the restricted optimum distances. Thus, below $CI \approx$1.4 kg/s the optimal solution is to fly higher (starting at FL300), whereas above that value the optimal solution is to fly lower (starting at FL280). Of course, for $CI \approx$1.4 kg/s both optimized restricted procedures, starting at FL280 and at FL300, have approximately the same cost; in the first case one has $r_1 < r_3$, whereas in the second case $r_1 > r_3$.

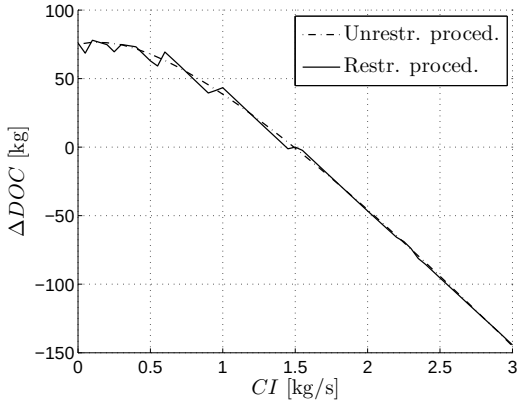

Figure 4.9: Difference in DOC between the lower and higher-altitude procedures vs CI when h_j are fixed parameters.

4.1.2.3 Influence of the initial aircraft weight

Now, the effect of the initial aircraft weight on the minimum-DOC cruise is analyzed. In this analysis the values of weight considered range from $W_i = 1500$ kN to 1700 kN and results are presented for $CI = 1$ kg/s and $w = 0$.

The evolution of the free parameters h_j, M_j, and r_j as a function of W_i is depicted in Fig. 4.10, for both the restricted and the unrestricted procedures. It can be seen that the unrestricted altitudes decrease almost linearly as W_i increases, with a variation of approximately 2000 ft every 150 kN. The restricted altitudes also decrease, dropping one level at $W_i = 1638$ kN (from FL300, FL320 and FL340, to FL280, FL300 and FL320).

The three unrestricted Mach numbers are very close to each other and their variation with W_i is very small, decreasing slightly as W_i increases. In the restricted procedure, the three speeds coincide from $W_i = 1500$ kN to 1658 kN, $M_1 = M_2 = M_3 = 0.80$. Then, M_1 drops to 0.79 and, at $W_i = 1698$ kN, M_2 also drops to 0.79. In general, one has $M_1 \leq M_2 \leq M_3$.

The distances r_j in the unrestricted procedure are almost independent of W_i and very close to each other. However, in the restricted procedure, the three distances are different, with r_1 increasing and r_3 decreasing as W_i increases, and r_2 almost independent of W_i. The large jumps in r_1 and r_3 at $W_i = 1638$ kN are due to the change in the flight levels, similarly

to what was observed in Fig. 4.6c.

These results show that the initial aircraft weight does have an important effect on the optimized procedures.

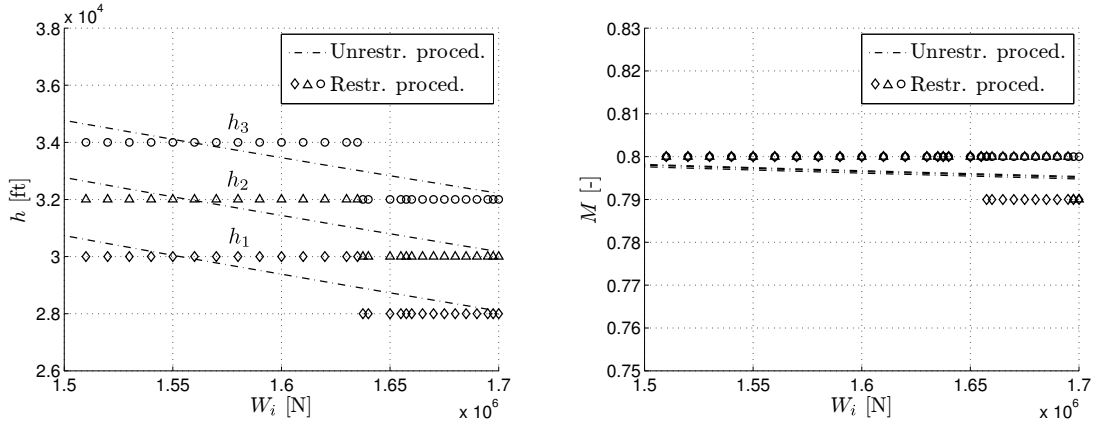

(a) Altitudes.

(b) Mach numbers.

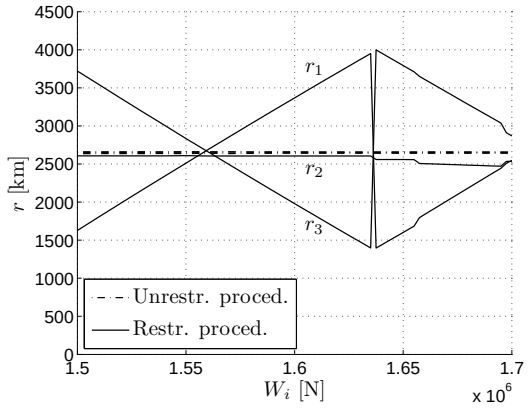

(c) Distances.

Figure 4.10: Evolution of the free parameters vs W_i for $CI = 1$ kg/s.

The evolution of the global properties as a function of W_i is shown in Fig. 4.11. As expected, the fuel consumed in both procedures increases as the initial aircraft weight increases. In general (except for very large weights, $W_i \approx 1700$ kN), more fuel is consumed in the restricted procedures, with a maximum difference of 252 kg (0.61% of the total).

The flight time in the unrestricted procedures decreases as W_i increases, because even though the Mach numbers decrease as W_i increases, the altitudes also decrease, which corresponds to an increase of the speed of sound that leads to an increase of the aerodynamic speeds $V_j = M_j a(h_j)$ (a being the speed of sound). In the restricted procedures, from $W_i = 1500$ kN to 1638 kN, the flight time also decreases because even though the Mach numbers M_j and the altitudes h_j are now the same for all values of W_i, r_1 increases and r_3 decreases as W_i increases, and therefore the aircraft flies more distance at the lower altitude, with larger speed of sound and, as a consequence, larger aerodynamic speed. Then, when the altitudes drop one level, at $W_i = 1638$ kN, the flight time reduces in approximately 100 s. At

$W_i = 1658$ kN the flight time increases because M_1 decreases, and at $W_i = 1698$ kN increases again when M_2 decreases. In general (except for very large weights, $W_i \approx 1700$ kN) the flight time is smaller in the restricted procedures, with a maximum difference of 211 s (0.64% of the total).

Although the differences in fuel consumed and flight time are about 0.6%, these differences compensate each other resulting in a maximum difference in the DOC of just 40 kg (0.05% of the total), being the cost larger in the case of the restricted procedures.

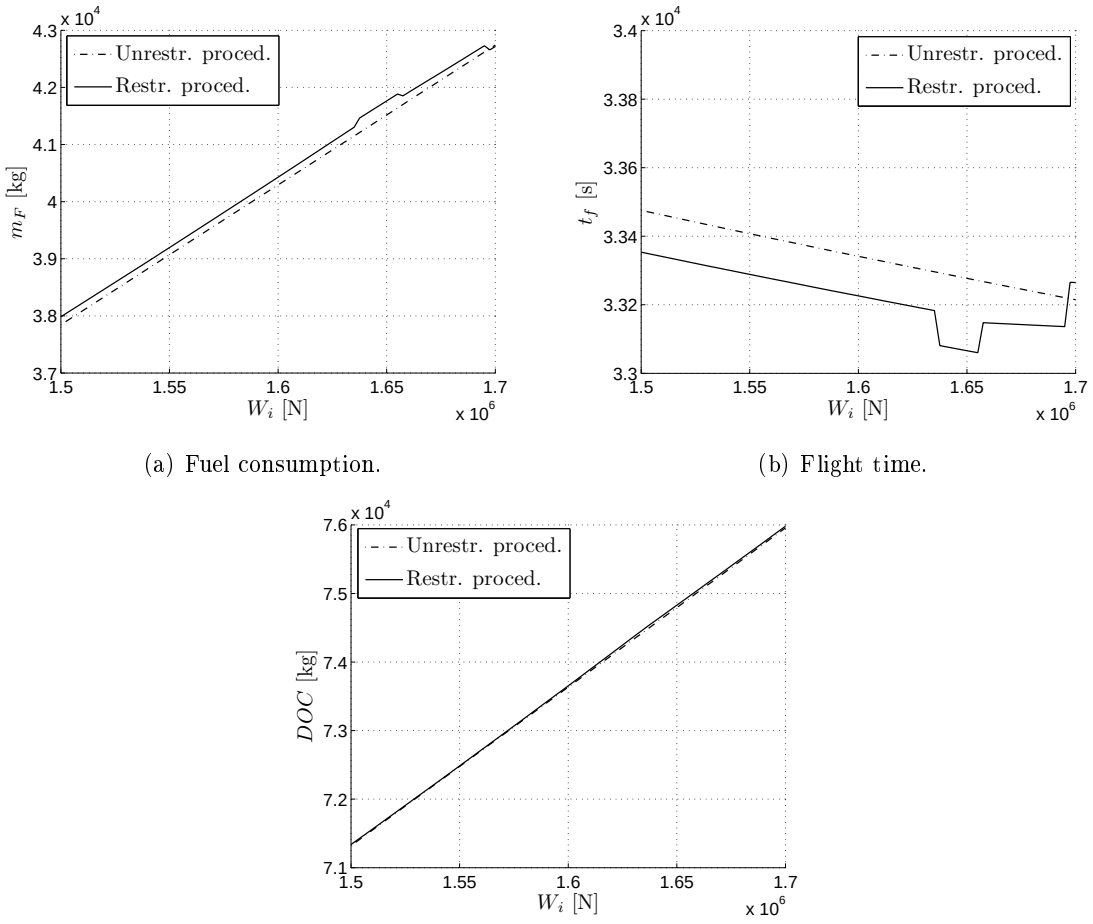

(a) Fuel consumption.

(b) Flight time.

(c) Direct operating cost.

Figure 4.11: Evolution of global properties vs W_i for $CI = 1$ kg/s.

4.1.2.4 Wind effects

In this section the effect of an average horizontal wind on the minimum-DOC cruise is analyzed. In particular, the effects of the wind speed on the optimized procedures is studied. Even though the theoretical analysis made in the chapter is general and valid for any altitude-dependent wind profile, so that results could be presented for any choice of profile, for simplicity a constant profile is considered. The values of wind speed used range from $w = -20$ to 20 m/s. Results are presented for $CI = 1$ kg/s and $W_i = 1600$ kN.

The evolution of the free parameters h_j, M_j, and r_j as a function of the wind speed w is depicted in Fig. 4.12, for both the restricted and the unrestricted procedures. In the unrestricted case the variation of the altitudes h_j is very small, and in the restricted case the flight levels used are the same for all the wind speeds considered, namely, FL300, FL320 and FL340.

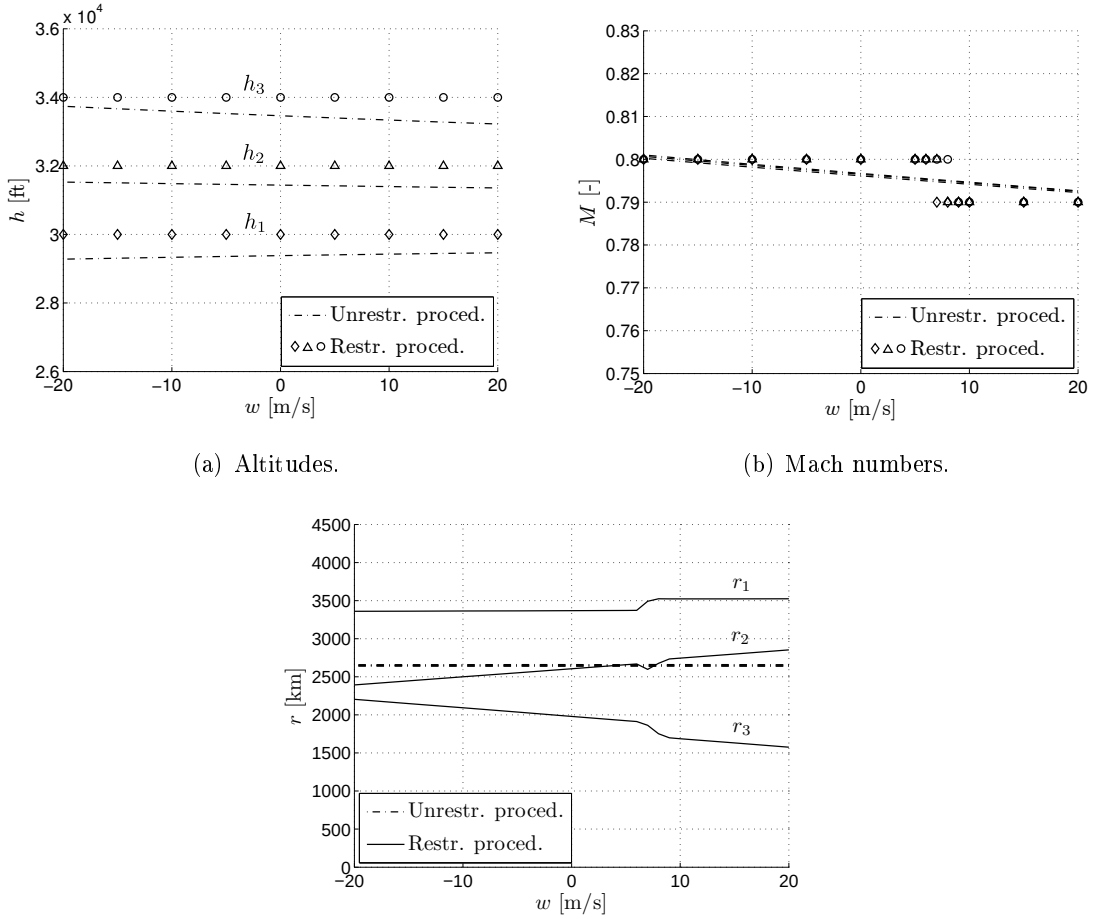

(a) Altitudes.

(b) Mach numbers.

(c) Distances.

Figure 4.12: Evolution of the free parameters vs w for $CI = 1$ kg/s and $W_i = 1600$ kN.

The three unrestricted Mach numbers are very close to each other and their variation with w is small, decreasing as w increases. In the restricted procedure, the variation with w is also small: the three Mach numbers coincide for $w \leq 6$ m/s ($M_j = 0.80$) and for $w \geq 9$ m/s ($M_j = 0.79$), and for $w \in (6, 9)$ m/s the Mach numbers take two different values (for example, for $w = 7$ m/s one has $M_1 = 0.79$ and $M_2 = M_3 = 0.80$, and for $w = 8$ m/s $M_1 = M_2 = 0.79$ and $M_3 = 0.80$). In general, one has $M_1 \leq M_2 \leq M_3$, with a maximum difference of just 0.01.

The distances r_j in the unrestricted procedure are almost independent of w and very close to each other. However, in the restricted procedure, the three distances are different, slightly changing with w, especially r_2 which increases and r_3 which decreases as w increases; for example, for a headwind of $w = -20$ m/s the distances are $(r_1, r_2, r_3) = (3360, 2394, 2204)$ km

and for a tailwind of $w = 20$ m/s they are $(3524, 2853, 1575)$ km. In the evolution of r_j with w, there is a little jump between $w = 7$ and 8 m/s which matches with the speed change just remarked.

In summary, it can be said that the effect of the wind on the optimized procedures is small.

The evolution of the global properties as a function of w is shown in Fig. 4.13. The fuel consumption, the flight time and the minimum DOC of the optimized restricted and unrestricted procedures are very close to each other; the maximum difference in the DOC found between both procedures is just 26.8 kg (0.04% of the total). These three global properties decrease as w increases: they are, as expected, larger for headwinds than for tailwinds, with the only exception of the flight time for some wind speeds in the interval $(6, 9)$ m/s, where the decrease of the Mach numbers (from 0.80 to 0.79) leads to a slight increase of t_f.

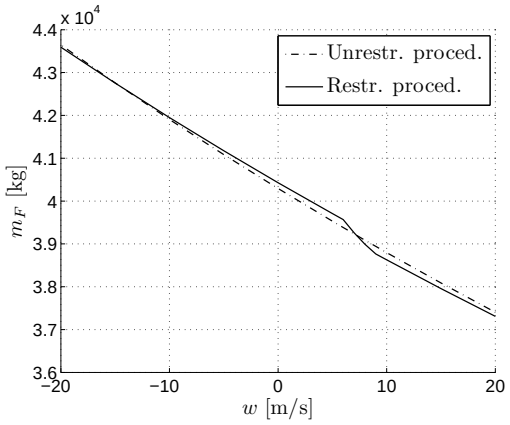

(a) Fuel consumption.

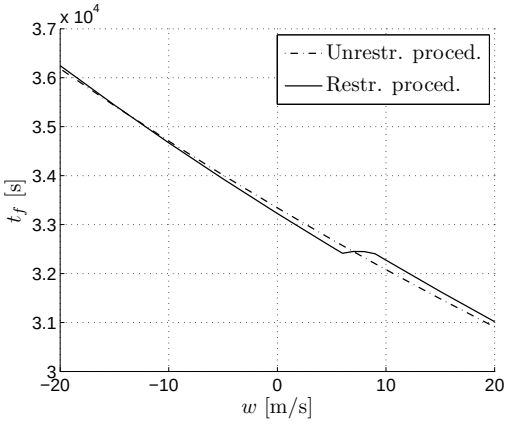

(b) Flight time.

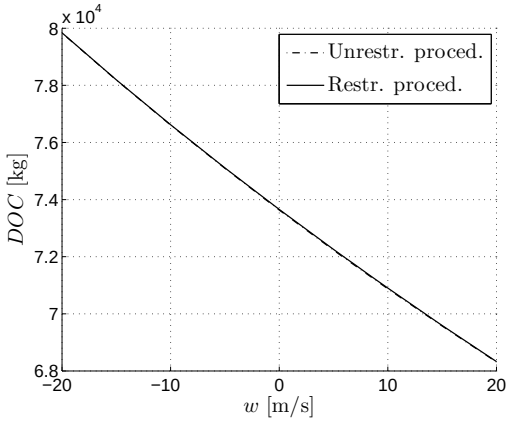

(c) Direct operating cost.

Figure 4.13: Evolution of global properties vs w for $CI = 1$ kg/s and $W_i = 1600$ kN.

4.2 Minimum-Fuel Cruise with Given Flight Time

An important problem in air traffic management is the design of aircraft trajectories that meet certain arrival time constraints at given waypoints, for instance, at the top of descent, at the initial approach fix (IAF), or at the runway threshold. The objective in this section is to minimize the fuel consumption, in a cruise flight at constant altitude where the range, flight time and initial and final conditions are given.

In this problem there exists an optimal solution obtained using the theory of singular optimal control. The structure of the optimal trajectory is formed by a singular arc and two min/max thrust arcs joining the singular arc with the given initial and final points. The problem is analyzed by Franco et al. in Refs. [Fran 10, Fran 11].

Ideally, aircraft should follow optimal trajectories, but these trajectories may not be flyable according to present-day air traffic procedures and regulations. However, they represent best performance and can be used either as references to design improved flight procedures or to determine the optimality of flight procedures commonly used in practice.

In this section a flyable flight procedure is defined based on flight segments at constant Mach numbers, which is called stepped-Mach procedure. This procedure is optimized while subject to the additional constraint of fixed arrival time, and the results are compared with the optimal trajectories. The comparison shows that the minimum fuel consumption is very close to optimal.

4.2.1 Problem Formulation

In this section, the optimization approach is used to solve the unsteady problem of minimum fuel cruise with arrival time and altitude constrained to take given values. In the following, the equations that describe the aircraft motion in a vertical plane at constant altitude, the trajectory pattern that models the cruise flight and the parametric optimization problem are described. The results and the comparison with optimal trajectories are presented in Section 4.2.2.

4.2.1.1 Equations of motion

In this problem, the flight takes place in a vertical plane, at constant altitude, h_A, and with no wind. If the equations of motion (3.1) and Eq. (3.4) are particularized for these conditions, then one obtains:

$$\begin{aligned} m\frac{\mathrm{d}V}{\mathrm{d}t} &= T - D(V, m, h_A) \\ \frac{\mathrm{d}m}{\mathrm{d}t} &= -c(V, h_A)T \\ \frac{\mathrm{d}r}{\mathrm{d}t} &= V \end{aligned} \tag{4.3}$$

In these equations, the drag takes into account the remaining equation of motion $L = mg$ and the control variable is T.

4.2.1.2 Trajectory pattern

The stepped-Mach procedure is modeled by a pattern formed of n steps, Fig. 4.14, which is similar to the pattern shown in Fig. 4.1 but without the climb/descent segments.

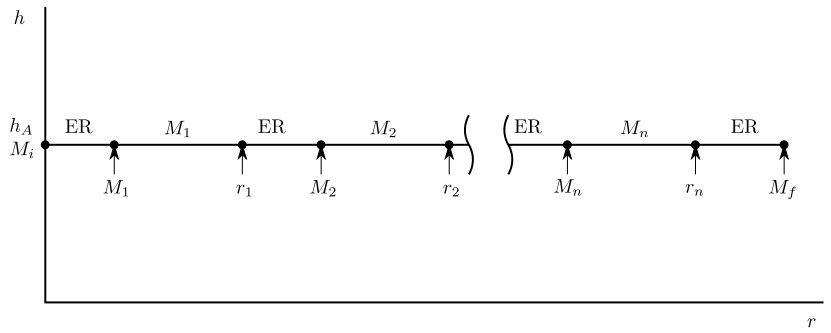

Figure 4.14: Trajectory pattern for cruise optimization at constant altitude.

Initially, the pattern starts from the altitude h_A and the initial Mach number M_i. Then, each step j, $j = 1, \ldots, n$, is formed by two flight segments. The first one is a transition segment, a deceleration/acceleration at constant altitude and with idle/maximum cruise engine rating, ending at M_j. The second one is a segment at constant Mach, M_j, and constant altitude which ends when a distance r_j is flown. Finally, because the cruise flight has to end at the final condition M_f, another transition segment completes the pattern.

Each step j is defined by 2 parameters: Mach number M_j and flown distance r_j. The altitude h_A, and the initial and final Mach numbers, M_i and M_f, are also parameters of the trajectory pattern. Thus, the total number of parameters of the pattern is $2n + 3$.

4.2.1.3 Optimization problem

The problem of minimizing the fuel consumption in a flight where the range and flight time are given values, r_A and t_A, respectively, can be written as

$$\begin{array}{lll} \text{minimize} & m_F(\mathbf{x}) & \\ \text{subject to} & r_f(\mathbf{x}) - r_A = 0 & \\ & t_f(\mathbf{x}) - t_A = 0 & \\ & \mathbf{x} \in X, & x_i \text{ discrete } \forall i \in I \end{array} \tag{4.4}$$

In all cases solved in this application, h_A, M_i, and M_f are fixed parameters. Thus, in this application the total number of free parameters is $2n$: r_j and M_j. The feasible region is given by $r_j \in [0, r_A]$ and $M_j \in [0.68, 0.86]$.

As it was done in the previous application, in the starting point to initialize the SQP method all the segments at constant speed have the same length, $r_j = r_A/n$, and the Mach numbers are randomly generated within the feasible region.

4.2.2 Results and Comparison with Optimal Trajectories

In this application the following values are considered: range $r_A = 8000$ km and arrival time $t_A = 10$ h (this time corresponds to a delay of 0.26 h with respect to the problem of minimum fuel with free flight time, in which case the optimum flight time is 9.74 h). The initial weight of the aircraft is $W_i = 1600$ kN and the altitude is $h_A = 33000$ ft. To analyze the influence of the given initial and final conditions on the optimized procedures, the initial and final Mach numbers, M_i and M_f, take the values 0.75, 0.76, 0.77 and 0.78, so that 16 different combinations of initial and final conditions are considered. Results are presented for $n = 2$, 3, 4 and 5 steps.

The evolution of the Mach number as a function of the flown distance is shown in Figs. 4.15 and 4.16 for the optimal trajectories and the optimized unrestricted and restricted procedures, respectively. For each value of n, 16 optimal trajectories and 16 optimized procedures are plotted. It can be seen that the effect of the initial and final conditions on the optimized procedures is very small, as in the case of the optimal trajectories. In fact, the initial and final conditions are hard to see in the figures, because the length of the transition segments and the bangs are so small when compared to the range that they are seen as vertical lines.

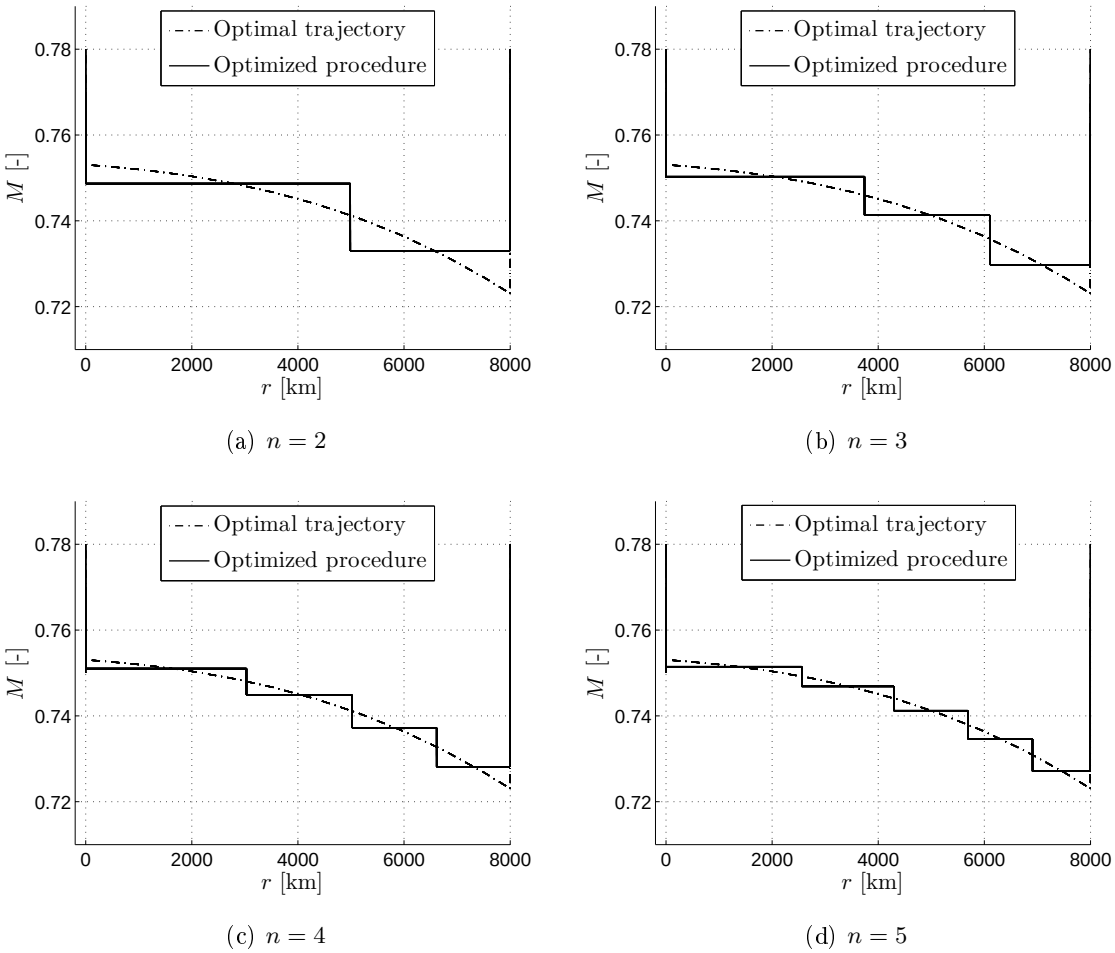

(a) $n = 2$ (b) $n = 3$

(c) $n = 4$ (d) $n = 5$

Figure 4.15: Comparison with optimal trajectories, optimized unrestricted procedures.

The optimized unrestricted procedures evolve around the optimal trajectories, providing an excellent fit. The approximation improves as n increases. To quantify how far the optimized unrestricted procedures are from the optimal trajectories, the fuel consumption in both problems is now compared. Among all the 16 combinations of initial and final conditions, the maximum and minimum values of the fuel consumption of the optimal trajectories, m_F^*, are 39920 and 39953 kg; the effect of considering different initial and final speeds is only of about 33 kg (0.08% of the total). The maximum and minimum differences in fuel consumption between the optimized unrestricted procedures and the optimal trajectories (for the 16 combinations of initial and final conditions), $\Delta m_F = m_F - m_F^*$, are given in Table 4.1 for the different number of steps n. It can be seen that the fuel differences decrease as n increases. The maximum difference in fuel consumption is about 4 kg (0.01% of the total) for $n = 2$, and decreases to less than 1 kg for $n = 5$.

Procedure	Δm_F [kg]							
	$n = 2$		$n = 3$		$n = 4$		$n = 5$	
	min	max	min	max	min	max	min	max
Unrestricted	4.42	4.43	1.92	1.93	1.07	1.08	0.684	0.686
Restricted	5.40	5.40	1.99	2.00	1.90	1.90	1.90	1.90

Table 4.1: Differences in fuel consumption between optimized procedures and optimal trajectories.

The effect of considering the Mach numbers as discrete variables is now analyzed. The evolution of the Mach number as a function of the flown distance is shown in Fig. 4.16 for the optimal trajectories and the optimized restricted procedures. Now, it can be seen that the approximation of the optimal trajectories is a bit worse than in the case of the optimized unrestricted procedures. Again, the approximation improves when n increases, until a limit is reached: no improvement is found in adding a new step when n goes from 4 to 5. Also notice that the improvement when n goes from 3 to 4 is very small, with the fourth step being of just 188 km. As before, the maximum and minimum differences in fuel consumption (among all the 16 combinations) between the optimized restricted procedures and the optimal trajectories, $\Delta m_F = m_F - m_F^*$, are given in Table 4.1 for the different number of steps n. The fuel differences initially decrease as n increases until a limit is reached. These differences cannot be smaller because the Mach numbers take discrete values.

As the results indicate, the differences between the optimized procedures and the optimal trajectories are very small in both cases, when the Mach numbers are restricted and when they are not. So it can be concluded that the optimization approach based on trajectory patterns generates optimized procedures whose performance is, in this problem, very close to optimal.

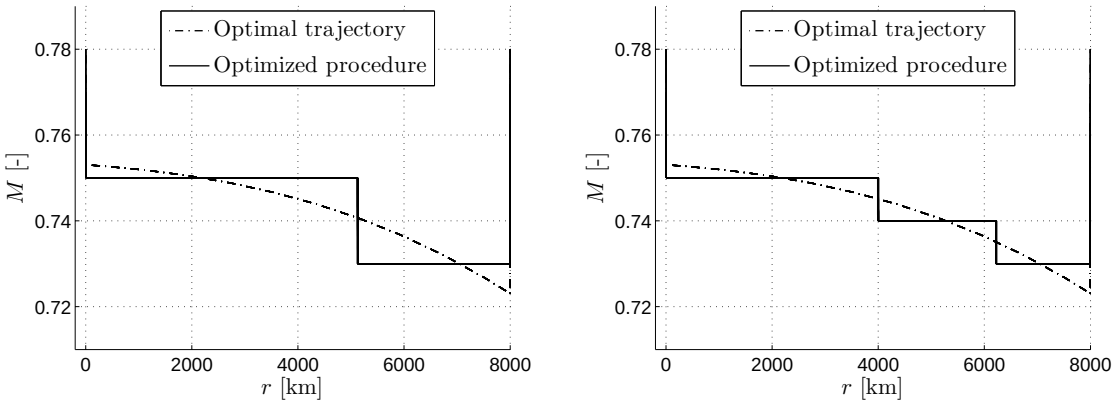

(a) $n = 2$

(b) $n = 3$

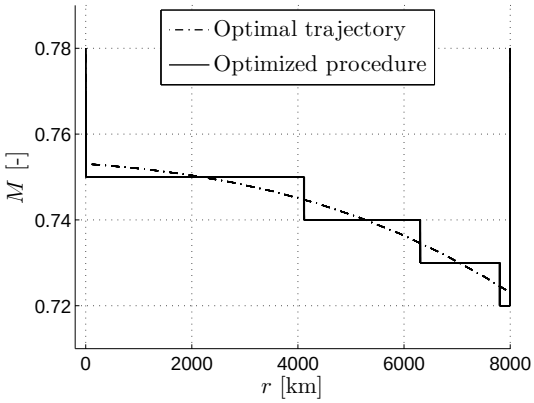

(c) $n = 4$

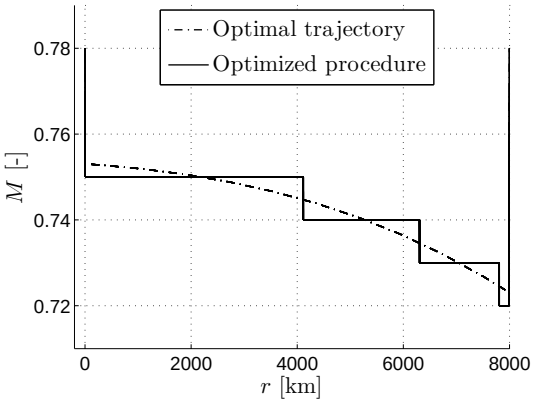

(d) $n = 5$

Figure 4.16: Comparison with optimal trajectories, optimized restricted procedures.

5 Optimization of Conflict-Free Trajectories in Converging Traffic

As it was discussed in the Introduction (Chapter 1) it is expected that the systems based on the TBO concept will improve the detection and resolution of conflicts among aircraft, making possible the automatic generation of conflict-free trajectories. Moreover, the aircraft will be able to fly optimal trajectories which will reduce the cost of the airlines and will allow an optimal management of the air space.

In this chapter, the optimization approach presented in Chapter 3 serves as a basis to develop a conflict resolution (CR) algorithm for converging traffic in a terminal area (TMA). This algorithm generates and optimizes conflict-free trajectories of a set of aircraft.

The conflict resolution algorithm devised to solve the CR problem yields the values of the parameters, for all aircraft involved, that solve the conflicts, while minimizing the deviation from the intended trajectories in the lateral profile (this is the chosen optimality criterion). The resolution strategy is composed of two phases: one in which a first valid solution is found by means of a random search, and another one in which this first valid solution is optimized (that is, another valid solution with smaller cost is found). The conflict detection (CD) algorithm that measures the separation among aircraft considers both horizontal and vertical separation standards.

Since the algorithm is applied to the case of converging traffic in a TMA, the trajectory patterns consider the flight segments usually flown by transport aircraft in cruise and descent (e.g. idle descents), and include standard airline procedures (e.g. standard arrival STAR) and air traffic control regulations (e.g. speed limitation below 10000 ft). In this work the nominal (intended) trajectories and the operator preferences are supposed known. The resolution trajectory patterns take into account changes of the nominal waypoints (*vectoring*) and changes of the aircraft speeds.

According to the taxonomy given by Kuchar and Yang [Kuch 00] the algorithm presented in this thesis can be categorized as: three-dimensional state information, nominal dynamic state propagation (without uncertainty), optimized conflict resolution, turns and speed changes maneuvers, global handling of the potential conflicts; it is also strategic and centralized, and considers multiple aircraft.

Bilimoria et al. [Bili 00b] propose the use of three metrics to evaluate the performance of a CR scheme: safety, efficiency and stability. The algorithm presented in this thesis is safe and stable, because it solves all the conflicts and is centralized and global, and its efficiency is stablished by assessing the cost of the global CR process, in terms of extra distance travelled,

extra flight time and extra fuel consumed for each aircraft.

As already mentioned, the CR algorithm is applied to the case of converging traffic in a TMA, and two different scenarios are considered. First, one in which all aircraft are unlocked, that is, their trajectories are subject to change in the resolution process; and a second one in which there are some unlocked aircraft and some locked aircraft, that is, aircraft whose trajectories are known and fixed. Unlocked aircraft can be in conflict both with the other unlocked and with the locked aircraft. The resolution of the problem requires that the unlocked aircraft be conflict free with all aircraft, both locked and unlocked. Results for the case of multiple conflicts among commercial transport aircraft in the TMA of Madrid are presented.

The outline of this chapter is as follows: the trajectory patterns, the CD and the CR algorithms are described in Section 5.1, the scenarios considered are defined in Section 5.2, and the results are presented in Section 5.3; the aircraft models used (based on BADA 3.6) are described in Appendix D.

5.1 Problem Formulation

In general, the TMA scenario is defined by a limited region of airspace where there are a set of aircraft whose nominal trajectories (the intended trajectories) are in conflict. One can consider two kinds of aircraft: *locked* and *unlocked* (Ref. [Vila 06]). The trajectories of the unlocked aircraft are free (these are the only trajectories the CR algorithm can modify), whereas the trajectories of the locked aircraft are fixed and conflict free among them. The resolution of the problem requires that the unlocked aircraft be conflict free with all aircraft (locked and unlocked). Let N_u be the number of unlocked aircraft and N_l the number of locked aircraft.

The resolution process is centralized, that is, there exists a *control station* that determines the resolution trajectories and all the aircraft exactly perform the resolution trajectories proposed by the control station (uncertainties are not considered). The process is also strategic, that is, the intended trajectories are known to the control station well in advance, to carry out the resolution process before the aircraft enter the TMA.

Next, the equations of motion, the trajectory patterns, the conflict detection and the conflict resolution algorithms are described.

5.1.1 Equations of Motion

Since no wind is considered in this application, Eqs. (3.1) and (3.4) reduce to:

$$
\begin{aligned}
m\frac{\mathrm{d}V}{\mathrm{d}t} &= T - D(V,h,L) - mg\sin\gamma \\
mV\cos\gamma\frac{\mathrm{d}\chi}{\mathrm{d}t} &= L\sin\mu \\
mV\frac{\mathrm{d}\gamma}{\mathrm{d}t} &= L\cos\mu - mg\cos\gamma \\
\frac{\mathrm{d}m}{\mathrm{d}t} &= -c(V,h)T \\
(R_E+h)\frac{\mathrm{d}\varphi}{\mathrm{d}t} &= V\cos\gamma\cos\chi \\
(R_E+h)\cos\varphi\frac{\mathrm{d}\lambda}{\mathrm{d}t} &= V\cos\gamma\sin\chi \\
\frac{\mathrm{d}h}{\mathrm{d}t} &= V\sin\gamma \\
\frac{\mathrm{d}r}{\mathrm{d}t} &= \frac{R_E}{R_E+h}V\cos\gamma
\end{aligned}
\tag{5.1}
$$

In these equations T, L and μ are the control variables.

Different aircraft models are considered in this application, namely, Boeing 737-400, Airbus 320-212 and CRJ 200. The aerodynamic and propulsive models of these aircraft are based on BADA 3.6. The models are described in detail in Appendix D.

5.1.2 Trajectory Patterns

To define the trajectory patterns the operator preferences are supposed known. Two types of trajectory patterns are considered:

- **Nominal trajectory patterns**, which model the aircraft intended trajectories.
- **Resolution trajectory patterns**, which model the aircraft resolution trajectories. These are modifications of the nominal trajectory patterns assigned to the aircraft, which must be physically executable. Either one or both of the vertical and lateral profiles can be modified. The modifications may change the parameters defining some flight segments, may eliminate some segments, and may also add new segments. The resolution trajectory patterns take into account changes of the nominal waypoints (vectoring) and changes of the aircraft speeds. Each aircraft can have a different resolution trajectory pattern assigned.

In this work conflict detection and resolution in converging traffic within a TMA is analyzed. Hence, we consider trajectory patterns that model the cruise and descent phases.

5.1.2.1 Nominal trajectory patterns

In principle, each aircraft can have a different nominal trajectory pattern assigned, although in this work all aircraft have the same one, as follows (note that one could choose a different flight intent):

- *Lateral profile*:
  - defined by waypoints,
  - turns at constant bank angle.
- *Vertical profile* (see Fig. 5.1):
  - constant Mach (M_c), constant altitude (h_c) cruise, until the cruise speed reduction (CSR) point (defined in Section 3.2),
  - horizontal deceleration at cruise altitude, with idle engine rating, until the Mach of descent (M_d) is reached, from the CSR point to the TOD point,
  - Mach/CAS descent (speeds M_d, CAS_d), with idle engine rating, until 10000 ft,
  - horizontal deceleration at 10000 ft, with idle engine rating, until 250 kt,
  - constant CAS descent (250 kt), with idle engine rating, until glide-path interception altitude h_{ILS},
  - horizontal deceleration at glide-path interception altitude, with idle engine rating, until the approach speed CAS_{AP} (lift devices for approach are deployed during this segment when CAS_{CR} is reached),
  - constant CAS (CAS_{AP}), constant altitude (h_{ILS}) segment of length 0.5 nmi (landing gear and lift devices for landing are deployed during this segment),
  - glide path segment at constant CAS (CAS_{AP}) and constant path angle ($\gamma = -3^{\mathrm{o}}$).

This vertical profile is quite similar to the flight profile used in the Experimental Flight Management System of the PHARE program (see Ref. [Gill 97]).

The aircraft can enter the TMA while flying any of the above segments above 10000 ft. The CSR point (and, as a consequence, the TOD point) is determined iteratively, as indicated in Appendix C.

5.1.2.2 Resolution trajectory patterns

The resolution trajectory patterns are now modifications of the nominal trajectory pattern both in the lateral and vertical profiles. The modification in the lateral profile is as follows: all the waypoints of the nominal trajectory pattern in the TMA, except the TMA entry point, the IAF and those after the IAF, may be changed, keeping fixed the total number of waypoints (it has been decided not to change the lateral profile after the IAF). The modification in the vertical profile consists in introducing speed changes, in cruise and in descent above 10000 ft (it has been decided not to change the speed profile below 10000 ft); moreover, it has been decided not to introduce altitude changes.

Thus, in general, besides the coordinates of the modifiable waypoints (longitude and latitude), the parameters of the nominal trajectory pattern that can be modified are the following speeds: cruise Mach, descent Mach and descent CAS; let M_c^*, M_d^*, CAS_d^* be the modified values.

Different patterns are considered depending on the flight phase (cruise, descent, ...) the aircraft is flying when it enters the TMA. These patterns are described next.

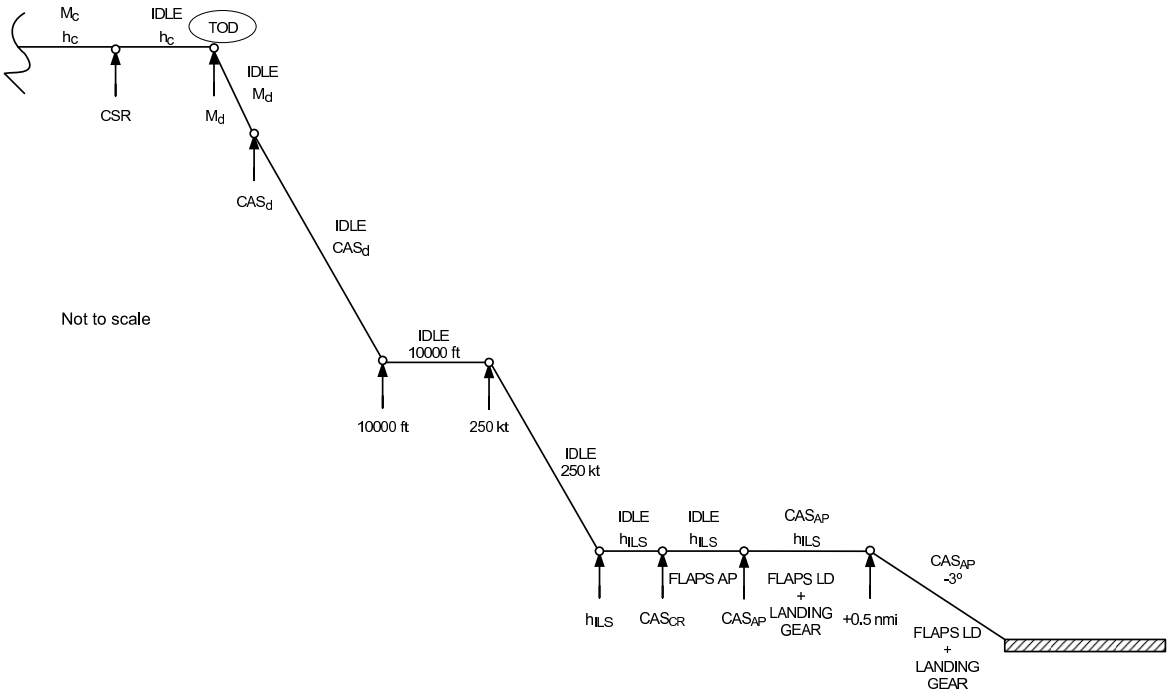

Figure 5.1: Sketch of the nominal trajectory pattern (flight intent).

Pattern A

The aircraft enters the TMA while cruising (before reaching the CSR point), see Fig. 5.2. The parameters free to be changed and define the resolution trajectory in this case are the speeds M_c, M_d, CAS_d and the coordinates of the modifiable waypoints λ_i, φ_i. The change in cruise speed requires a new flight segment: horizontal acceleration/deceleration at cruise altitude, from the nominal to the modified cruise Mach (M_c^*), with maximum cruise/idle engine rating. To define the resolution trajectory the new CSR point must be calculated (by iteration), say CSR*, which in general is different from the CSR point of the nominal trajectory. The horizontal distance between the TMA entry point and the IAF can be larger or smaller than the one corresponding to the nominal trajectory, that is, the nominal route can be lengthened or shortened.

The changes in the speed profile parameters are subject to the following constraints:

a) They must be changed within some limits. We consider changes within $\pm 10\%$ of the nominal values:

$$\begin{aligned} |M_c^* - M_c| &\leq 0.1 M_c \\ |M_d^* - M_d| &\leq 0.1 M_d \\ |CAS_d^* - CAS_d| &\leq 0.1 CAS_d \end{aligned} \tag{5.2}$$

b) The descent Mach is always smaller than or equal to the cruise Mach:

$$M_d^* \leq M_c^* \tag{5.3}$$

c) The descent CAS is always larger than or equal to 250 kt:

$$CAS_d^* \geq 250 \text{ kt} \tag{5.4}$$

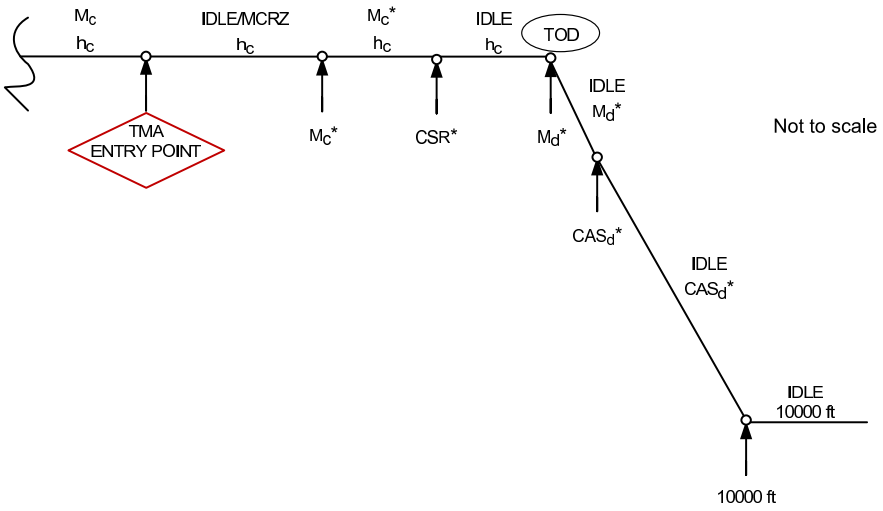

Figure 5.2: Resolution trajectory pattern A.

d) The descent Mach and CAS must be such that the transition altitude (h_{TR}) is smaller than or equal to the cruise altitude and larger than or equal to 10000 ft:

$$10000 \text{ ft} \leq h_{TR}(M_d^*, CAS_d^*) \leq h_c \tag{5.5}$$

The changes in the waypoints coordinates are subject to the constraint that they must be inside boxes centered on the nominal waypoints, that is,

$$\begin{aligned} |\lambda_i - \lambda_i^0| &\leq 0.3 \text{ deg} \\ |\varphi_i - \varphi_i^0| &\leq 0.3 \text{ deg} \end{aligned} \tag{5.6}$$

This constraint enforces that the resolution trajectory does not deviate too much from the preferred trajectory.

Pattern B

The aircraft enters the TMA flying the last cruise deceleration segment, between the CSR and the TOD points, see Fig. 5.3. The parameters free to be changed in this case are the descent speeds M_d, CAS_d and the coordinates of the modifiable waypoints λ_i, φ_i. The cruise deceleration segment now ends when the new descent Mach (M_d^*) is reached. After the deceleration, a new flight segment is added: cruise altitude and constant Mach (M_d^*), ending at the new TOD point, say TOD*, which must be determined iteratively.

The changes in the speed profile parameters are subject to the following constraints:

a) They must be changed within ±10% of the nominal values:

$$\begin{aligned} |M_d^* - M_d| &\leq 0.1 M_d \\ |CAS_d^* - CAS_d| &\leq 0.1 CAS_d \end{aligned} \tag{5.7}$$

b) The descent Mach is always smaller than or equal to the Mach at the TMA entry point (M_{TMA}):

$$M_d^* \leq M_{TMA} \tag{5.8}$$

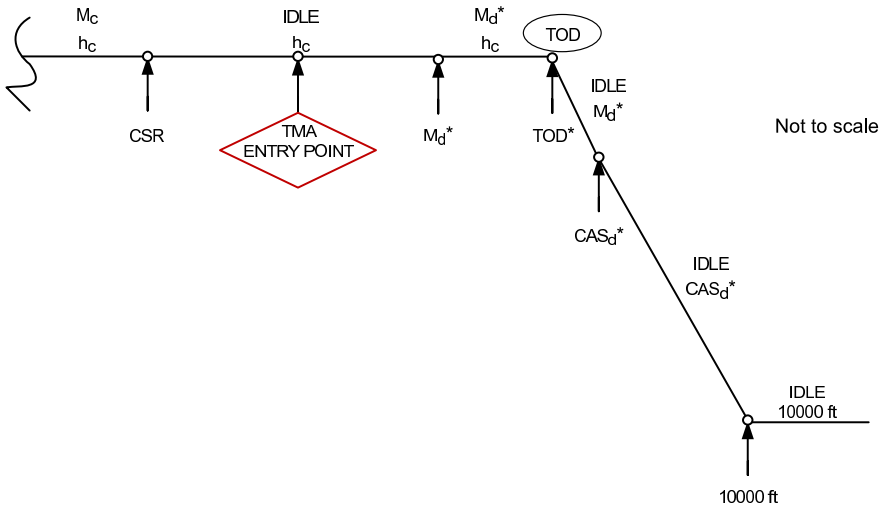

Figure 5.3: Resolution trajectory pattern B.

c) The descent CAS is always larger than or equal to 250 kt, as given by Eq. (5.4).

d) The descent Mach and CAS must be such that the transition altitude (h_{TR}) is smaller than or equal to the cruise altitude and larger than or equal to 10000 ft, as given by Eq. (5.5).

As in pattern A, the changes in waypoints coordinates must be inside boxes centered on the nominal waypoints; the constraints are given by Eq. (5.6).

Pattern C

The aircraft enters the TMA flying the constant-Mach descent segment, see Fig. 5.4. In this case, the parameters free to be changed and define the resolution trajectory are the CAS descent speed CAS_d and the coordinates of the modifiable waypoints λ_i, φ_i. The constant-Mach descent segment is flown with the nominal Mach (M_d), ending now when the new descent CAS (CAS_d^*) is reached. After the deceleration at 10000 ft, a new segment is added: constant CAS (250 kt) at 10000 ft, ending at a metering fix (MF*) that must be determined iteratively.

The changes in the speed profile parameters are subject to the following constraints:

a) They must be changed within ±10% of the nominal values:

$$|CAS_d^* - CAS_d| \leq 0.1 CAS_d \tag{5.9}$$

b) The descent CAS is larger than or equal to 250 kt, as given by Eq. (5.4).

c) The descent Mach and CAS must be such that the transition altitude (h_{TR}) is smaller than or equal to the altitude of the TMA entry point (h_{TMA}) and larger than or equal to 10000 ft:

$$10000 \text{ ft} \leq h_{TR}(M_d, CAS_d^*) \leq h_{TMA} \tag{5.10}$$

Again, the changes in waypoints coordinates must be inside boxes centered on the nominal waypoints; the constraints are given by Eq. (5.6).

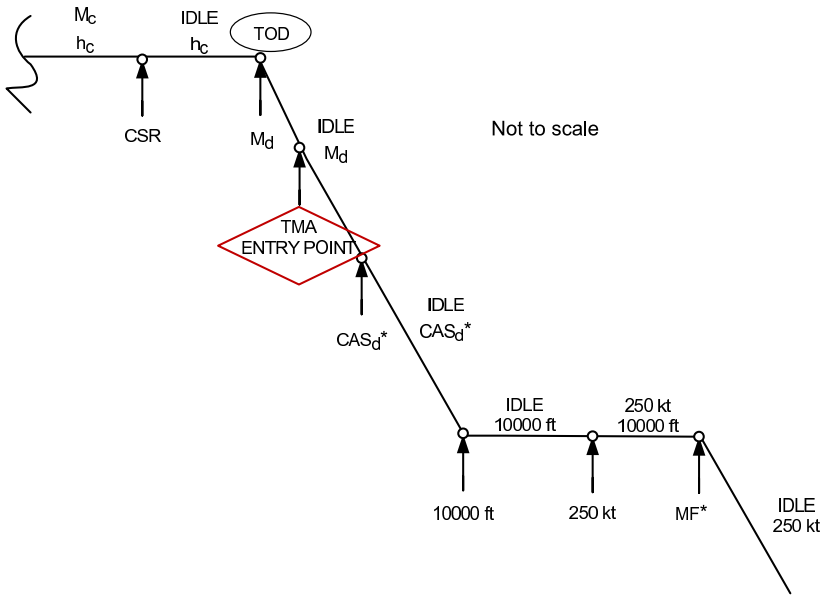

Figure 5.4: Resolution trajectory pattern C.

Pattern D

The aircraft enters the TMA flying the constant-CAS descent segment, see Fig. 5.5. Now, the parameters free to be changed and define the resolution trajectory are just the coordinates of the modifiable waypoints λ_i, φ_i. The constant-CAS descent segment is flown with the nominal CAS (CAS_d). After the deceleration at 10000 ft, a new segment is added: constant CAS (250 kt) at 10000 ft, ending at a metering fix (MF*) that must be determined iteratively.

The changes in the coordinates of the modifiable waypoints are subject to the constraint that, as in previous cases, they must be inside boxes centered on the nominal waypoints, that is, as given by Eq. (5.6).

5.1.3 Conflict Detection

The conflict detection (CD) algorithm evaluates the separation between any pair of aircraft during their flights, by comparing the separation between them with the separation minima applicable. In this work distance separation is considered, hence the CD algorithm measures distance between pairs of aircraft.

The input to the algorithm is the state vector of all aircraft, $\mathbf{y}_i(t)$, $i = 1, ..., N_u + N_l$, and the output are the horizontal and vertical distances between all pairs of aircraft, except the pairs of locked aircraft, $d_{ij}(t_k)$ and $h_{ij}(t_k)$, $i = 1, ..., N_u$, $j = 1, ..., N_u + N_l$, $i \neq j$, respectively. The distances are measured at discrete times $t_k = t_0 + k\Delta t$, $k = 1, 2, 3, ...$, during the time they both are in the TMA (when the state variables are not known at time t_k, linear interpolation is used). The horizontal and vertical distances are computed at every discrete time and compared with the separation minima, d_s and h_s, that correspond to each pair of aircraft; a conflict between aircraft i and j is detected if exists a time t_k at which both distances are

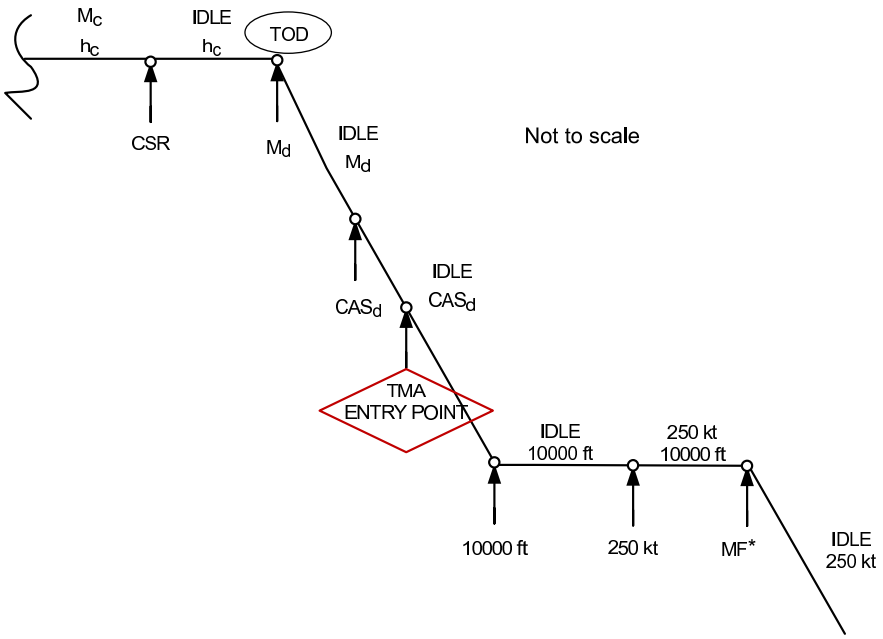

Figure 5.5: Resolution trajectory pattern D.

smaller than the separation minima

$$\min_{t_k}\left(\max\left(\frac{d_{ij}(t_k)}{d_s},\frac{h_{ij}(t_k)}{h_s}\right)\right)<1 \tag{5.11}$$

(this definition of conflict is an extension of that given in Ref. [Dowe 07]).

This way of detecting the conflicts allows one to consider altogether all the violations of the separation minima that can occur between two aircraft trajectories along the whole flight, so that in case that a proposed trajectory modification solves one loss of separation but leads to new losses, the aircraft trajectory will be still in conflict and the proposed modification will not be accepted.

The horizontal distance between two aircraft is measured along a great circle (minimum distance) on the Earth surface, which is given by

$$d_{ij}=R_E\cos^{-1}\left[\sin\varphi_i\sin\varphi_j+\cos\varphi_i\cos\varphi_j\cos(\lambda_j-\lambda_i)\right] \tag{5.12}$$

where (λ_i,φ_i) and (λ_j,φ_j) are the geodetic coordinates of the aircraft horizontal positions and R_E is the Earth radius. The vertical distance is just

$$h_{ij}=|h_i-h_j| \tag{5.13}$$

Other CD algorithms with more complex logics can be found in Refs. [Isaa 97] and [Krem 99], developed for CTAS and PHARE, respectively.

5.1.4 Conflict Resolution

The conflict resolution (CR) algorithm generates a set of trajectories that resolves the potential conflicts detected by the CD algorithm (i.e. a set of trajectories that meet the separation criteria), while optimizing a given performance index.

In general, each unlocked aircraft i has assigned a resolution trajectory pattern. The corresponding resolution trajectory is then described in terms of a set of free parameters $\mathbf{x}_i$ (waypoints coordinates and speeds in our case). The set of trajectories corresponding to the N_u unlocked aircraft is collected in a vector of free parameters $\mathbf{x}$:

$$\mathbf{x} = \left[\begin{array}{ccccc} \mathbf{x}_1^T & \dots & \mathbf{x}_i^T & \dots & \mathbf{x}_{N_u}^T \end{array} \right]^T \tag{5.14}$$

so that the CR problem is formulated as a constrained parametric optimization problem, including equality and inequality constraints, as the optimization problem given by Eqs. (3.5), described in Section 3.3.

Next, the free parameters, the cost function and the constraints of the optimization problem are described. Afterwards, a resolution strategy to solve the optimization problem is proposed.

5.1.4.1 Free parameters

The free parameters considered in the resolution process depend on the resolution trajectory pattern under consideration (namely, A, B, C or D), as described above in Section 5.1.2.2.

5.1.4.2 Cost function

In principle, the optimality criterium defining the cost function can be the minimization (or maximization) of any property or combination of properties that can be derived from the resolution trajectories. In this work the optimality criterium is to minimize the deviation from the nominal trajectories in the lateral profile. The objective function selected is:

$$J(\mathbf{x}) = \sqrt{\sum_{i=1}^{q} \left[(\lambda_i - \lambda_i^0)^2 + (\varphi_i - \varphi_i^0)^2 \right]} \tag{5.15}$$

where $(\lambda_i^0, \varphi_i^0)$ are the nominal location of the waypoints and q is the total number of waypoints that can be changed.

5.1.4.3 Constraints

The constraints considered in this work can be classified as follows:

- traffic constraints: 1) the resolution trajectories have to be conflict free ($(d_{ij})_{min} \geq d_s$ or $(h_{ij})_{min} \geq h_s$), among themselves and with the fixed trajectories of the locked aircraft; 2) all the waypoints must be inside the TMA; and 3) the resolution trajectories have to end in the runway threshold;
- method constraints: constraints defined by the trajectory patterns (see Section 5.1.2.2), which depend on the resolution trajectory pattern under consideration (namely, A, B, C or D);
- aircraft constraints: all the speeds have to be inside the operational envelopes.

These constraints can be also classified as *individual* constraints and *dual* constraints. Individual constraints affect only one trajectory $\mathbf{x}_i$ (e.g., aircraft constraints). Dual constraints link pairs of trajectories $\mathbf{x}_i$ and $\mathbf{x}_j$ (e.g., loss of separation between unlocked aircraft). As it is shown below, this classification is important in the resolution strategy.

5.1.4.4 Resolution strategy

The resolution process is divided into two phases:

(i) Random search of a first valid solution. The objective is to find a set of resolution trajectories that solve the conflicts, although the trajectories found may not be too efficient (that is, to find a set of free parameters $\mathbf{x}$ that satisfy the constraints). This phase is carried out following the iterative procedure described next.

First, a resolution trajectory is randomly generated for each unlocked aircraft, that is, for each unlocked aircraft a vector $\mathbf{x}_i$ that meets the individual constraints is randomly generated (in the random search, a uniform distribution is used). Thus, at iteration p, p randomly generated resolution trajectories and 1 nominal trajectory are available for each aircraft, that is, $p+1$ trajectories that meet the individual constraints. This means that, for the N_u aircraft, one has $(p+1)^{N_u}$ possible combinations of trajectories, formed by choosing one trajectory from the $p+1$ that correspond to each aircraft, so that each combination is a candidate solution of the conflict resolution process.

Next, for each of the $(p+1)^{N_u}$ trajectory combinations, the dual constraints are checked. In fact, because at iteration $p-1$ many of these combinations were checked, only those combinations that have at least one of the new resolution trajectories generated at this iteration are checked (in total, $(p+1)^{N_u} - p^{N_u}$ combinations).

If one or more combinations meet all the constraints, then the lowest-cost combination is chosen as first valid solution. If, on the other hand, no combination meets the constraints, then a new iteration is performed.

The objective of this combinatorial approach is to reduce the number of trajectory computations, which is the most time-consuming step in the whole resolution process.

Note that, in this first phase, in the process of finding a feasible initial point, one could have also considered other more advanced algorithms such as penalty methods (see Ref. [Rao 96]). In our approach, we have combined the simple random algorithm with the combinatorial approach just described in order to make the overall method efficient and suitable to our problem, in the sense of performing a small number of trajectory computations. Indeed, it is shown below that, with the computation of only 9 trajectories for each aircraft, a total of 10000 combinations of trajectories are analyzed in Scenario 1 (Section 5.3.1.2), and with the computation of 16 trajectories for each aircraft, a total of 83521 combinations are analyzed in Scenario 2 (Section 5.3.2.2).

(ii) Improvement of the first valid solution. The objective now is to improve the first valid solution found in the first phase, that is, to find another valid solution with smaller cost. This second phase is carried out by solving the parametric optimization problem (3.5), using that first valid solution as the starting point. Note that the landing sequence of the first valid solution is not imposed as a constraint, so that it can change during the optimization process.

5.2 Scenarios

In this work two scenarios are analyzed, one without locked aircraft and another with locked aircraft. In both cases the same TMA is considered: MADRID-BARAJAS airport (LEMD), RWY 18R, two TMA entry points (BARAHONA and TERSA) and one IAF (TAGOM).

In Scenario 1 the following traffic is considered:

- Boeing 737-400, with TERSA as TMA entry point (labeled as A1 in the figures of Section 5.3). The aircraft enters the scenario at $t = 0\,\text{s}$, in cruise flight, at altitude h_c =30000 ft, and with initial mass m_i =50631 kg.
- Airbus 320, with TERSA as TMA entry point (labeled as A2 in the figures of Section 5.3). The aircraft enters the scenario at $t = 60\,\text{s}$, in cruise flight, at altitude h_c =33000 ft, and with initial mass m_i =59163 kg.
- Airbus 320, with BARAHONA as TMA entry point (labeled as A3 in the figures of Section 5.3). The aircraft enters the scenario at $t = 300\,\text{s}$, in descent flight, flying the constant CAS segment, at an altitude h_{TMA} =25822 ft, and with initial mass m_i =59896 kg.
- CRJ 200, with BARAHONA as TMA entry point (labeled as A4 in the figures of Section 5.3). The aircraft enters the scenario at $t = 360\,\text{s}$, in descent flight, flying the constant Mach segment, at an altitude h_{TMA} =28985 ft, and with initial mass m_i =19944 kg.

In Scenario 2 the traffic considered has the same four unlocked aircraft of Scenario 1 plus the two following locked aircraft:

- Boeing 737-400, with TERSA as TMA entry point (labeled as AL1 in the figures of Section 5.3). The aircraft enters the scenario at $t = -60\,\text{s}$, in cruise flight, at altitude h_c =30000 ft, and with initial mass m_i =50631 kg.
- Airbus 320, with BARAHONA as TMA entry point (labeled as AL2 in the figures of Section 5.3). The aircraft enters the scenario at $t = 120\,\text{s}$, in descent flight, flying the constant CAS segment, at an altitude h_{TMA} =25822 ft, and with initial mass m_i =59896 kg.

The presence of the locked aircraft makes this second scenario more demanding than Scenario 1 (although the parameters are the same, the number of constraints is larger). Hence, a higher cost of the resolution process is expected.

In these scenarios the same separation minima are considered for all pairs of aircraft, namely, $d_s = 3$ nmi and $h_s = 1000$ ft, and the conflict detection time step is $\Delta t = 0.1$ s. All turns are performed with bank angle $\mu_A = 25$ deg. The operational speeds are taken from BADA 3.6.

5.3 Results

Results are presented first for Scenario 1 (without locked aircraft) and then for Scenario 2 (with locked aircraft). In the following graphs, runways are represented by thick lines, VORs are circles, fix points are triangles, nominal waypoints are pentagrams, and aircraft are stars. Each aircraft is bounded by a cylinder of radius $d_s/2$ and height h_s; hence, when two cylinders intersect the distance between the aircraft is less than the separation minima (d_s and h_s) and a conflict exists.

In the results presented below, two types of conflict arise: *merging* and *catching up* (other types of conflicts are defined in Ref. [Isaa 01]).

5.3.1 Scenario 1

5.3.1.1 Nominal trajectories

The nominal trajectories are depicted at different times in Fig. 5.6. In Fig. 5.6a (at 480 s) all aircraft have entered the TMA and there is a catching-up conflict between aircraft A1 and A2; in Fig. 5.6b (at 650 s) a merging conflict between A1 and A3 arises; in Fig. 5.6c (at 700 s) one has multiple mergings; and in Fig. 5.6d (at 1100 s) one has multiple catching ups. Even though the aircraft are in conflict during the final approach, the landing sequence for these nominal trajectories is A1-A3-A2-A4. Note that all those conflicts do exist, even though in Fig. 5.6 we only see the horizontal loss of separation (this same comment applies below, except in one case, stated explicitly, in which there is a horizontal loss of separation but there is not a conflict).

For aircraft A1 and A2 there are 3 waypoints that can be changed to resolve the conflicts, and for aircraft A3 and A4 there is only one. For A1 and A2, M_c, M_d and CAS_d can be changed (since they enter the TMA in cruise flight); for A3 no speed can be changed (since it enters the TMA flying the constant CAS segment); and for A4 only CAS_d can be modified (since it enters the TMA flying the constant Mach segment).

The vertical profiles during the final approach (at 1100 s) are depicted in Fig. 5.7a, in which the multiple conflicts are clearly seen (for comparison, the vertical profiles for the resolution, conflict-free trajectories are also shown; they are analyzed below).

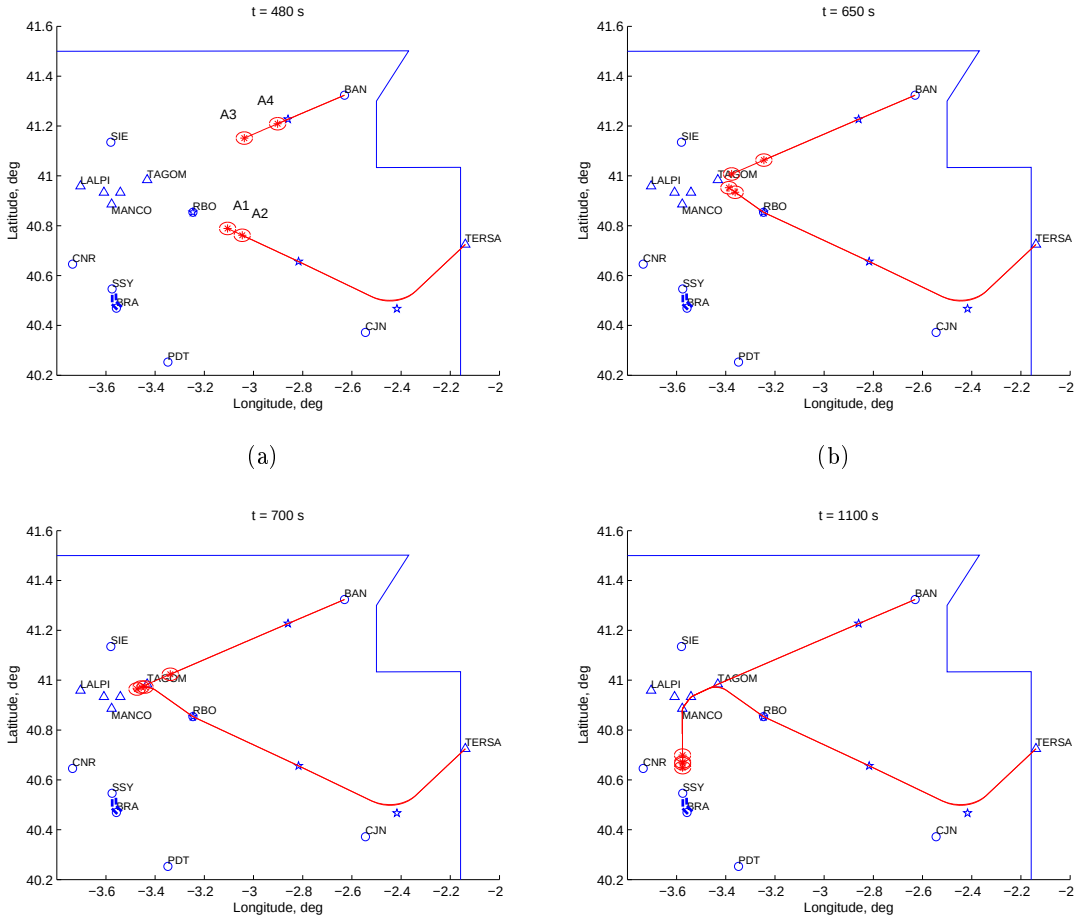

Figure 5.6: Scenario 1: nominal trajectories without locked aircraft, at different times: (a) 480 s, (b) 650 s, (c) 700 s, (d) 1100 s.

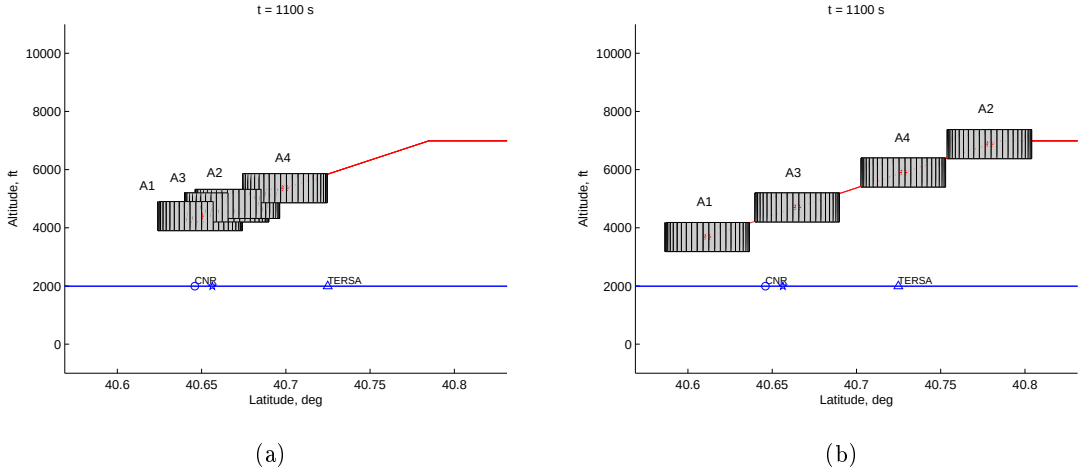

Figure 5.7: Scenario 1: vertical profiles during the final approach. (a) Nominal trajectories, (b) resolution trajectories after phase 2.

5.3.1.2 Resolution trajectories

In the execution of the first phase of the resolution strategy, 9 iterations were performed, hence 9 trajectories were randomly generated for each aircraft. These trajectories and the nominal ones are shown in Fig. 5.8. In the last iteration of this first phase, 34 combinations of trajectories (out of a total of 10000) met all the constraints. The lowest-cost combination, depicted in Fig. 5.9 at different times, was chosen as first valid solution; the cost of this solution is J=0.625 deg. The landing sequence in this solution is A1-A3-A4-A2.

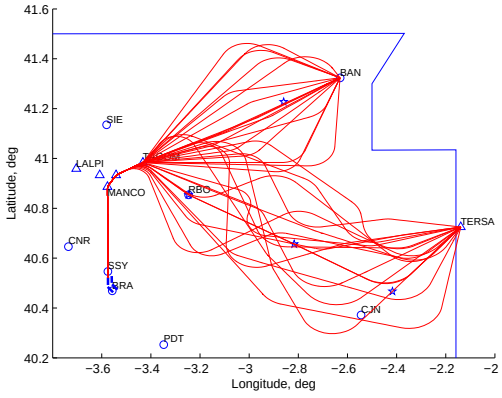

Figure 5.8: Scenario 1: proposed trajectories in phase 1.

The resolution trajectories obtained after the second phase of the resolution strategy are depicted at different times in Fig. 5.10. In Fig. 5.10a (at 480 s) A2 and A4 are deviated; in Fig. 5.10b (at 650 s) A1 has crossed the IAF (TAGOM); in Fig. 5.10c (at 850 s) A3 and A4 have crossed the IAF and the landing sequence can be seen; and in Fig. 5.10d (at 1100 s) all aircraft are in the final approach conflict free. The landing sequence obtained in the resolution process is A1-A3-A4-A2 (the same as in the first phase). Note that A3 has followed very closely its nominal trajectory. The cost of this solution is J=0.223 deg. The vertical profiles during the final approach of these conflict-free resolution trajectories (at 1100 s) were depicted above in Fig. 5.7b.

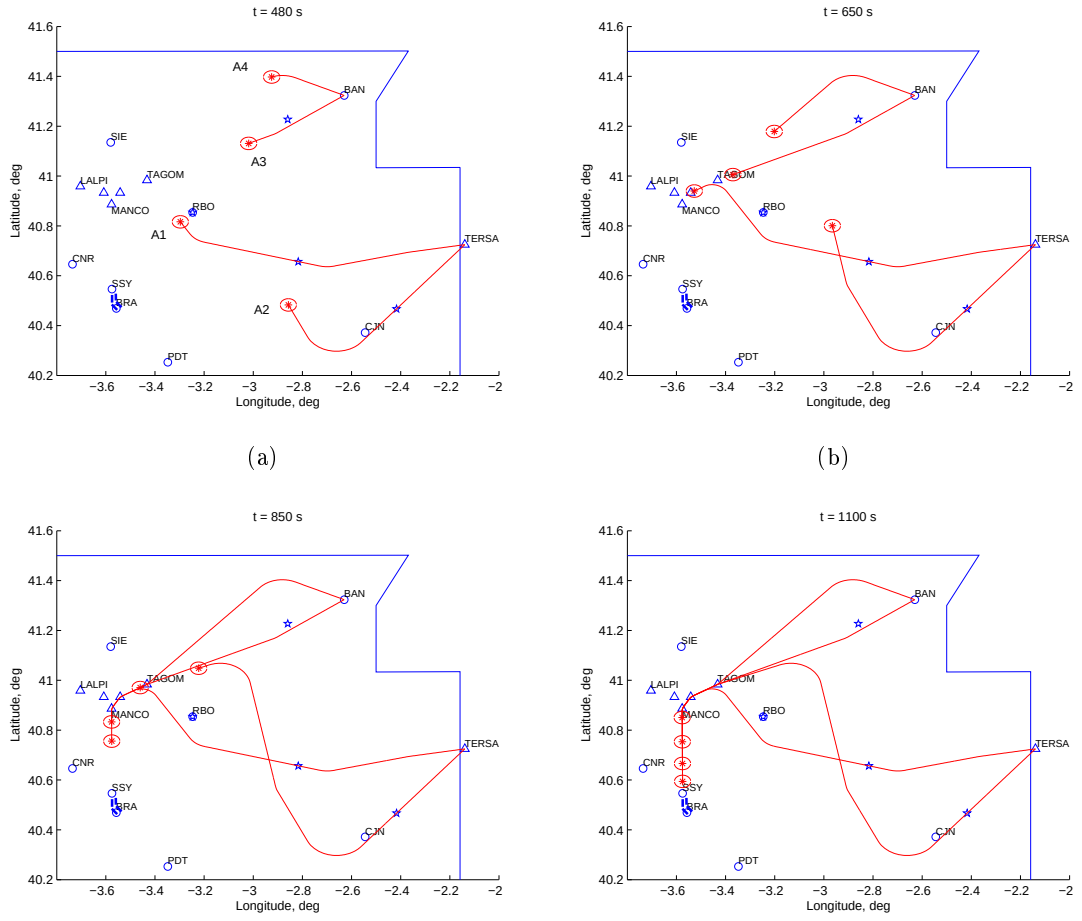

Figure 5.9: Scenario 1: resolution trajectories after phase 1 without locked aircraft, at different times: (a) 480 s, (b) 650 s, (c) 850 s, (d) 1100 s.

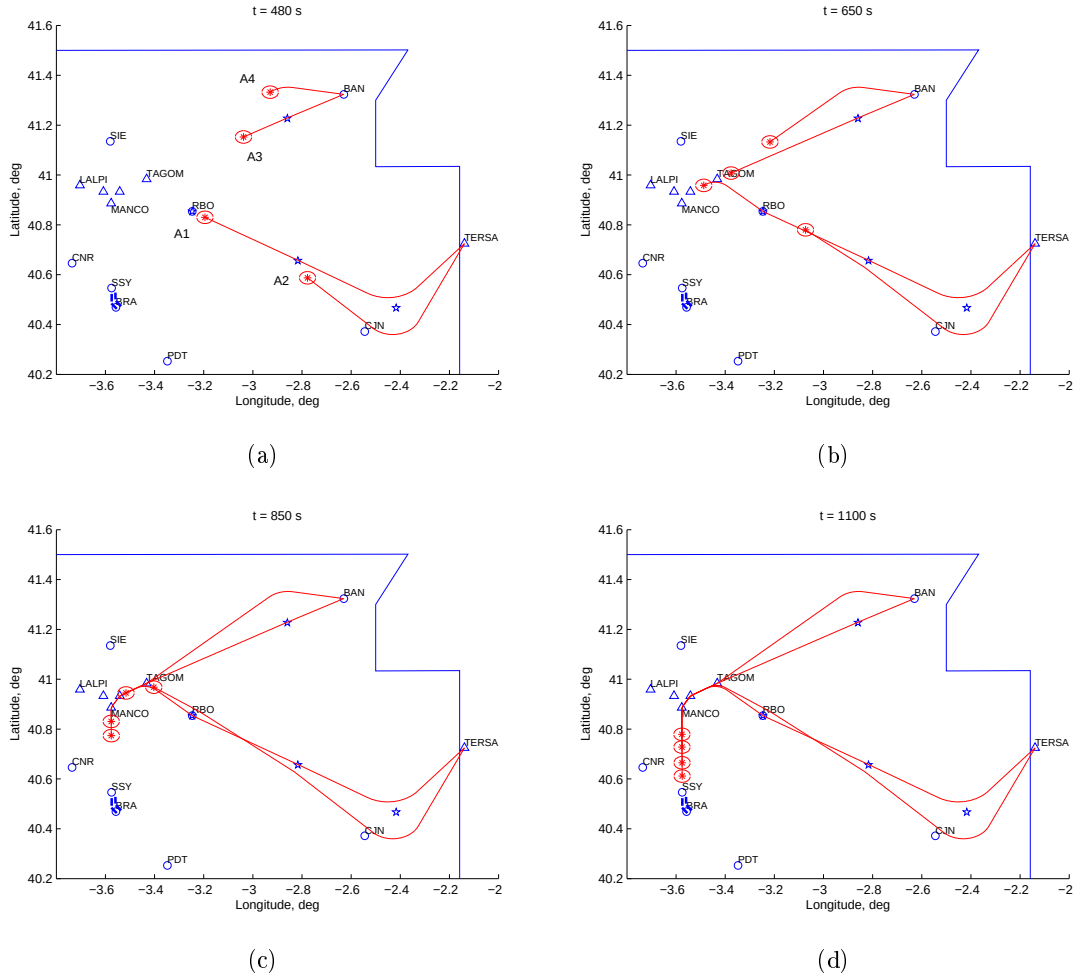

Figure 5.10: Scenario 1: resolution trajectories after phase 2 without locked aircraft, at different times: (a) 480 s, (b) 650 s, (c) 850 s, (d) 1100 s.

With respect to the resolution strategy, the cost reduction (from 0.625 deg obtained in the first phase to 0.223 deg) indicates the improvement obtained with the second phase.

The speed variations corresponding to these resolution trajectories are presented in Table 5.1 (along with the nominal values). A1 (that arrives in first place) has increased its speeds, whereas A2 and A4 have decreased theirs (in order to arrive later). Note that some speed changes have been the maximum 10% (recall that the cost function selected does not penalize speed variations).

Some global properties of the resolution trajectories are also presented in Table 5.1, namely, the increments in distance travelled (Δr), flight time (Δt_f) and fuel consumption (Δm_F), between resolution and nominal trajectories. These increments are almost nil for A3, since it has followed its nominal trajectory. A1 has shortened its route slightly, decreasing the flight time, whereas A2 and A4 have lengthened theirs, increasing the flight time; Δr and Δt_f vary according to the landing sequence.

The total increase in fuel consumption is about 54 kg, which is a measure of the cost of the resolution process. Another performance indicator is the final value of the objective function, namely, f=0.223 deg.

Aircraft	M_c [-]	ΔM_c [-]	M_d [-]	ΔM_d [-]	CAS_d kt	ΔCAS_d kt	Δr [m]	Δt_f [s]	Δm_F [kg]
A1	0.740	0.074	0.740	0.024	280.0	28.0	-1230	-59.0	27.3
A2	0.780	-0.078	0.780	-0.078	310.0	-31.0	23038	172.4	20.0
A3	-	-	-	-	310.0	-	3	0.0	0.0
A4	-	-	0.740	-	290.0	-4.1	5936	42.1	6.8

Table 5.1: Scenario 1: properties of the resolution trajectories.

5.3.2 Scenario 2

5.3.2.1 Nominal trajectories

The nominal trajectories in this second scenario are depicted at different times in Fig. 5.11. The trajectories of the two locked aircraft are such that there are no conflicts between them, but there exists a catching up between AL1 and A1 (see Fig. 5.11d). The landing sequence for these nominal trajectories is AL2-AL1-A1-A3-A2-A4.

As in Scenario 1, for aircraft A1 and A2 there are 3 waypoints that can be changed to resolve the conflicts, and for aircraft A3 and A4 there is only one. For A1 and A2, M_c, M_d and CAS_d can be changed; for A3 no speed can be changed; and for A4 only CAS_d can be modified.

The vertical profiles during the final approach (at 1100 s) are depicted in Fig. 5.12a, in which the multiple conflicts among unlocked aircraft, as well as the catching up between A1 and AL1, are seen (for comparison, the vertical profiles for the resolution trajectories, which are analyzed below, are also shown; all the aircraft are there free of conflicts).

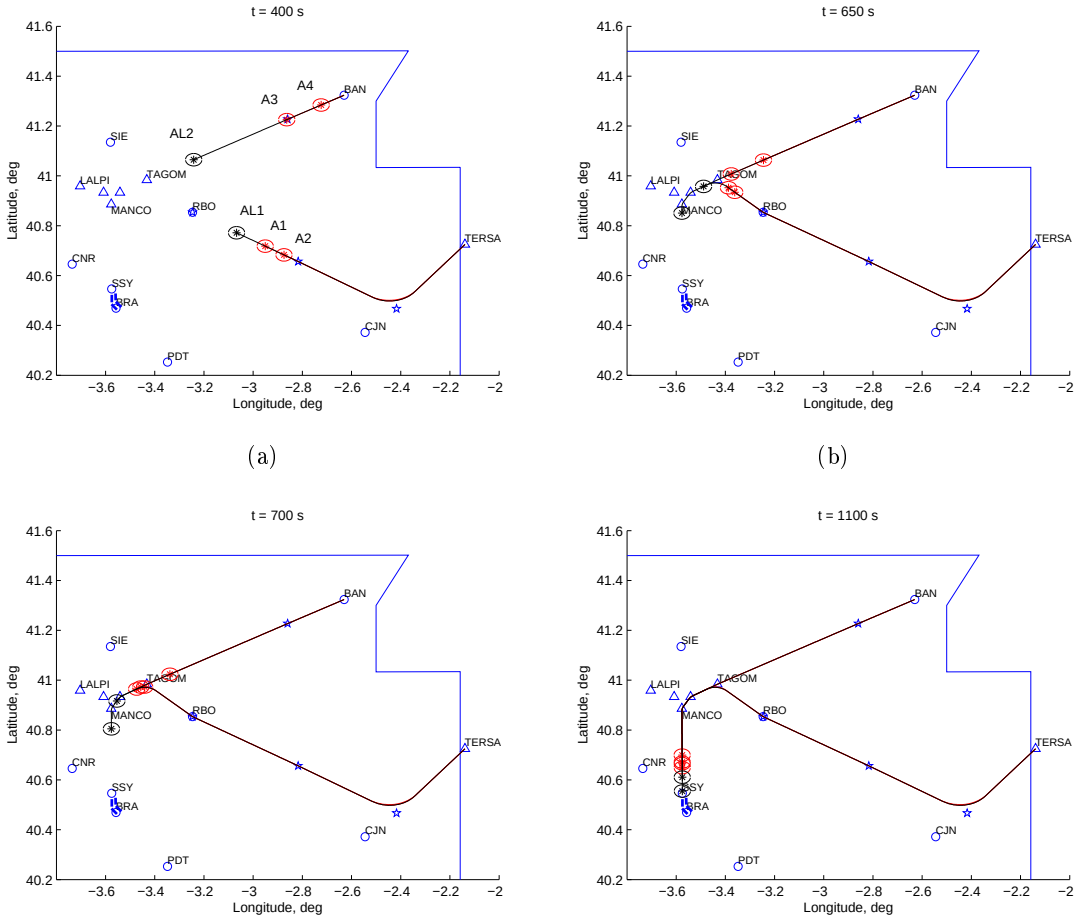

Figure 5.11: Scenario 2: nominal trajectories with locked aircraft, at different times: (a) 400 s, (b) 650 s, (c) 700 s, (d) 1100 s.

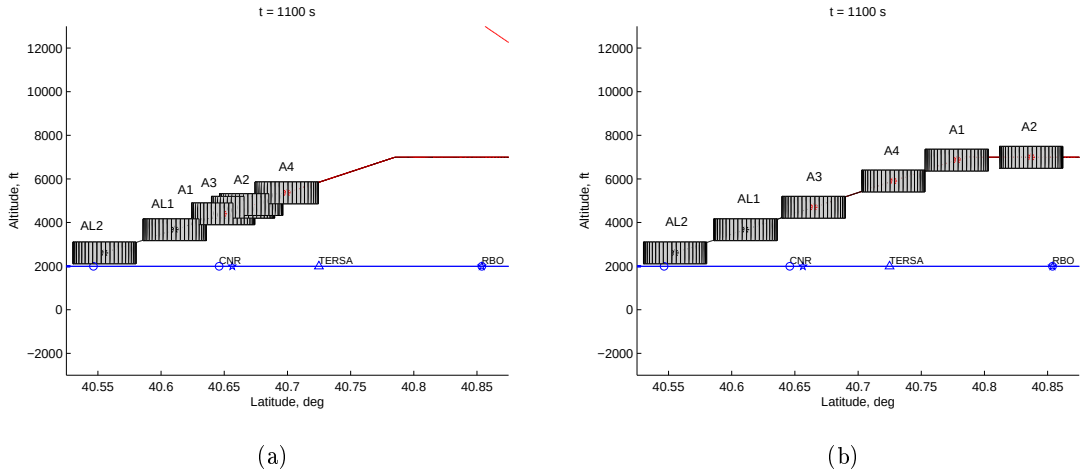

Figure 5.12: Scenario 2: vertical profiles during the final approach. (a) Nominal trajectories, (b) resolution trajectories after phase 2.

5.3.2.2 Resolution trajectories

In the execution of the first phase in this second scenario 16 iterations were performed, hence 16 trajectories were randomly generated for each aircraft. Because of the higher exigency of this scenario, more iterations are performed than in Scenario 1. In the last iteration of this first phase, 17 combinations of trajectories (out of a total of 83521) met all the constraints. The generated trajectories and the nominal ones are shown in Fig. 5.13; since the changes in the waypoints coordinates are constrained to be enclosed inside given boxes, the proposed trajectories are contained in a sort of bands around the nominal trajectories, which can be seen in the figure. The lowest-cost combination, depicted in Fig. 5.14 at different times, was chosen as first valid solution. The cost of this solution is J=0.675 deg. The landing sequence in this solution is AL2-AL1-A3-A4-A1-A2.

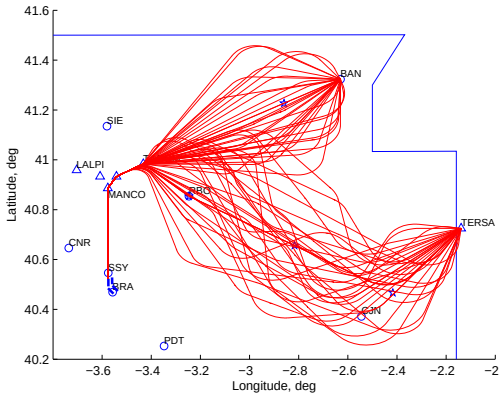

Figure 5.13: Scenario 2: proposed trajectories in phase 1.

In Fig. 5.15 we represent the resolution trajectories after phase 1 at 270 s. In this figure we can see a case in which the horizontal separation minimum is violated (the horizontal distance between A1 and A2 is smaller than d_s), but the vertical separation minimum is not (the vertical separation distance is larger than h_s), so that there is not a conflict.

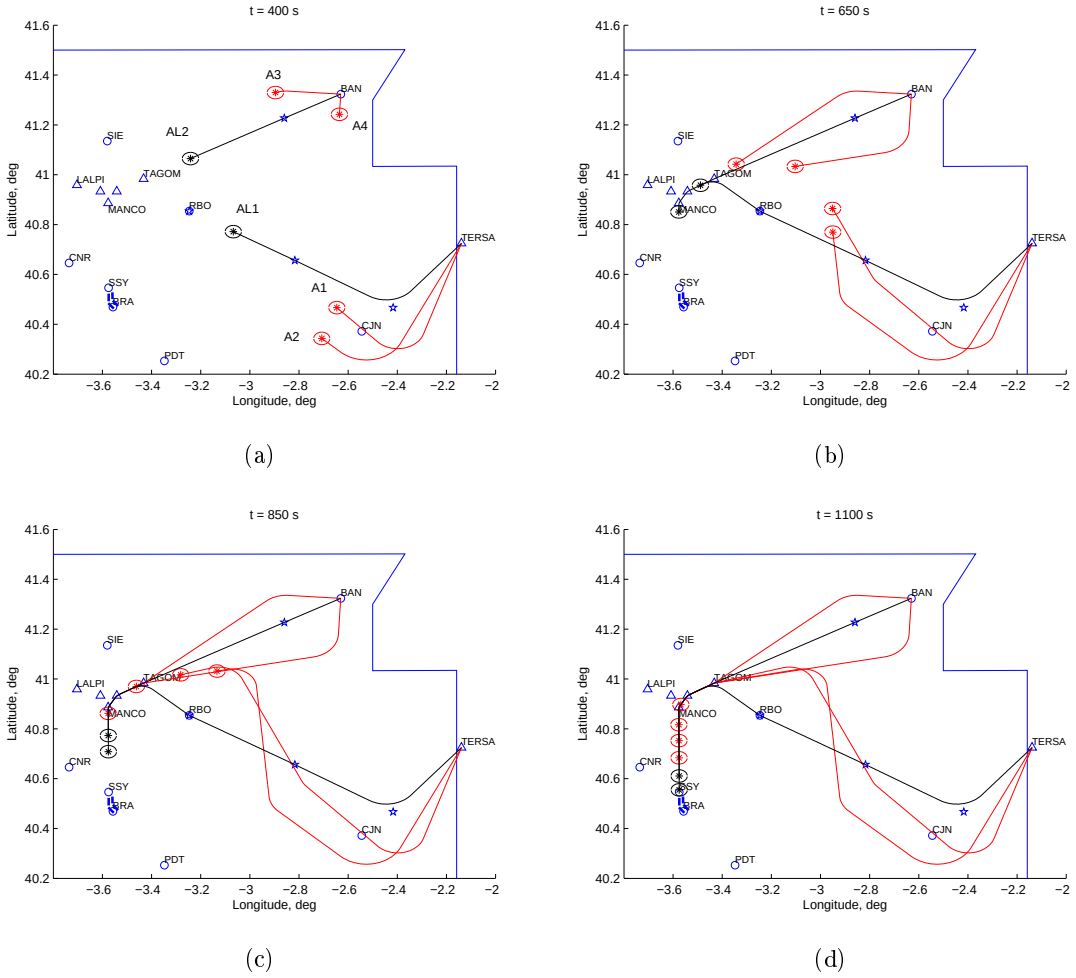

Figure 5.14: Scenario 2: resolution trajectories after phase 1 with locked aircraft, at different times: (a) 400 s, (b) 650 s, (c) 850 s, (d) 1100 s.

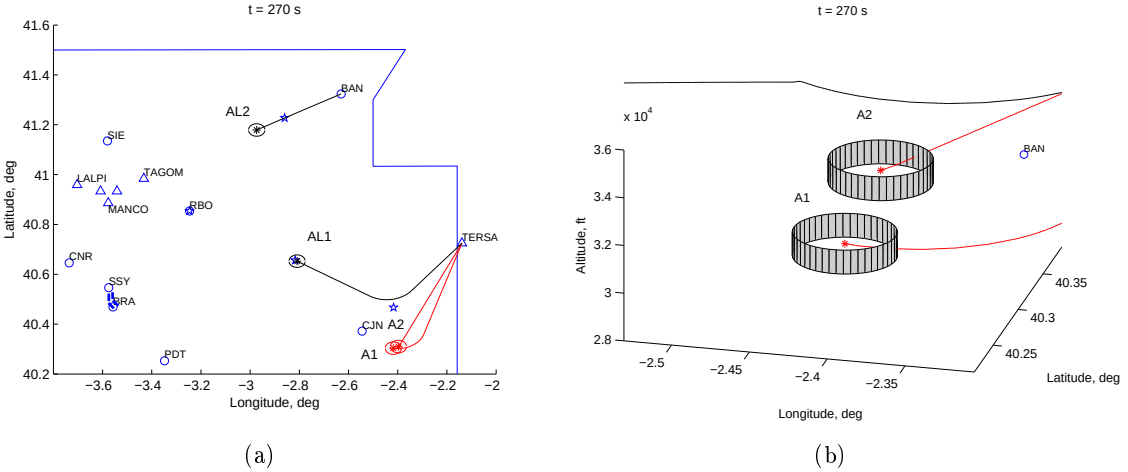

Figure 5.15: Scenario 2: resolution trajectories after phase 1 with locked aircraft, at 270 s: (a) horizontal profile, (b) 3-dimensional view.

The resolution trajectories obtained after the second phase are depicted at different times in Fig. 5.16. In Fig. 5.16a (at 400 s) A1, A2 and A4 are deviated; in Fig. 5.16b (at 650 s) A3 is reaching the IAF; in Fig. 5.16c (at 850 s) A4 has crossed the IAF; and in Fig. 5.16d (at 1100 s) all aircraft are in the final approach conflict free. Note that A3 has followed very closely its nominal trajectory. The landing sequence obtained in the resolution process is AL2-AL1-A3-A4-A1-A2 (the same as in the first phase). In this scenario the landing sequence of the unlocked aircraft is different from the sequence in Scenario 1. The cost of this solution is J=0.365 deg. The vertical profiles during the final approach of these conflict-free resolution trajectories (at 1100 s) were depicted in Fig. 5.12b.

Again, the cost reduction (from 0.675 deg to 0.365 deg) indicates the improvement obtained with the second phase of the resolution strategy.

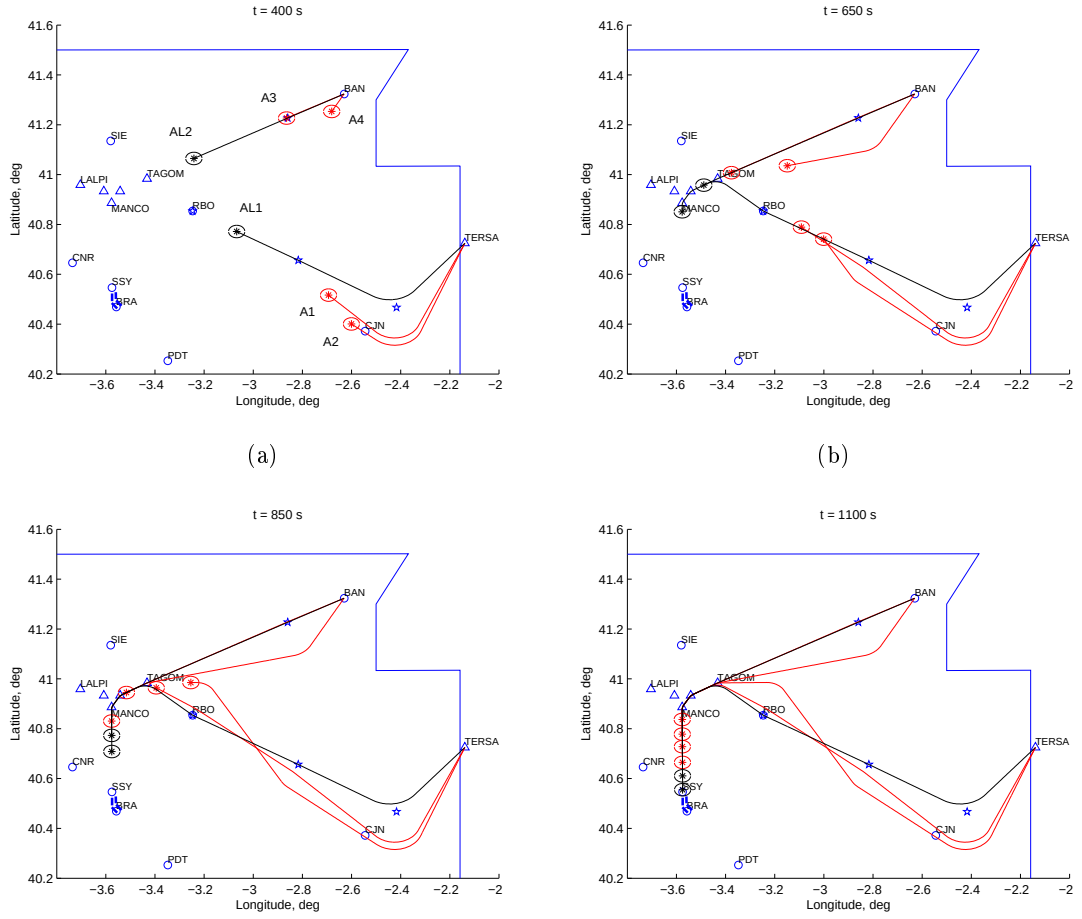

Figure 5.16: Scenario 2: resolution trajectories after phase 2 with locked aircraft, at different times: (a) 400 s, (b) 650 s, (c) 850 s, (d) 1100 s.

The speed variations and the global properties corresponding to these resolution trajectories are presented in Table 5.2. Except for ΔCAS_d for A4, all speed changes have been maximum (10%), and in all cases the speeds have decreased.

The global properties indicate that A3 has followed almost exactly its nominal trajectory, whereas A1, A2 and A4 have lengthened their routes, increasing the flight time; Δr and Δt_f vary according to the landing sequence.

The total increase in fuel consumption is about 114 kg, significantly greater than in Scenario 1, as well as the final value of the objective function (J=0.365 deg), as expected for this more demanding scenario.

Aircraft	M_c [-]	ΔM_c [-]	M_d [-]	ΔM_d [-]	CAS_d kt	ΔCAS_d kt	Δr [m]	Δt_f [s]	Δm_F [kg]
A1	0.740	-0.074	0.740	-0.074	280.0	-28.0	25526	197.8	43.1
A2	0.780	-0.078	0.780	-0.078	310.0	-31.0	38845	247.9	63.9
A3	-	-	-	-	310.0	-	3	0.0	0.0
A4	-	-	0.740	-	290.0	-4.1	5948	42.1	6.8

Table 5.2: Scenario 2: properties of the resolution trajectories.

This page intentionally left blank

6 Optimization of Conflict-Free Trajectories with Scheduled Times of Arrival

In this chapter, the optimization approach presented in Chapter 3 is applied to solve the problem of generating and optimizing conflict-free trajectories that meet scheduled times of arrival, which is a key component in arrival management, as shown next.

Arrival management is the process of safely and effectively arranging arrivals into a smooth efficient flow for landing at a destination airport [Hase 10]. It involves two high-level functions at the strategic level: traffic management and separation management, both in the en-route arrival transition, and in the terminal area (Boeing [Berg 08]). Traffic management performs runway assignment, sequencing and scheduling, that is, it creates a strategic arrival plan, and separation management synthesizes intents that meet the traffic management schedule and ensures that the arrival plan is conflict free.

The separation management function relies on the iterative combination of Trajectory Prediction (TP), Conflict Detection (CD) and Conflict Resolution (CR) functions. How this iterative process is carried out depends strongly on the particular algorithmic solution used to implement the task. The TP function translates intent into a predicted trajectory; the CD function uses the predicted trajectories to determine whether conflicts exist; and, the CR function determines intents that meet the objectives and constraints. The primary hard constraint is to maintain safe separation throughout the conflict area; in addition to this, there are other constraints such as those arising from procedures, terrain and/or airspace avoidance. On the other hand, the primary objective is to stay close to the schedule provided by the traffic management function; secondary objectives can include for example fairness, operating cost, and environmental impact.

In this thesis, the TP function is performed through the computation of flight segments, as it was described in Chapter 3. The CD function is performed by an algorithm that considers horizontal separation among aircraft and takes into account their wake turbulence categories. And the CR function is performed by a resolution algorithm which is as an extension of that one proposed in Chapter 5, and it is formed by three steps: avoidance, recovery and optimization. In fact, two different algorithms are developed, depending on whether the optimization step is applied globally (to all aircraft) or locally (to each aircraft); this second algorithm is efficient when the scenario is very demanding (in which the global optimization is not effective). These algorithms are tested in two different scenarios in the TMA of Canarias.

Their performance is evaluated applying a set of key performance indicators (KPI), defined in Appendix E, to the obtained resolution trajectories.

The outline of this chapter is as follows: the trajectory patterns, the CD algorithm and the two CR algorithms developed for this application are defined in Section 6.1, the scenarios considered are described in Section 6.2, and the results are presented in Section 6.3; the aircraft models used (based on BADA 3.6) are described in Appendix D.

6.1 Problem Formulation

The TMA scenario considered in this application is similar to the scenario considered in the previous chapter: there exists a limited region of airspace where there are some locked and unlocked aircraft, whose intended trajectories may be in conflict. The main difference is that now the trajectories of the unlocked aircraft must also meet an arrival time at a given point (in this application the runway threshold). The resolution of the problem requires that the unlocked aircraft be conflict free with all aircraft (locked and unlocked) and arrive at times as close as possible to the scheduled arrival times.

In the considered scenarios (Section 6.2) about 30 aircraft must land in one hour, a number of aircraft much higher than in Chapter 5. In order to reduce the computation time of the conflict detection and resolution process, the CD algorithm is simplified to consider only horizontal separation and the trajectory patterns consider instantaneous turns.

Next, the equations of motion, the trajectory patterns, the conflict detection and the conflict resolution algorithms are described.

6.1.1 Equations of Motion

If Eqs. (3.1) and (3.4) are particularized for flight in a vertical plane with no wind, then the equations reduce to:

$$\begin{aligned}
m\frac{\mathrm{d}V}{\mathrm{d}t} &= T - D(V,h,L) - mg\sin\gamma \\
mV\frac{\mathrm{d}\gamma}{\mathrm{d}t} &= L - mg\cos\gamma \\
\frac{\mathrm{d}m}{\mathrm{d}t} &= -c(V,h)T \\
(R_E+h)\frac{\mathrm{d}\varphi}{\mathrm{d}t} &= V\cos\gamma\cos\chi_A \\
(R_E+h)\cos\varphi\frac{\mathrm{d}\lambda}{\mathrm{d}t} &= V\cos\gamma\sin\chi_A \\
\frac{\mathrm{d}h}{\mathrm{d}t} &= V\sin\gamma \\
\frac{\mathrm{d}r}{\mathrm{d}t} &= \frac{R_E}{R_E+h}V\cos\gamma
\end{aligned} \tag{6.1}$$

where χ_A is the heading angle of the corresponding segment. The control variables are T and L.

Different aircraft models are considered, namely, Boeing 737-400, Airbus 320-212, CRJ 200, and Boeing 777-300. As in Chapter 5, the aerodynamic and propulsive models are based

on BADA 3.6, which are described in detail in Appendix D.

6.1.2 Trajectory Patterns

The nominal and resolution trajectory patterns considered in this application are very similar to the trajectory patterns defined in Section 5.1.2. The only differences are that in this application: 1) turns are performed instantaneously (to save computation time), and 2) the changes in the waypoints coordinates are not subject to be inside boxes centered on the nominal waypoints (to have more available solutions).

6.1.3 Conflict Detection

In the CD algorithm the horizontal distance d_{ij} between any pair of aircraft i and j is measured at discrete times $t_k = t_0 + k\Delta t$ during the time they both are in the TMA. The minimum distances $(d_{ij})_{min}$ are computed and compared with the corresponding separation minimum $d_{s,ij}$. In case $(d_{ij})_{min} < d_{s,ij}$ a conflict is detected between aircraft i and j. This CD algorithm is simpler than the one presented in Section 5.1.3 since it does not consider vertical separation. As a result, this algorithm is more conservative, it detects conflicts although the vertical separation is large enough for not having a conflict.

In exchange, the CD algorithm considers the wake turbulence categories of aircraft (light, medium and heavy) and the wake turbulence separation minima, which are defined in ICAO Doc. 4444 [ICAO 07a]. The separation minima used are shown in Table 6.1. In this table it is considered that if aircraft i is succeeding aircraft j, then aircraft j is preceding aircraft i, or vice versa. This situation takes place in a nominal scenario in which all the aircraft fly predefined tracks. However, the aircraft trajectories proposed by the CR process allow the aircraft to be located at any point and with any heading. Therefore, to properly select the separation minimum between two aircraft it is necessary to determine at each time the relative position between them.

		Preceding aircraft		
		Heavy	Medium	Light
Succeeding aircraft	Heavy	4	3	3
	Medium	5	3	3
	Light	6	5	3

Table 6.1: Separation minima [nmi] (ICAO Doc. 4444)

The horizontal distance between two aircraft is measured along a great circle (minimum distance) on the Earth surface, which is given by Eq. (5.12).

6.1.4 Conflict Resolution

The objective of the CR algorithm is to determine intents that result in conflict-free, on-time trajectories, that is, deconflicted trajectories that meet the scheduled times of arrival associated either to waypoints or runway threshold. As stated in Ref. [Berg 08], to maintain

safe separation is considered as a *hard constraint* that must be always met. The scheduling requirement is a *primary objective* that has to be met as close as possible. Other objectives which should be met, called *secondary objectives*, are fairness (to attempt to distribute among all the aircraft the costs incurred in deviating from the user preferred trajectory), reduced operating costs and environmental impact.

As in Chapter 5, one can consider locked and unlocked aircraft. In this application, the resolution of the problem requires that the unlocked aircraft be conflict free with all aircraft (locked and unlocked) and meet their scheduled arrival times. In practice, which aircraft are locked and which unlocked is decided by the separation management function.

The inputs to the CR algorithm are a set of N_u unlocked aircraft (their nominal trajectories or intents and their scheduled times of arrival) and a set of N_l locked aircraft (their intents), which represent constraints for the resolution process. The CR function relies on the TP and CD functions.

In the following, two CR algorithms are presented. The first one turns out to be inefficient when the scenario is very demanding, as shown in Section 6.3.2, so that the second algorithm is a modification of the first one to make it efficient in such very-demanding scenarios.

6.1.4.1 2-step CR algorithm

This algorithm is divided into two phases: Phase 1 (with 2 steps) and Phase 2. The structure of this algorithm can be seen in Fig. 6.1. Phase 1 deals with hard constraints and primary objectives (conflict-free, on-time trajectories), whereas Phase 2 deals with secondary objectives (fairness, cost optimization, ...). According to this structure, Phase 2 is not performed until Phase 1 is completed.

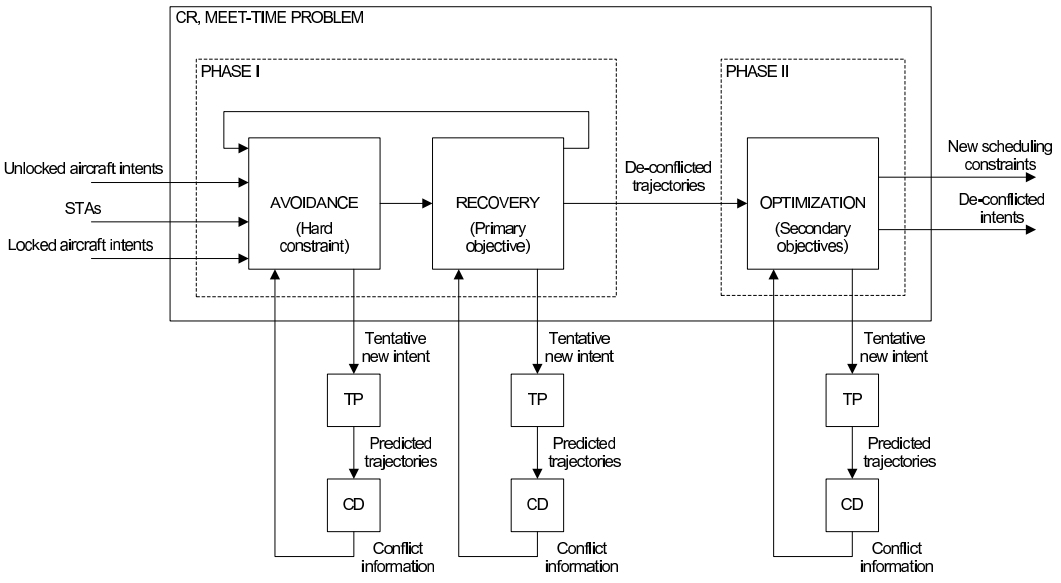

Figure 6.1: Structure of the 2-step CR algorithm.

Phase 1

The objective of this phase is to generate conflict-free trajectories (hard constraint) that meet the scheduling requirement (primary objective). To achieve this goal, two steps are carried out for each unlocked aircraft: *avoidance* and *recovery* (using the nomenclature of Ref. [Bili 02]).

These two steps are applied sequentially to the unlocked aircraft according to the arrival sequence. While aircraft i is processed (as it will be seen later), the only conflicts considered are those with the locked aircraft and the $i-1$ previous unlocked aircraft already processed (when the first aircraft is processed, only the conflicts with the locked aircraft are considered).

The two steps of this phase applied to each aircraft are carried out as follows:

1. Avoidance

   In the avoidance step, two requirements are imposed: the trajectories must be conflict free and they have to meet a sequencing requirement (notice that the scheduled arrival times define an arrival sequence). The last requirement is imposed as a new constraint: the arrival time of a given aircraft must be greater than the scheduled arrival time of the previously sequenced aircraft (either locked or unlocked). The output of this step is a set of conflict-free trajectories that comply with the pre-determined arrival sequence.

   This step then consists in generating a trajectory for aircraft i that satisfies the following set of constraints:

$$\begin{aligned} &\mathbf{g}_{TPi} \leq 0 \\ &(d_{i,j})_{min} \geq d_{s,ij}, \quad \forall j = 1, \ldots, i-1 \\ &(\hat{d}_{i,k})_{min} \geq d_{s,ik}, \quad \forall k = 1, \ldots, N_l \\ &t_{ETA,i} > t_{STA,prev} \end{aligned} \tag{6.2}$$

   where $\mathbf{g}_{TPi}$ is the set of inequality constraints imposed by the resolution trajectory pattern assigned to aircraft i (described in Section 5.1.2.2), $(d_{i,j})_{min}$ the minimum distance between the unlocked aircraft i and j, $(\hat{d}_{i,k})_{min}$ the minimum distance between the unlocked aircraft i and the locked aircraft k, $d_{s,ij}$ the separation minimum that corresponds to aircraft i and j, $t_{ETA,i}$ the estimated time of arrival of the unlocked aircraft i, and $t_{STA,prev}$ the scheduled time of arrival of the previously sequenced aircraft (either locked or unlocked).

   Besides the constraints imposed by the resolution trajectory pattern, the second constraint refers to the conflicts between aircraft i and the $i-1$ previously processed aircraft, the third constraint refers to the conflicts between aircraft i and the N_l locked aircraft, and the last constraint is the sequencing constraint: the arrival time of the aircraft i must be greater than the arrival time of the previously sequenced aircraft.

   In the avoidance algorithm, first, it is checked if all the given constraints are met by the nominal trajectory; if not, a random search is performed to obtain a first valid solution. If the vector $\mathbf{x}_i$ contains the parameters that define the trajectory of aircraft i, then this step reduces to randomly generate a vector $\mathbf{x}_i$ that satisfies all the constraints. The method followed to perform the random search is based on a normal distribution. A new vector $\mathbf{x}_i$ is generated around $\mathbf{x}_i^0$, which represents the nominal trajectory for aircraft i.

2. Recovery

   In the recovery step, the conflict-free trajectories obtained in the avoidance step are modified in order to have arrival times as close as possible to the scheduled ones. The output of this step is a new set of conflict-free trajectories with arrival times very close to the scheduled ones.

   To meet the scheduled arrival time, an optimization problem is formulated: minimize the deviation from the scheduled arrival time, $t_{STA,i}$, keeping the trajectory conflict free, that is,

$$\begin{aligned} &\text{minimize} \quad (t_{ETA,i} - t_{STA,i})^2 \\ &\text{subject to Eqs. (6.2)} \end{aligned} \tag{6.3}$$

   Note that deviations in both directions are penalized.

   If after solving this optimization problem the scheduled arrival time is met, then the next unlocked aircraft is processed. Otherwise, the avoidance step is repeated in order to generate a new starting random trajectory. This process can be repeated up to 5 times if necessary. In case that after 5 repetitions it is not found any trajectory that meets $t_{STA,i}$, it is considered that the best solution is that trajectory with a $t_{ETA,i}$ closer to $t_{STA,i}$, and the next unlocked aircraft is processed.

Phase 2

After executing Phase 1, all the trajectories are conflict-free with estimated arrival times equal or close to the scheduled ones. However, the resolution trajectories obtained may not meet the secondary objectives: have a high cost (for example, a high deviation from the nominal trajectories). Thus, this optimization phase aims at minimizing a combination of costs considering such secondary objectives; in this work only the lateral deviation from the nominal trajectories is considered. Starting from the trajectories found in Phase 1, a global optimization is performed. The modification of all the intents at once implies a high computational cost.

The following optimization problem is formulated:

$$\begin{aligned} \text{minimize} \quad & \frac{1}{N_u}\sqrt{\sum_{i=1}^{q}\left[\left(\lambda_i-\lambda_i^0\right)^2+\left(\varphi_i-\varphi_i^0\right)^2\right]} \\ \text{subject to} \quad & \mathbf{g}_{TPi} \le 0 && \forall i = 1,\ldots,N_u \\ & (d_{i,j})_{min} \ge d_{s,ij} && \forall i,j = 1,\ldots,N_u,\ \ j \ne i \\ & (\hat{d}_{i,k})_{min} \ge d_{s,ik} && \forall i = 1,\ldots,N_u,\ \ \forall k = 1,\ldots,N_l \\ & t_{ETA,i} - t^1_{ETA,i} = 0 && \forall i = 1,\ldots,N_u \end{aligned} \tag{6.4}$$

where $\left(\lambda_i^0, \varphi_i^0\right)$ are the nominal location of the waypoints, q the total number of waypoints that can be changed, and $t^1_{ETA,i}$ is the t_{ETA} of aircraft i obtained in Phase 1. Note that the last constraint represents that the arrival time obtained in Phase 1 is to be maintained.

6.1.4.2 3-step CR algorithm

The poor performance obtained in the lateral optimization of the 2-step CR algorithm (Phase 2) with a very demanding scenario, as it will be shown in Section 6.3.2, makes it necessary the definition of a new algorithm. We consider a modification of the 2-step CR algorithm in which Phase 2 is eliminated and a third step is added after the avoidance and recovery steps, as can be seen in Fig. 6.2. The three steps are performed sequentially for each unlocked aircraft. The first two steps are as before (Section 6.1.4.1). Once these steps have been executed an optimization of the lateral deviation of aircraft i is performed keeping fixed its $t^1_{ETA,i}$ (as in Phase 2 before). In this third step, while aircraft i is processed, the only conflicts considered are those with the locked aircraft and the $i-1$ previous unlocked aircraft already processed, as in the two first steps. Once this last step is executed, the next unlocked aircraft is processed.

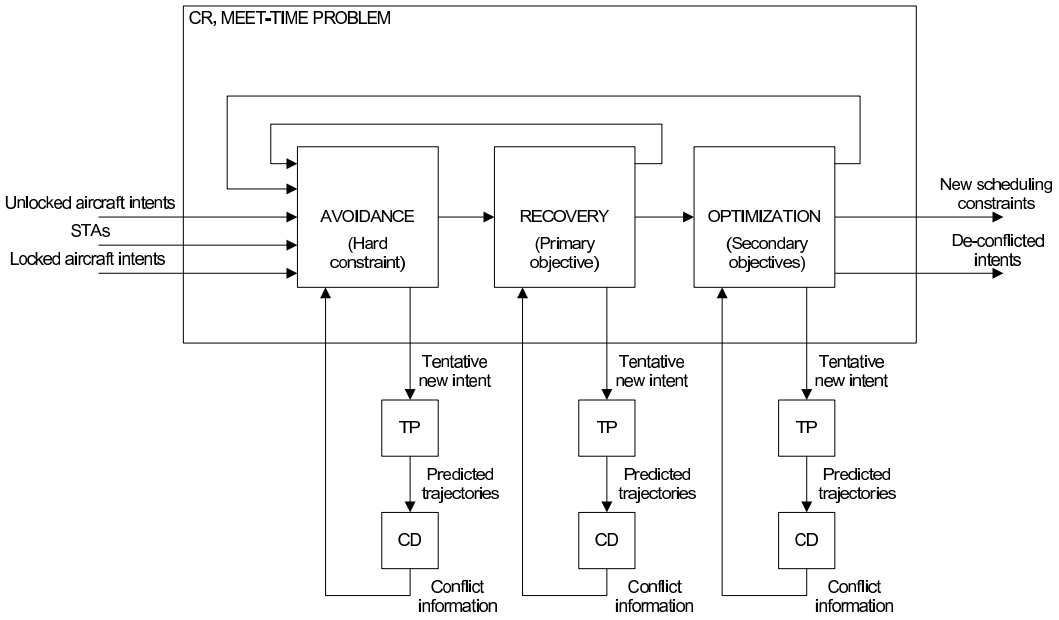

Figure 6.2: Structure of the 3-step CR algorithm.

The optimization problem solved in the third step while aircraft i is processed is formulated as:

$$\begin{aligned} \text{minimize} \quad & \sqrt{\sum_{j=1}^{q_i}\left[\left(\lambda_j-\lambda_j^0\right)^2+\left(\varphi_j-\varphi_j^0\right)^2\right]} \\ \text{subject to} \quad & \mathbf{g}_{TPi} \leq 0 \\ & (d_{i,j})_{min} \geq d_{s,ij} \qquad \forall j=1,\ldots,i-1 \\ & (\hat{d}_{i,k})_{min} \geq d_{s,ik} \qquad \forall k=1,\ldots,N_l \\ & t_{ETA,i}-t^1_{ETA,i}=0 \end{aligned} \tag{6.5}$$

where only the waypoints of aircraft i are considered, being q_i the total number of waypoints that can be changed for this aircraft.

6.2 Scenarios

Two scenarios are considered: one in which the 2-step CR algorithm is efficient, and another, more demanding, in which the 3-step CR algorithm must be used to meet the secondary objectives.

6.2.1 Scenario 1

Scenario 1 corresponds to the TMA of Canarias with three entry points (TERTO, RUSIK and WPT1), and two merging points (FAYTA and CANIS). The waypoint WPT1 is placed South-East of FAYTA, at (φ, λ)=(27°40'00"N,13°30'00"W). In this scenario one has 30 aircraft arriving in one hour, with the scheduled arrival times equally spaced 120 s. The traffic generated for this scenario can be found in Appendix F. All aircraft are of the same category (medium), and there are no locked aircraft.

The properties of this scenario are: number of aircraft, 30; mean aircraft mass at TMA entry point, 41372 kg; maximum deviation time, 148.0 s; mean deviation time, 61.3 s; conflicts between nominal trajectories, 12; and mean conflict intensity, 7.84. In these properties, the deviation time is the difference between the nominal ETA and STA, and the conflict intensity among aircraft i and j is calculated as $10 \cdot (d_s - (d_{ij})_{min}) / d_s$ (with 0 being the lowest level of severity and 10 the highest), as stated in Ref. [Vila 06], where d_s is the corresponding separation minimum.

In this scenario a separation minimum of 3 nmi and a time tolerance (difference between ETA and STA) of 0.1 s have been considered. The nominal trajectories are represented in Fig. 6.3. Each aircraft is bounded by a circle of radius 1.5 nmi.

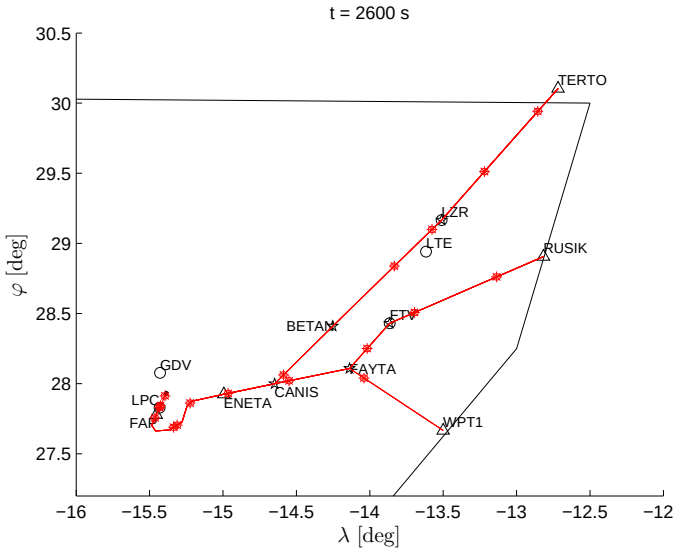

Figure 6.3: Scenario 1: nominal trajectories, $t = 2600$ s.

6.2.2 Scenario 2

Scenario 2 is a modification of Scenario 1 with an additional entry point (WPT2). Now it has four entry points (TERTO, RUSIK, WPT1 and WPT2), and three merging points (FAYTA, BETAN and CANIS). The arrival procedure that starts at WPT2 is composed of the following waypoints: WPT2 (φ, λ)=(30°15'34"N,14°30'11"W), WPT3 (φ, λ)=(29°19'07"N,14°25'51"W), BETAN, CANIS, ENETA, and RWY. The traffic generated for this scenario can be found in Appendix F. The aircraft have different categories (medium and heavy), and there are no locked aircraft.

In this scenario 35 aircraft arrive in one hour: 9 CRJ (medium aircraft), 9 Boeing 737-400 (medium aircraft), 8 Airbus A320 (medium aircraft), and 9 Boeing 777-300 (heavy aircraft). The scheduled arrival times are equally spaced 120 s. Thus, the deviation time (difference between the nominal ETA and STA) of the last arriving aircraft is at least 600 s.

The properties of this scenario are: number of aircraft, 35; mean aircraft mass at TMA entry point, 96657 kg; maximum deviation time, 630.8 s; mean deviation time, 274.1 s; conflicts among nominal trajectories, 30; and mean conflict intensity, 5.63.

Note that this scenario is more demanding than Scenario 1: the number of aircraft, the mean mass, the maximum deviation time, the mean deviation time, and the number of conflicts are significantly greater, even though the mean conflict intensity is smaller.

The nominal trajectories are represented in Fig. 6.4. Each aircraft is bounded by a circle of radius 1.5 nmi. The medium aircraft are bounded by red circles and the heavy ones by blue circles.

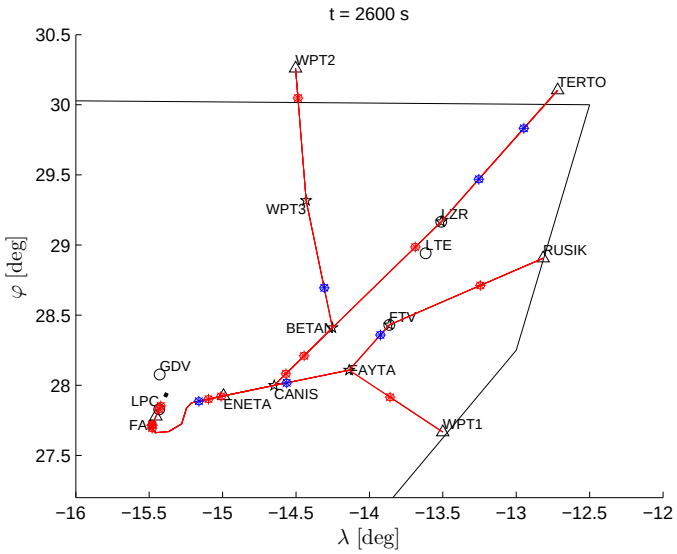

Figure 6.4: Scenario 2: nominal trajectories, $t = 2600$ s.

6.3 Results

In this section the results obtained in the generation of conflict-free, on-time trajectories are presented. The 2-step CR algorithm is used in Scenarios 1 and 2, and the 3-step CR algorithm in Scenario 2.

6.3.1 Scenario 1

The conflict-free, on-time trajectories obtained after Phase 1 are represented in Fig. 6.5, and those obtained after Phase 2 in Fig. 6.6 (in these figures, some aircraft have already landed, and some others have not yet entered the TMA). After Phase 1 the value of the objective function is 0.1324 deg and after Phase 2 it reduces to 0.0048 deg. This objective function measures the deviation of the resolution waypoints from the nominal waypoints (see Section 6.1.4.1). The improvement obtained after executing Phase 2 is notorious.

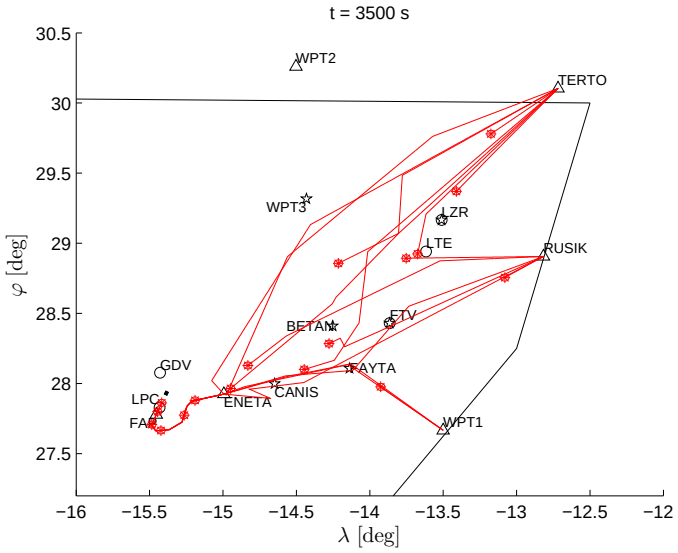

Figure 6.5: 2-step CR: resolution trajectories, Phase 1, $t = 3500$ s (Scenario 1).

After the CR execution call, the number of conflicts is 0 and the mean deviation time is 0.04 seconds. These and other indicators of the solution are provided in Table 6.2. The resolution speeds, deviation times from the STA, and the increase in fuel consumption for each aircraft are given in Appendix F. These results indicate that all aircraft are on time.

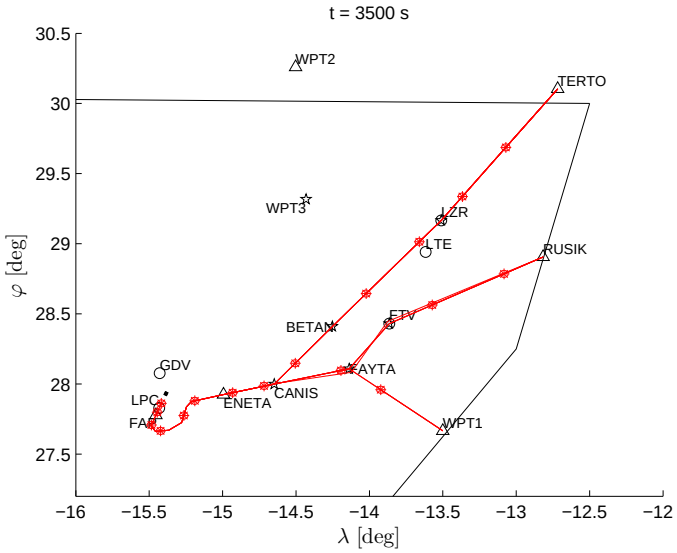

Figure 6.6: 2-step CR: resolution trajectories, Phase 2, $t = 3500$ s (Scenario 1).

Indicator	Value
Objective function value after phase 1, J_1 [deg]	0.1324
Objective function value after phase 2, J_2 [deg]	0.0048
Maximum deviation time, KPI_1 [s]	0.10
Mean deviation time, KPI_2 [s]	0.04
Mean fuel cost, KPI_3 [kg]	-16.71
Cost distribution, KPI_4 [kg]	14.64
Mean deviation from nominal trajectories, KPI_5 [m]	7226

Table 6.2: 2-step CR: resolution indicators (Scenario 1).

6.3.2 Scenario 2

If one uses the 2-step CR algorithm in the second scenario, Phase 2 does not provide any improvement: the global optimization (considering all the aircraft) is not effective. One possible explanation to this poor performance of Phase 2 is that Scenario 2 is more demanding than Scenario 1 due to: 1) the higher number of aircraft (35 opposed to 30), which determines the number of free parameters and constraints; 2) the mean deviation time (274.2 s opposed to 61.3 s), which indicates that aircraft have to spend more time flying inside the TMA; and 3) the number of conflicts among nominal trajectories (30 opposed to 12), which suggests a greater interaction among trajectories.

The resolution trajectories obtained with the 2-step CR algorithm (in Phases 1 and 2) are represented in Fig. 6.7. After the CR execution call, the value of the objective function is 0.2053 deg, the number of conflicts is 0 and the mean deviation time is 4.66 s; other indicators of the solution are provided in Table 6.3. The mean deviation time indicates that several aircraft are not on time. The resolution speeds, deviation times from the STA, and the increase in fuel consumption for each aircraft can be found in Appendix F. It can be seen that all the medium aircraft that arrive after heavy aircraft do not meet the STA. This is due to the separation of 2 minutes at the runway threshold, which is not compatible with the separation minimum applied of 5 nmi (Table 6.1). Therefore, bigger separation between STA should be used between medium and heavy aircraft.

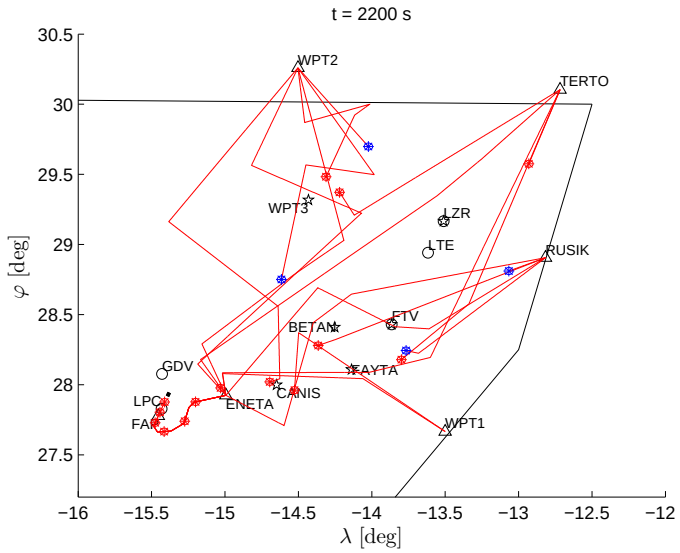

Figure 6.7: 2-step CR: resolution trajectories, Phases 1 and 2, $t = 2200$ s (Scenario 2).

The poor performance of the Phase 2 of the 2-step CR algorithm in this scenario motivates the development of the 3-step CR algorithm described in Section 6.1.4.2. In this new algorithm the global optimization performed in Phase 2 of the 2-step algorithm is replaced by an additional optimization step. The aim of this change in the algorithm is to solve smaller

Indicator	Value
Objective function value after phase 1, J_1 [deg]	0.2053
Objective function value after phase 2, J_2 [deg]	0.2053
Maximum deviation time, KPI_1 [s]	37.95
Mean deviation time, KPI_2 [s]	4.66
Mean fuel cost, KPI_3 [kg]	466.66
Cost distribution, KPI_4 [kg]	609.74
Mean deviation from nominal trajectories, KPI_5 [m]	33811

Table 6.3: 2-step CR: resolution indicators (Scenario 2).

optimization problems with less aircraft, that leads to a lower number of parameters and constraints and lower interactions.

The resolution trajectories obtained with the 3-step CR algorithm are plotted at two different times in Figs. 6.8 and 6.9. It can be seen that the horizontal deviation in the latter is greater because the differences between the ETA and the STA of the last aircraft are much bigger than the differences in the first ones.

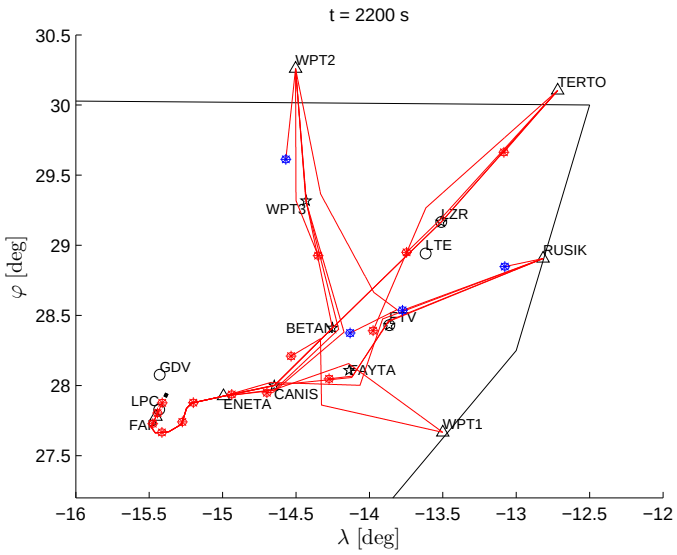

Figure 6.8: 3-step CR: resolution trajectories, t=2200 s (Scenario 2).

Now, the value of the objective function is 0.0873 deg, which is significantly lower than the value obtained with the 2-step algorithm (0.2053 deg). This difference can be graphically observed by comparing Figs. 6.7 and 6.8, in which the trajectories are plotted for the same time (t = 2200 s). The mean fuel cost, cost distribution and deviation from the nominal trajectories, shown in Table 6.4, are also lower than those obtained with the 2-step algorithm. The deviation times are similar, and the differences are of the order of the time tolerances.

The mean fuel cost and cost distribution are significantly greater than in Scenario 1. This is due to: the higher deviation time of the scenario (the delay is absorbed in the TMA), the increase in the mean mass (the fuel consumption is also increased), and the presence of

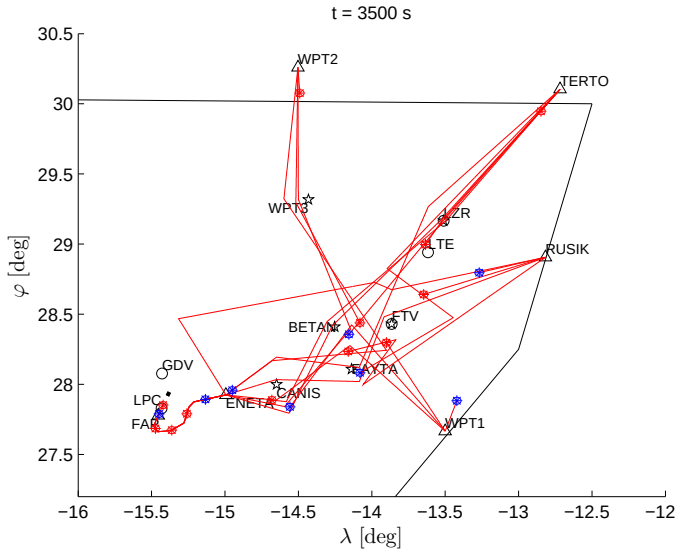

Figure 6.9: 3-step CR: resolution trajectories, t=3500 s (Scenario 2).

aircraft of different categories (the fuel consumption is heterogeneous).

Indicator	Value
Objective function value after phase 1, J_1 [deg]	0.0873
Maximum deviation time, KPI_1 [s]	38.47
Mean deviation time, KPI_2 [s]	4.84
Mean fuel cost, KPI_3 [kg]	323.96
Cost distribution, KPI_4 [kg]	516.36
Mean deviation from nominal trajectories, KPI_5 [m]	26296

Table 6.4: 3-step CR: resolution indicators (Scenario 2).

7 Conclusions

The research theme in this thesis has been the optimization of aircraft trajectories using parametric optimization theory. In this work, the parameterization of the trajectories is based on the use of predefined trajectory patterns which are, in fact, a parameterization of the flight intents, that model the aircraft trajectories actually flown. In this parameterization, the aircraft trajectory is described by flight segments, and the segments are defined by a small number of parameters, some of which are fixed whereas others are free, on which the optimization is performed. The optimization algorithm is chosen according to the characteristics of the optimization problem and the recommendations found in the literature.

This approach based on the use of trajectory patterns has been applied to the optimization of the cruise trajectory of one single aircraft as well as to a set of aircraft, taking into account the conflicts that may arise among them. For each application, the dynamic equations of motion have been particularized, an appropriate trajectory pattern has been defined, the parameters free to change have been selected, and the optimization problem has been formulated and solved.

In the first application, the general problem of minimum direct-operating-cost cruise (unsteady, with variable mass and without any constraint on speed or altitude) with given range has been addressed. Two types of problems have been solved: one in which all the parameters are continuous variables, and another one in which some parameters are discrete variables (Mach numbers multiple of 0.01, and altitudes defined by flight levels), defining what have been called unrestricted and restricted procedures, respectively. The results have shown that the optimal procedures are always cruise climbs (in fact, stepped cruise climbs, according to the trajectory pattern) with roughly constant Mach numbers, for all values of the cost index. The optimal procedures define not only the optimum values of speed and altitude for the different cruise segments, but also, and more importantly, the optimum distances to be flown in each segment.

The main objective of this application has been to analyze how the optimal procedures change when the altitudes and speeds are restricted to take discrete values. It has been shown that the changes in the procedures (with respect to the unrestricted case) are important, especially in the optimum lengths of each cruise segment, although the changes in cost are very small. It has been shown that the altitudes play a key role in the selection of the optimum distances to be flown in each cruise segment. The influences of the initial aircraft weight and of an average horizontal wind on the optimal procedures have also been analyzed. The initial weight has an important effect on the selection of the optimum altitudes, while the effect of the wind has been shown to be quite small. Although results have been presented for constant average winds, the analysis has been general, valid for any altitude-dependent

wind profile.

Next, the problem of minimum-fuel cruise at constant altitude with fixed range and fixed arrival time has been solved. The objective in this application has been to analyze the optimized procedures when they are subject to the additional equality constraint of fixed arrival time. In this case, it has been possible to compare the results with known optimal laws obtained with singular optimal control theory. As in the previous application, restricted and unrestricted procedures have been considered. The comparison has shown that the optimized procedures approximate very well the optimal laws and give results that are very close to the optimal values, in both the unrestricted and restricted cases. The differences between the optimized procedures and the optimal trajectories decrease as the number of steps increases, but in the case of restricted procedures a limit is reached and no further improvement is found in adding more steps.

In the next application, the proposed optimization approach has served as a basis to develop an algorithm for conflict resolution in converging traffic in the terminal area which minimizes the deviation from the intended trajectories. The resolution trajectory patterns take into account changes of the nominal waypoints (vectoring) and changes of the aircraft speeds. The algorithm has been applied to the case of global traffic (multiple conflicts) in two different scenarios: one with only unlocked aircraft, and another one with some additional locked aircraft. The resolution strategy is composed of two phases: one in which a first valid solution is found by means of a random search, and another one in which this first valid solution is optimized. The two-phase resolution strategy considered has proven to be an efficient approach in, both, finding a first valid solution with a relatively small number of trajectory computations, and improving it by reducing the total cost. The cost of the resolution process has been assessed, in terms of extra distance travelled, extra flight time and extra fuel consumption for each aircraft. As expected, the scenario with additional locked aircraft has been more demanding in computing effort, and the cost of the resolution process has been larger.

As already mentioned, the conflict resolution algorithm is global, meaning that all the aircraft present in the scenario are handled altogether, which in fact limits the number of aircraft that can be handled, especially in the second phase of the resolution strategy (optimization) since the number of parameters becomes excessively large. However, if the arrival sequence is known, this information can be used to develop different resolution strategies, as shown in the last application considered in the thesis.

Finally, the previous algorithm has been extended to solve the problem of generating conflict-free, on-time trajectories in arrival management. The resolution strategy is formed by 3 steps. First, the avoidance step, in which the objective is to obtain resolution trajectories that are conflict free and meet the sequencing constraint; second, the recovery step, in which these resolution trajectories are modified to meet the scheduled arrival times as close as possible; and, third, an optimization step in which the goal is to minimize a given combination of costs. Two algorithms have been presented. One in which the 3rd step (optimization) is applied globally (to all aircraft) after steps 1 and 2 are performed for all aircraft, and another one in which the 3rd step is applied locally to each aircraft after steps 1 and 2 are performed for the given aircraft. The results have shown that the first algorithm is adequate for scenarios which are not very demanding, in which the global optimization is effective

(that is, it improves the results obtained with the avoidance and recovery steps). On the other hand, for very-demanding scenarios, the global optimization is not effective and the 2nd algorithm must be used.

As it has been shown throughout the document, this optimization approach presents the following advantages: 1) it allows to optimize any property or combination of properties derived from the trajectory (e.g., fuel consumption, flight time, deviation from waypoints, etc.); 2) it allows to generate trajectories based on flight procedures usually flown by the aircraft (acceleration/deceleration at constant altitude, Mach/CAS descent, turns at constant bank angle, etc.); 3) it allows to readily incorporate any kind of restriction on the trajectory (discrete values of the parameters, given range, given arrival time, etc); and 4) the optimization is performed on a small number of parameters (in the applications considered in this thesis, about ten parameters per aircraft).

The versatility shown by this approach allows to solve different problems by just defining the appropriate trajectory patterns, cost functions and constraints. For example, the approach has already been applied in the optimality assessment of a constant-CAS, unpowered descent procedure in the presence of altitude-dependent winds. These results are presented in the following journal paper

- A. Franco, D. Rivas and A. Valenzuela. "Optimization of Unpowered Descents of Commercial Aircraft in the Presence of Altitude-Dependent Winds". *Journal of Aircraft*, Vol. 49, No. 5, pp. 1460–1470, 2012.

The approach has also been applied in the project CENIT SINTONIA, in the generation of optimal trajectories for UAVs which serve as references for the guidance and control system onboard the aircraft. This work was presented in the conference paper

- A. Valenzuela, D. Rivas, F. Gavilán and R. Vázquez. "Optimal Trajectory Generation for UAVs Using Dynamic Trajectory Modeling". *First Workshop on Research, Development and Education on Unmanned Aerial Systems (RED-UAS 2011)*, Seville, Spain, Nov. 30 - Dec. 1, 2011.

This page intentionally left blank

8 Future Work

As already mentioned, the optimization approach presented in this thesis can be generalized straightforwardly to solve other problems, which only requires the definition of an appropriate trajectory pattern, and the corresponding cost function and constraints.

For example, the approach can be applied to the optimization of other flight phases, such as climb, a very fuel-demanding phase. In this sense, a new paper is in preparation to assess the optimality of the standard CAS/Mach climb procedure:

- A. Franco, D. Rivas and A. Valenzuela, "Analysis of minimum-fuel, constant-rating aircraft climbs in altitude-dependent winds". In preparation.

The approach can also be applied to the global trajectory, from liftoff to touchdown, by just defining a trajectory pattern that models all the flight phases. An example of this kind of pattern has already been used in a trajectory computation tool designed to compute global trajectories of commercial transport aircraft:

- D. Rivas, A. Valenzuela and J. L. de Augusto, "Computation of Global Trajectories of Commercial Transport Aircraft". *Proceedings of the Institution of Mechanical Engineers, Part G: Journal of Aerospace Engineering*, accepted for publication, 2012.

Other cost functions may be considered, provided that they depend, directly or indirectly, on the state or the control variables; for example, noise perceived at ground and pollutants emissions (e.g., nitrogen oxides or hydrocarbons), which are of special importance in the surroundings of airports. The noise is mainly a function of the power generated at the engines and the distance between the aircraft and the ground [ICAO 08], while the pollutants emissions are functions of the fuel flow and the time [ICAO 07c].

Other constraints can be taken into account, such as to keep a minimum distance from an obstacle or a restricted area. For example, in the case that forecast models for adverse weather are available, the approach can be used to obtain trajectories that circumnavigate the bad-weather regions.

The availability of more realistic supplementary models can also lead to new applications. For example, if an atmosphere model that includes the distribution of winds along the Earth surface is available then the approach can be used to determine routes that would take advantage of the winds, as for example, the northern jet streams.

The proposed CR algorithm developed for convergent traffic can be also applied to other types of traffic, for example, en-route traffic (free flight), and can incorporate other features such as altitude changes, which would just require the definition of the appropriate trajectory patterns.

The proposed CR algorithm is global and centralized, meaning that all the aircraft present in the scenario are handled altogether by a control station which computes resolution trajectories for all of them. Another approach to this problem is to consider distributed algorithms, where each aircraft computes its own resolution trajectory, which must be coordinated with the resolution trajectories of the other aircraft. In this sense, a visit of two months was made to the National Institute of Aerospace, NIA, in which a collaboration with the NASA Langley Formal Methods Research Group was made. In this visit, intent-based implicit coordination criteria were developed, as an extension of the already existing state-based criteria [Nark 11]. These criteria can be easily incorporated as inequality constraints to the conflict resolution problem.

All these applications are left for future work.

Bibliography

[AIRE 12] *AIRE: Atlantic Interoperability Initiative to Reduce Emissions. Summary of results 2010/2011.* 2012. doi: 10.2829/17266.

[Arde 76] M. D. Ardema. "Solution of the Minimum Time-to-Climb Problem by Matched Asymptotic Expansions". *AIAA Journal*, Vol. 14, No. 7, pp. 843–850, 1976.

[Asse 97] M. Asselin. *An introduction to Aircraft Performance.* AIAA Education Series, Reston, VA, 1997.

[Barm 76] J. F. Barman and H. Erzberger. "Fixed-Range Optimum Trajectories for Short-Haul Aircraft". *Journal of Aircraft*, Vol. 13, No. 10, pp. 748–754, 1976.

[Barr 99] J. N. Barrer. "Integrating the Flight Management System with Air Traffic Control Functions - The Concept of Path Objects". Tech. Rep. MTR 99W000011, MITRE Corporation, 1999.

[Berg 08] M. Berger, I. del Pozo de Poza, A. Haraldsdottir, J. López-Leonés, J. Scharl, and M. Vilaplana. *AMAN Technologies. Arrival Management Modeling Collaboration. Functional Architecture. D 1.0.* Boeing Research & Technology Europe, 2008.

[Bett 95] J. T. Betts and E. J. Cramer. "Application of Direct Transcription to Commercial Aircraft Trajectory Optimization". *Journal of Guidance, Control, and Dynamics*, Vol. 18, No. 1, pp. 151–159, 1995.

[Bieg 04] L. T. Biegler and I. E. Grossmann. "Retrospective on Optimization". *Computers and Chemical Engineering*, Vol. 28, No. 8, pp. 1169–1192, 2004.

[Bili 00a] K. D. Bilimoria. "A Geometric Optimization Approach to Aircraft Conflict Resolution". In: *AIAA Guidance, Navigation, and Control Conference and Exhibit, Denver, CO, Aug. 14-17.* No. AIAA-2000-4265, pp. 1–11, 2000.

[Bili 00b] K. D. Bilimoria, K. S. Sheth, H. Q. Lee, and S. R. Grabbe. "Performance Evaluation of Airborne Separation Assurance for Free Flight". In: *AIAA Guidance, Navigation, and Control Conference and Exhibit, Denver, CO, Aug. 14-17.* No. AIAA-2000-4269, 2000.

[Bili 02] K. D. Bilimoria and H. Q. Lee. "Aircraft Conflict Resolution with an Arrival Time Constraint". In: *AIAA Guidance, Navigation, and Control Conference and Exhibit, Monterey, Aug. 5-8.* No. AIAA-2002-4444, pp. 1–11, 2002.

[Bili 85] K. D. Bilimoria, E. M. Cliff, and H. J. Kelley. "Classical and Neo-Classical Cruise-Dash Optimization". *Journal of Aircraft*, Vol. 22, No. 7, pp. 555–560, 1985.

[Broy 70a] C. G. Broyden. "The Convergence of a Class of Double-rank Minimization Algorithms. 1 General Considerations". *IMA Journal of Applied Mathematics*, Vol. 6, No. 1, pp. 76–90, 1970.

[Broy 70b] C. G. Broyden. "The Convergence of a Class of Double-rank Minimization Algorithms. 2 The New Algorithm". *IMA Journal of Applied Mathematics*, Vol. 6, No. 3, pp. 222–231, 1970.

[Brys 62] A. E. Bryson and W. F. Denham. "A Steepest-Ascent Method for Solving Optimum Programming Problems". *Journal of Applied Mechanics*, Vol. 29, No. 2, pp. 247–257, 1962.

[Brys 69] A. E. Bryson Jr., M. N. Desai, and W. C. Hoffman. "Energy-State Approximation in Performance Optimization of Supersonic Aircraft". *Journal of Aircraft*, Vol. 6, No. 6, pp. 481–488, 1969.

[Brys 75] A. E. Bryson and Y.-C. Ho. *Applied Optimal Control: Optimization, Estimation and Control.* Taylor & Francis, revised Ed., 1975.

[Burr 82] J. W. Burrows. "Fuel Optimal Trajectory Computation". *Journal of Aircraft*, Vol. 19, No. 4, pp. 324–329, 1982.

[Burr 83] J. W. Burrows. "Fuel-Optimal Aircraft Trajectories with Fixed Arrival Times". *Journal of Guidance, Control, and Dynamics*, Vol. 6, No. 1, pp. 14–19, 1983.

[Cali 77] A. J. Calise. "Extended Energy Management Methods for Flight Performance Optimization". *AIAA Journal*, Vol. 15, No. 3, pp. 314–321, 1977.

[Cavc 04] A. Cavcar and M. Cavcar. "Approximate Solutions of Range for Constant Altitude - Constant High Subsonic Speed Flight of Transport Aircraft". *Aerospace Science and Technology*, Vol. 8, pp. 557–567, 2004.

[Chak 85] A. Chakravarty. "Four-Dimensional Fuel-Optimal Guidance in the Presence of Winds". *Journal of Guidance, Control, and Dynamics*, Vol. 8, No. 1, pp. 16–22, 1985.

[Clem 02] J. C. Clements. "Optimal Simultaneous Pairwise Conflict Resolution Maneuvers in Air Traffic Management". *Journal of Guidance, Control, and Dynamics*, Vol. 25, No. 4, pp. 815–818, 2002.

[Copp 04] R. A. Coppenbarger, R. Lanier, D. Sweet, and S. Dorsky. "Design and Development of the En Route Descent Advisor (EDA) for Conflict-Free Arrival Metering". In: *AIAA Guidance, Navigation, and Control Conference and Exhibit, Providence, Rhode Island, Aug. 16-19.* No. AIAA-2004-4875, pp. 1–19, 2004.

[Cour 43] R. Courant. "Variational Methods for the Solution of Problems of Equilibrium and Vibrations". *Bulletin of the American Mathematical Society*, Vol. 49, No. 1, pp. 1–23, 1943.

[Dai 09] R. Dai and J. E. Cochran Jr. "Three-Dimensional Trajectory Optimization in Constrained Airspace". *Journal of Aircraft*, Vol. 46, No. 2, pp. 627–634, 2009.

[Daki 65] R. J. Dakin. "A Tree-Search Algorithm for Mixed Integer Programming Problems". *The Computer Journal*, Vol. 8, No. 3, pp. 250–255, 1965.

[Deb 00] K. Deb. "An Efficient Constraint Handling Method for Genetic Algorithms". *Computer Methods in Applied Mechanics and Engineering*, Vol. 186, No. 2-4, pp. 311–338, June 2000.

[Dowe 07] G. Dowek and C. Muñoz. "Conflict Detection and Resolution for 1,2,...N Aircraft". In: *7th AIAA Aviation Technology, Integration and Operations (ATIO) Conference, Belfast, Northern Ireland, Sep. 18-20.* No. AIAA-2007-7737, pp. 1–13, 2007.

[Erzb 80] H. Erzberger and H. Lee. "Constrained Optimum Trajectories with Specified Range". *Journal of Guidance, Control, and Dynamics*, Vol. 3, No. 1, pp. 78–85, 1980.

[EURO 10] *EUROCONTROL Long-Term Forecast: Flight Movements 2010-2030.* EUROCONTROL, 2010.

[FAA 11] *FAA Aerospace Forecast: Fiscal Years 2011-2030.* FAA, 2011.

[Flet 64] R. Fletcher and C. M. Reeves. "Function Minimization by Conjugate Gradients". *The Computer Journal*, Vol. 7, No. 2, pp. 149–154, 1964.

[Flet 70] R. Fletcher. "A New Approach to Variable Metric Algorithms". *The Computer Journal*, Vol. 13, No. 3, pp. 317–322, 1970.

[Flet 87] R. Fletcher. *Practical Methods of Optimization.* John Wiley & Sons, Inc., second Ed., 1987.

[Flet 94] R. Fletcher and S. Leyffer. "Solving Mixed Integer Nonlinear Programs by Outer Approximation". *Mathematical Programming*, Vol. 66, pp. 327–349, 1994.

[Flip 93] O. E. Flippo and A. H. G. R. Kan. "Decomposition in General Mathematical Programming". *Mathematical Programming*, Vol. 60, pp. 361–382, 1993.

[Fran 10] A. Franco, D. Rivas, and A. Valenzuela. "Minimum-Fuel Cruise at Constant Altitude with Fixed Arrival Time". *Journal of Guidance, Control, and Dynamics*, Vol. 33, No. 1, pp. 280–285, 2010.

[Fran 11] A. Franco and D. Rivas. "Minimum-Cost Cruise at Constant Altitude of Commercial Aircraft Including Wind Effects". *Journal of Guidance, Control, and Dynamics*, Vol. 34, No. 4, pp. 1253–1260, 2011.

[Fran 12] A. Franco, D. Rivas, and A. Valenzuela. "Optimization of Unpowered Descents of Commercial Aircraft in the Presence of Altitude-Dependent Winds". *Journal of Aircraft*, 2012. Accepted for publication.

[Fraz 01] E. Frazzoli, Z.-H. Mao, J.-H. Oh, and E. Feron. "Resolution of Conflicts Involving Many Aircraft via Semidefinite Programming". *Journal of Guidance, Control, and Dynamics*, Vol. 24, No. 1, pp. 79–86, 2001.

[Garc 95] F. García Benítez. *Optimización No Lineal.* Universidad de Sevilla, 1995.

[Gill 89] P. E. Gill, W. Murray, M. A. Saunders, and M. H. Wright. *Handbooks in Operations Research and Management Science, Vol. 1, Optimization*, Chap. Constrained Nonlinear Programming. Elsevier Science B.V., 1989.

[Gill 97] W. Gill and R. Maddock. "EFMS Prediction of Optimal 4D Trajectories in the Presence of Time and Altitude Constraints". Tech. Rep. PHARE DOC 97-70-09, EUROCONTROL, 1997.

[Gold 70] D. Goldfarb. "A Family of Variable-Metric Methods Derived by Variational Means". *Mathematics of Computation*, Vol. 24, No. 109, pp. 23–26, 1970.

[Han 77] S. P. Han. "A Globally Convergent Method for Nonlinear Programming". *Journal of Optimization Theory and Applications*, Vol. 22, No. 3, pp. 297–309, 1977.

[Hase 10] N. Haseuoets and P. Conroy. *Arrival Manager. Implementation Guidelines and Lessons Learned.* EUROCONTROL, 2010.

[Hest 69] M. R. Hestenes. "Multiplier and Gradient Methods". *Journal of Optimization Theory and Applications*, Vol. 4, No. 4, pp. 303–320, 1969.

[Holl 92] J. H. Holland. *Adaptation in Natural and Artificial Systems: An Introductory Analysis with Applications to Biology, Control, and Artificial Intelligence.* MIT Press, 1992.

[Hu 02] J. Hu, M. Prandini, and S. Sastry. "Optimal Coordinated Maneuvers for Three-Dimensional Aircraft Conflict Resolution". *Journal of Guidance, Control, and Dynamics*, Vol. 25, No. 2, pp. 888–900, 2002.

[ICAO 06] *ICAO Doc. 8168, Aircraft Operations. Procedures for Air Navigation Services. Volume I, Flight Procedures.* ICAO, 5th Ed., 2006.

[ICAO 07a] *ICAO Doc. 4444, Air Traffic Management. Procedures for Air Navigation Services.* ICAO, 15th Ed., 2007.

[ICAO 07b] *ICAO Doc. 9750, Global Air Navigation Plan.* ICAO, 3rd Ed., 2007.

[ICAO 07c] *ICAO Doc. 9889, Airport Air Quality Guidance Manual.* ICAO, preliminary Ed., 2007.

[ICAO 08] *ICAO Doc. 9911, Recommended Method for Computing Noise Contours Around Airports.* ICAO, 1st Ed., 2008.

[Isaa 01] D. R. Isaacson and J. E. Robinson III. "A Knowledge-Based Conflict Resolution Algorithm for Terminal Area Air Traffic Control Advisory Generation". In: *AIAA Guidance, Navigation, and Control Conference and Exhibit, Montreal, Canada, Aug. 6-9.* No. AIAA-2001-4116, pp. 1–11, 2001.

[Isaa 97] D. R. Isaacson and H. Erzberger. "Design of a Conflict Detection Algorithm for the Center/TRACON Automation System". In: *Proceedings 16th Digital Avionics Systems Conference, AIAA/IEEE, Oct. 26-30.* pp. 9.3–1–9.3–9, 1997.

[Jack 99] M. R. Jackson, Y. Zhao, and R. A. Slattery. "Sensitivity of Trajectory Prediction in Air Traffic Management". *Journal of Guidance, Control, and Dynamics*, Vol. 22, No. 2, pp. 219–228, 1999.

[Kenn 95] J. Kennedy and R. Eberhart. "Particle Swarm Optimization". In: *Proceedings of the IEEE International Conference on Neural Networks.* pp. 1942–1948, 1995.

[Kirk 83] S. Kirkpatrick, C. D. Gelatt, and M. P. Vecchi. "Optimization by Simulated Annealing". *Science, New Series*, Vol. 220, No. 4598, pp. 671–680, May 1983.

[Krem 99] H. J. Kremer, W. C. Vertegaal, and R. Jansen. "PHARE Advanced Tools: Conflict Probe". Tech. Rep. PHARE DOC 98-70-18, EUROCONTROL, 1999.

[Kuch 00] J. K. Kuchar and L. C. Yang. "A Reviwe of Conflict Detection and Resolution Modeling Methods". *IEEE Transactions on Intelligent Transportation Systems*, Vol. 1, pp. 179–189, 2000.

[Lope 07] J. López-Leonés, M. A. Vilaplana, E. Gallo, F. A. Navarro, and C. Querejeta. "The Aircraft Intent Description Language: a Key Enabler for Air-Ground Synchronization in Trajectory Based Operations". In: *Proceedings of the 26th Digital Avionics Systems Conference, AIAA/IEEE, Oct. 21–25.* pp. 1.D.4–1–1.D.4–12, 2007.

[Matt 02] J. D. Mattingly, W. H. Heiser, and D. T. Pratt. *Aircraft Engine Design.* AIAA Education Series, Reston, Virginia, 2nd edition Ed., 2002.

[Meno 89] P. K. A. Menon. "Study of Aircraft Cruise". *Journal of Guidance, Control, and Dynamics*, Vol. 12, No. 5, pp. 631–639, 1989.

[Meno 99] P. K. Menon, G. D. Swediruk, and B. Sridhar. "Optimal Strategies for Free-Flight Air Traffic Conflict Resolution". *Journal of Guidance, Control, and Dynamics*, Vol. 22, No. 2, pp. 202–211, 1999.

[Miel 55] A. Miele. "General Solutions of Optimum Problems in Nonstationary Flight". Tech. Rep. NACA TM 1388, National Advisory Comittee for Aeronautics, 1955.

[Miel 62] A. Miele. *Flight Mechanics. Theory of Flight Paths.* Addison-Wesley, 1962.

[Nark 11] A. J. Narkawicz and C. A. Muñoz. "Sate-Based Implicit Coordination and Applications". Tech. Rep. NASA/TP-2011-217067, NASA, March 2011.

[Nuic 04] A. Nuic. "User Manual for the Base of Aircraft Data (BADA) - Revision 3.6. EEC Note No. 10/04". Tech. Rep., Eurocontrol Experimental Centre, 2004.

[Nuic 09] A. Nuic. "Base of Aircraft DAta (BADA) Product Management Document". Tech. Rep. EEC Technical/Scientific Report No. 2009-008, EUROCONTROL, 2009.

[Paie 03] R. A. Paielli. "Modeling Maneuver Dynamics in Air Traffic Conflict Resolution". *Journal of Guidance, Control, and Dynamics*, Vol. 26, No. 3, pp. 407–415, 2003.

[Parg 07] D. M. Pargett and M. D. Ardema. "Flight Path Optimization at Constant Altitude". *Journal of Guidance, Control, and Dynamics*, Vol. 30, No. 4, pp. 1197–1201, 2007.

[Powe 64] M. J. D. Powell. "An efficient method for finding the minimum of a function of several variables without calculating derivatives". *The Computer Journal*, Vol. 7, No. 2, pp. 155–162, 1964.

[Prat 11] X. Prats, V. Puig, and J. Quevedo. "Equitable Aircraft Noise-Abatement Departure Procedures". *Journal of Guidance, Control, and Dynamics*, Vol. 34, No. 1, pp. 192–203, 2011.

[Ragh 04] A. U. Raghunathan, V. Gopal, D. Subramanian, L. T. Biegler, and T. Samad. "Dynamic Optimization Strategies for Three-Dimensional Conflict Resolution of Multiple Aircraft". *Journal of Guidance, Control, and Dynamics*, Vol. 27, No. 4, pp. 586–594, 2004.

[Rao 96] S. S. Rao. *Engineering Optimization. Theory and Practice*. John Wiley & Sons, Inc., 3rd Ed., 1996.

[Riva 09] D. Rivas and A. Valenzuela. "Compressibility Effects on Maximum Range Cruise at Constant Altitude". *Journal of Guidance, Control, and Dynamics*, Vol. 32, No. 5, pp. 1654–1658, 2009.

[Riva 10] D. Rivas, O. Lopez Garcia, S. Esteban, and E. Gallo. "An Analysis of Maximum Range Cruise Including Wind Effects". *Aerospace Science and Technology*, Vol. 14, pp. 38–48, 2010.

[Schi 85] K. Schittkowski. "NLPQL: A Fortran Subroutine Solving Constrained Nonlinear Programming Problems". *Annals of Operations Research*, Vol. 5, pp. 485–500, 1985.

[Schu 72] R. L. Schultz and N. R. Zagalsky. "Aircraft Performance Optimization". *Journal of Aircraft*, Vol. 9, No. 2, pp. 108–114, 1972.

[Sham 97] L. Shampine and M. W. Reichelt. "The MATLAB ODE Suite". *SIAM Journal on Scientific Computing*, Vol. 18, No. 1, pp. 1–22, 1997.

[Shan 70] D. F. Shanno. "Conditioning of Quasi-Newton Methods for Function Minimization". *Mathematics of Computation*, Vol. 24, No. 111, pp. 647–656, 1970.

[Shap 04] I. Shapira and J. Z. Ben-Asher. "Singular Perturbation Analysis of Optimal Glide". *Journal of Guidance, Control, and Dynamics*, Vol. 27, No. 5, pp. 915–918, 2004.

[Shap 05] I. Shapira and J. Ben-Asher. "Range Maximization for Emergency Landing After Engine Cutoff". *Journal of Aircraft*, Vol. 42, No. 5, pp. 1296–1306, 2005.

[Slat 97] R. Slattery and Y. Zhao. "Trajectory Synthesis for Air Traffic Automation". *Journal of Guidance, Control, and Dynamics*, Vol. 20, No. 2, pp. 232–238, 1997.

[Sole 10] M. Soler, A. Olivares, and E. Staffetti. "Hybrid Optimal Control Approach to Commercial Aircraft Trajectory Planning". *Journal of Guidance, Control, and Dynamics*, Vol. 33, No. 3, pp. 985–991, 2010.

[Sore 81] J. A. Sorensen and M. H. Waters. "Airborne Method to Minimize Fuel with Fixed Time-of-Arrival Constraints". *Journal of Guidance, Control, and Dynamics*, Vol. 4, No. 3, pp. 348–349, 1981.

[Tore 97] E. Torenbeek. "Cruise Performance and Range Prediction Reconsidered". *Progress in Aerospace Sciences*, Vol. 33, pp. 285–321, 1997.

[Torr 11] R. Torres, J. Chaptal, C. Bès, and J.-B. Hiriart-Urruty. "Optimal, Environmentally Friendly Departure Procedures for Civil Aircraft". *Journal of Aircraft*, Vol. 48, No. 1, pp. 11–22, 2011.

[Vila 02] M. A. Vilaplana. *Co-Operative Conflict Resolution in Autonomous Aircraft Operations Using a Multi-Agent Approach.* PhD thesis, University of Glasgow, 2002.

[Vila 06] M. Vilaplana, F. García de Blanes, E. Valls, and I. del Pozo. *ISPOC (Intent Synchronization Proof Of Concept). Concept Document.* Boeing Research & Technology Europe, 2006.

[Vivo 06] R. A. Vivona, D. A. Karr, and D. A. Roscoe. "Pattern-Based Genetic Algorithm for Airborne Conflict Resolution". In: *AIAA Guidance, Navigation, and Control Conference and Exhibit, Keystone, Colorado, Aug. 21-24.* No. AIAA-2006-6060, pp. 1–23, 2006.

[Vorm 06] F. J. Vormer, M. Mulder, M. M. van Paasen, and J. A. Mulder. "Optimization of Flexible Approach Trajectories Using a Genetic Algorithm". *Journal of Aircraft*, Vol. 43, No. 4, pp. 941–952, 2006.

[West 95] T. Westerlund and F. Pettersson. "An Extended Cutting Plane Method for Solving Convex MINLP Problems". *Computers and Chemical Engineering*, Vol. 19, pp. S131–S136, 1995.

[Will 91] D. H. Williams and S. M. Green. "Airborne Four-Dimensional Flight Management in a Time-Based Air Traffic Control Environment". Tech. Rep. NASA TM-4249, NASA, 1991.

[Wu 09] D. Wu and Y. J. Zhao. "Performances and Sensitivities of Optimal Trajectory Generation for Air Traffic Control Automation". In: *AIAA Guidance, Navigation, and Control Conference and Exhibit, Chicago, Illinois, Aug. 10-13.* No. AIAA-2009-6167, pp. 1–22, 2009.

A Math Notation

a	speed of sound
c	specific fuel consumption
CAS	calibrated air speed
C_C	specific fuel consumption coefficient
C_D	drag coefficient
C_L	lift coefficient
C_T	thrust coefficient
CI	cost index
d	distance
d_{ij}	horizontal distance between aircraft i and j
d_s	horizontal separation minimum
D	drag
DOC	direct operating cost
$\mathbf{f}$	equality constraints
$\mathbf{F}$	state equations
g	gravity acceleration
$\mathbf{g}$	inequality constraints
$\mathbf{G}$	flight constraint equations
h	altitude
h_{ij}	vertical distance between aircraft i and j
h_s	vertical separation minimum
J	objective function
KPI	key performance indicator
L	lift
m	aircraft mass
m_F	fuel mass
M	Mach number
n	number of steps in a pattern
N_l	number of locked aircraft
N_u	number of unlocked aircraft
p	pressure
r	horizontal distance
r_f	range
R	turn radius
R_a	air gas constant

R_E	Earth radius
S	wing area
t	time
t_f	flight time
T	thrust
$\mathbf{u}$	control vector
V	aerodynamic speed
w	horizontal wind component in the vertical plane
w_1, w_2, w_3	wind components in the local-axes system (north, east and down)
$\dot{w}_V, \dot{w}_\gamma, \dot{w}_\chi$	wind acceleration components
$\mathbf{x}$	parameter vector
$\mathbf{y}$	state vector
γ	flight-path angle
δ	pressure ratio
Δ	difference
θ	temperature ratio
Θ	temperature
κ	ratio of specific heats
λ	geodetic longitude
μ	bank angle
ρ	density
φ	geodetic latitude
χ	heading angle

Subindices

A	given value
AP	approach
c	cruise
d	descent
ETA	estimated time of arrival
f	final
i	initial or counter
j	counter
SL	sea level (ISA model)
STA	scheduled time of arrival

B Acronyms

AIRE	Atlantic Interoperability Initiative to Reduce Emissions
ATC	Air Traffic Control
ATLANTIDA	Aplicación de Tecnologías Líder a Aeronaves No Tripuladas para la Investigación y Desarrollo en ATM
ATM	Air Traffic Management
BADA	Base of Aircraft DAta
BB	Branch and Bound
BFGS	Broyden-Fletcher-Goldfarb-Shanno
CAS	Calibrated Air Speed
CD	Conflict Detection
CD&R	Conflict Detection and Resolution
CDTI	Comisión para el Desarrollo Tecnológico e Industrial
CI	Cost Index
CNS	Communications, Navigation, and Surveillance
CR	Conflict Resolution
CSR	Cruise Speed Reduction
CTAS	Center-TRACON Automation System
DAE	Differential Algebraic Equations
DOC	Direct Operating Cost
ER	Engine Rating
ETA	Estimated Time of Arrival
FAA	Federal Aviation Administration
FANS	Future Air Navigation Systems
FL	Flight Level
GRG	Generalized Reduced Gradient
HALA	Higher Automation Levels in ATM
IAF	Initial Approach Fix
ICAO	International Civil Aviation Organization
IMPACT	Advanced Multi-Purpose Infrastructure for Trajectory Computation
ISA	International Standard Atmosphere
JPDO	Joint Planning and Development Office
KPI	Key Performance Indicator
MINLP	Mixed-Integer NonLinear Programming
MF	Metering Fix
NIA	National Institute of Aerospace

NLP	NonLinear Programming
NASA	National Aeronautics and Space Administration
NextGen	Next Generation air transportation system
ODE	Ordinary Differential Equations
PHARE	Programme for Harmonized ATC Research in Europe
RWY	Runway
SESAR	Single European Sky ATM Research
SINTONIA	SIstemas No Tripulados Orientados al Nulo Impacto Ambiental
SQP	Sequential Quadratic Programming
STA	Scheduled Time of Arrival
STAR	STandard ARrival
TBO	Trajectory-Based Operations
TMA	Terminal Area
TOD	Top Of Descent
TP	Trajectory Prediction
UAV	Unmanned Air Vehicle

C Trajectory Computation

To compute each flight segment, it is required to solve the corresponding DAE system. In the solver used in this thesis, the control variables (T, L, μ) are determined explicitly (operation that can be accomplished in all the flight segments considered) and the DAE system is reduced to an ODE system, that can be solved using standard numerical procedures, such as a Runge-Kutta method. In the following, it is provided a description of the flight constraints, of the stopping conditions, and of how turns and the computation of the top-of-descent point are performed. Finally each type of flight segment is described, and the corresponding equations of motion (ODE system to be solved, obtained from Eqs. 3.1) are summarized.

C.1 Flight Constraints

The imposed flight constraints must be compatible and physically meaningful, that is, they must close the mathematical problem. In this thesis all the flight segments considered are defined by the following types of flight constraints:

a) Constant γ, χ, h, μ. In these cases, the constraint sets the value of a state variable (path angle, heading angle, altitude) or a control variable (bank angle).

b) Given T_{RATE}. In cases where the engine rating is given, this constraint defines the thrust law: $T_{MCRZ}(M,h)$ for maximum cruise or $T_{IDLE}(M,h)$ for idle.

c) Constant M. When the Mach number is constant, say M_A, this constraint is equivalent to

$$V = M_A\sqrt{\kappa R_a \Theta(h)} \tag{C.1}$$

that is, one has a known speed law $V(h)$, say $V = V_M(h)$ (κ and R_a are given in Appendix D).

d) Constant CAS. When the calibrated air speed (CAS) is constant, say CAS_A, this constraint is equivalent to (see Ref. [Asse 97])

$$V = \sqrt{\frac{2}{k}R_a\Theta(h)\left[\left(1+\frac{p_{SL}}{p(h)}\left[\left(1+\frac{k}{2}\frac{\rho_{SL}}{p_{SL}}CAS_A^2\right)^{1/k}-1\right]\right)^{k}-1\right]} \tag{C.2}$$

where $k = (\kappa-1)/\kappa$; that is, one has another known speed law $V(h)$, say $V = V_C(h)$.

C.2 Stopping Conditions

The computation of each flight segment ends when the appropriate stopping condition is reached. The following stopping conditions are considered in this thesis:

a) Reach a given Mach or CAS. In this case, from the computed values of V and h, the corresponding value of Mach or CAS, defined by Eqs. (C.1) and (C.2), must be monitored during the integration, in order to determine when the event is reached.

b) Reach a given altitude. Altitude is a computed variable that must be monitored.

c) Reach a given heading. Heading angle is a computed variable that must be monitored.

d) Reach a given horizontal distance. Distance travelled by the aircraft along the Earth surface is a computed variable that must be monitored.

C.3 Turns

In this thesis we consider inside turns at constant bank angle ($\mu = \mu_A$). Thus the turning segment is defined by the flight constraint of constant bank angle (which replaces that of constant heading) and the two other constraints that define the preceding segment, which are maintained (for example, constant altitude and constant Mach).

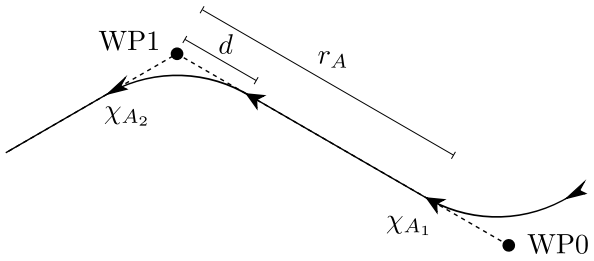

Figure C.1: Turn scheme.

The turn must be initiated some distance d before reaching the waypoint that triggers the heading change, see Fig. C.1. This distance is calculated iteratively. To start the iteration, a first estimate is obtained considering uniform horizontal turns, in which case it is given by

$$d = R \tan \frac{\chi_{A_2} - \chi_{A_1}}{2} \tag{C.3}$$

where χ_{A_1} and χ_{A_2} are the old and new heading angles, and R is the turn radius which is given by

$$R = \frac{V^2}{g \tan \mu_A} \tag{C.4}$$

where V is approximated by $V \approx V_i$, V_i being the initial value of V during the preceding segment, which is known.

The stopping condition for the preceding segment is reaching the horizontal distance $r_A - d$, where r_A is the horizontal distance between the beginning of the preceding segment and the next waypoint (WP1 in Fig. C.1), which is known. The stopping condition for the turning segment is reaching the new heading χ_{A_2}.

C.4 Top of Descent

The top-of-descent point is determined iteratively, in order to consider the actual weight of the aircraft (if the landing weight were known or guessed, the TOD point could be determined integrating backwards, as in Ref. [Will 91]).

As mentioned in Sections 3.2 and 5.1.2, we have defined the cruise speed reduction (CSR) point as the beginning of the last segment of the cruise phase. This segment is a deceleration at cruise altitude, that ends when the descent Mach number is reached. In the iteration procedure, the CSR point (instead of the TOD point) is determined iteratively, and, then, the TOD point is just the end of the segment; in this process, the trajectory is computed for different approximations of the CSR point until the touch-down point coincides with the runway location.

C.5 Flight Segments

The resolution of the DAE systems for the different flight segments is based on the reduction of the system of equations to a system of ordinary differential equations (ODE) through the explicit utilization of the flight constraints. A summary of this procedure, for the flight segments considered in this thesis, is shown next. In those segments which consider the presence of wind, the equations are particularized to the case of altitude-dependent horizontal winds $w(h)$.

C.5.1 Horizontal, Rectilinear, Uniform Flight in the Presence of Wind

Constraints:

- constant altitude $h = h_A$,
- constant Mach or constant CAS, that is, known speed law $V = V_M(h)$ or $V = V_C(h)$, respectively, that is, known speed law $V = V(h)$,
- constant heading angle $\chi = \chi_A$.

In this segment, since $h = const$, one has $V = const$, say $V = V(h_A) \equiv V_A$; one also has $L = mg$, $\mu = 0$ and $\gamma = 0$. Equations (3.1) and (3.4) reduce to:

$$\begin{aligned} \frac{\mathrm{d}m}{\mathrm{d}t} &= -c(M_A, h_A)T(m) \\ (R_E + h_A)\frac{\mathrm{d}\varphi}{\mathrm{d}t} &= (V_A + w(h_A))\cos\chi_A \\ (R_E + h_A)\cos\varphi\frac{\mathrm{d}\lambda}{\mathrm{d}t} &= (V_A + w(h_A))\sin\chi_A \\ \frac{\mathrm{d}r}{\mathrm{d}t} &= \frac{R_E}{R_E + h_A}(V_A + w(h_A)) \end{aligned} \tag{C.5}$$

where the required thrust $T(m)$ is given by

$$T = \frac{1}{2}\rho_A V_A^2 S C_D(M_A, C_L) \tag{C.6}$$

with

$$C_L = \frac{2mg}{\rho_A V_A^2 S} \tag{C.7}$$

C.5.2 Horizontal Acceleration/Deceleration in Rectilinear Flight in the Presence of Wind

Constraints:

- constant altitude $h = h_A$,
- given engine rating, either maximum cruise $T = T_{MCRZ}(M, h)$ or idle $T = T_{IDLE}(M, h)$, that is, a known function $T(M, h)$,
- constant heading angle $\chi = \chi_A$.

In this segment one has $L = mg$, $\mu = 0$ and $\gamma = 0$. Equations (3.1) and (3.4) reduce to:

$$\begin{aligned} m\frac{\mathrm{d}V}{\mathrm{d}t} &= T(M, h_A) - \frac{1}{2}\rho_A V^2 S C_D(M, C_L) \\ \frac{\mathrm{d}m}{\mathrm{d}t} &= -c(M, h_A) T(M, h_A) \\ (R_E + h_A)\frac{\mathrm{d}\varphi}{\mathrm{d}t} &= (V + w(h_A))\cos\chi_A \\ (R_E + h_A)\cos\varphi\frac{\mathrm{d}\lambda}{\mathrm{d}t} &= (V + w(h_A))\sin\chi_A \\ \frac{\mathrm{d}r}{\mathrm{d}t} &= \frac{R_E}{R_E + h_A}(V + w(h_A)) \end{aligned} \tag{C.8}$$

where the lift coefficient $C_L(V, m)$ is given by

$$C_L = \frac{2mg}{\rho_A V^2 S} \tag{C.9}$$

C.5.3 Mach/CAS Climb/Descent in the Presence of Wind

Constraints:

- constant Mach or constant CAS, that is, known speed law $V = V_M(h)$ or $V = V_C(h)$, respectively,
- given engine rating, either maximum cruise $T = T_{MCRZ}(M, h)$ or idle $T = T_{IDLE}(M, h)$, that is, a known function $T(M, h)$,
- constant heading angle $\chi = \chi_A$.

In general, in this segment one has known functions $V(h)$ and $T(M,h)$; one also has $\mu = 0$. The equations of motion (3.1) and Eq. (3.4) reduce to:

$$\begin{aligned} mV(h)\frac{\mathrm{d}\gamma}{\mathrm{d}t} &= L(m,h,\gamma) - mg\cos\gamma + m\frac{\mathrm{d}w}{\mathrm{d}h}V(h)\sin^2\gamma \\ \frac{\mathrm{d}m}{\mathrm{d}t} &= -c(M,h)T(M,h) \\ (R_E+h)\frac{\mathrm{d}\varphi}{\mathrm{d}t} &= (V(h)\cos\gamma + w(h))\cos\chi_A \\ (R_E+h)\cos\varphi\frac{\mathrm{d}\lambda}{\mathrm{d}t} &= (V(h)\cos\gamma + w(h))\sin\chi_A \\ \frac{\mathrm{d}h}{\mathrm{d}t} &= V(h)\sin\gamma \\ \frac{\mathrm{d}r}{\mathrm{d}t} &= \frac{R_E}{R_E+h}\left(V(h)\cos\gamma + w(h)\right) \end{aligned} \tag{C.10}$$

where the lift $L(m,h,\gamma)$ is given by

$$L = \frac{1}{2}\rho V^2(h) S C_L(m,h,\gamma) \tag{C.11}$$

and the lift coefficient $C_L(m,h,\gamma)$ is the solution of

$$\frac{1}{2}\rho V^2(h) S C_D(M,C_L) = T(M,h) - mg\sin\gamma - mV(h)\frac{\mathrm{d}V}{\mathrm{d}h}\sin\gamma - m\frac{\mathrm{d}w}{\mathrm{d}h}V(h)\sin\gamma\cos\gamma \tag{C.12}$$

C.5.4 Glide Path with No Wind

Constraints:

- constant path angle $\gamma = \gamma_A$ (defined by the ILS),
- constant CAS (in practice, the approach speed CAS_{AP}), that is, known speed law $V = V_C(h)$,
- constant heading angle $\chi = \chi_A$.

In this segment one has $L = mg\cos\gamma_A$ and $\mu = 0$. Equations (3.1) and (3.4) reduce to

$$\begin{aligned} \frac{\mathrm{d}m}{\mathrm{d}t} &= -c(M,h)T(h,m) \\ (R_E+h)\frac{\mathrm{d}\varphi}{\mathrm{d}t} &= V_C(h)\cos\gamma_A\cos\chi_A \\ (R_E+h)\cos\varphi\frac{\mathrm{d}\lambda}{\mathrm{d}t} &= V_C(h)\cos\gamma_A\sin\chi_A \\ \frac{\mathrm{d}h}{\mathrm{d}t} &= V_C(h)\sin\gamma_A \\ \frac{\mathrm{d}r}{\mathrm{d}t} &= \frac{R_E}{R_E+h}V_C(h)\cos\gamma_A \end{aligned} \tag{C.13}$$

where the required thrust $T(h,m)$ is given by

$$T = \frac{1}{2}\rho V_C^2(h) S C_D(M,C_L) + mg\sin\gamma_A + mV_C(h)\frac{\mathrm{d}V_C}{\mathrm{d}h}\sin\gamma_A \tag{C.14}$$

with

$$C_L = \frac{2mg\cos\gamma_A}{\rho V_C^2(h)S} \tag{C.15}$$

C.5.5 Horizontal Turn in Uniform Flight with No Wind

Constraints:

- constant altitude $h = h_A$,
- constant Mach or constant CAS, that is, known speed law $V = V_M(h)$ or $V = V_C(h)$, respectively,
- constant bank angle $\mu = \mu_A$.

In this segment, since $h = const$, one has $V = const$, say $V = V_A$; one also has $L = \dfrac{mg}{\cos\mu_A}$ and $\gamma = 0$. Equations (3.1) and (3.4) reduce to:

$$\begin{aligned} mV_A\frac{\mathrm{d}\chi}{\mathrm{d}t} &= L(m)\sin\mu_A \\ \frac{\mathrm{d}m}{\mathrm{d}t} &= -c(M_A,h_A)T(m) \\ (R_E+h_A)\frac{\mathrm{d}\varphi}{\mathrm{d}t} &= V_A\cos\chi \\ (R_E+h_A)\cos\varphi\frac{\mathrm{d}\lambda}{\mathrm{d}t} &= V_A\sin\chi \\ \frac{\mathrm{d}r}{\mathrm{d}t} &= \frac{R_E}{R_E+h_A}V_A \end{aligned} \tag{C.16}$$

where the required thrust $T(m)$ is given by Eq. (C.6), with the lift coefficient given by

$$C_L = \frac{2mg}{\rho_A V_A^2 S\cos\mu_A} \tag{C.17}$$

C.5.6 Horizontal Turn in Accelerating/Decelerating Flight with No Wind

Constraints:

- constant altitude $h = h_A$,
- given engine rating, either maximum cruise $T = T_{MCRZ}(M,h)$ or idle $T = T_{IDLE}(M,h)$, that is, a known function $T(M,h)$,
- constant bank angle $\mu = \mu_A$.

In this segment one has $L = \dfrac{mg}{\cos\mu_A}$ and $\gamma = 0$. The equations of motion (3.1) and Eq. (3.4) reduce to:

$$\begin{aligned} m\frac{\mathrm{d}V}{\mathrm{d}t} &= T(M,h_A) - \frac{1}{2}\rho_A V^2 S C_D(M,C_L) \\ mV\frac{\mathrm{d}\chi}{\mathrm{d}t} &= L(m)\sin\mu_A \\ \frac{\mathrm{d}m}{\mathrm{d}t} &= -c(M,h_A)T(M,h_A) \\ (R_E+h_A)\frac{\mathrm{d}\varphi}{\mathrm{d}t} &= V\cos\chi \\ (R_E+h_A)\cos\varphi\frac{\mathrm{d}\lambda}{\mathrm{d}t} &= V\sin\chi \\ \frac{\mathrm{d}r}{\mathrm{d}t} &= \frac{R_E}{R_E+h}V \end{aligned} \tag{C.18}$$

where the lift coefficient $C_L(V,m)$ is given by

$$C_L = \frac{2mg}{\rho_A V^2 S\cos\mu_A} \tag{C.19}$$

C.5.7 Turn in Mach/CAS Descent Flight with No Wind

Constraints:

- constant Mach or constant CAS, that is, known speed law $V = V_M(h)$ or $V = V_C(h)$, respectively,
- idle engine rating $T = T_{IDLE}(M,h)$,
- constant bank angle $\mu = \mu_A$.

In general, in this segment one has known functions $V(h)$ and $T(M,h)$. The equations of motion (3.1) and Eq. (3.4) reduce to

$$\begin{aligned} mV(h)\cos\gamma\frac{\mathrm{d}\chi}{\mathrm{d}t} &= L(m,h,\gamma)\sin\mu_A \\ mV(h)\frac{\mathrm{d}\gamma}{\mathrm{d}t} &= L(m,h,\gamma)\cos\mu_A - mg\cos\gamma \\ \frac{\mathrm{d}m}{\mathrm{d}t} &= -c(M,h)T(M,h) \\ (R_E+h)\frac{\mathrm{d}\varphi}{\mathrm{d}t} &= V(h)\cos\gamma\cos\chi \\ (R_E+h)\cos\varphi\frac{\mathrm{d}\lambda}{\mathrm{d}t} &= V(h)\cos\gamma\sin\chi \\ \frac{\mathrm{d}h}{\mathrm{d}t} &= V(h)\sin\gamma \\ \frac{\mathrm{d}r}{\mathrm{d}t} &= \frac{R_E}{R_E+h}V(h)\cos\gamma \end{aligned} \tag{C.20}$$

where the lift $L(m,h,\gamma)$ is given by Eq. (C.11) and the lift coefficient $C_L(m,h,\gamma)$ is defined by

$$\frac{1}{2}\rho V^2(h) S C_D(M,C_L) = T(M,h) - mg\sin\gamma - mV(h)\frac{\mathrm{d}V}{\mathrm{d}h}\sin\gamma \tag{C.21}$$

This page intentionally left blank

D Supplementary Models

D.1 Earth Model

The Earth model adopted has the following characteristics:

- spherical Earth of radius R_E=6356.766 km,
- constant gravity g=9.80665 m/s^2,
- air, a perfect gas defined by a gas constant R_a =287.053 J/(kgK) and a ratio of specific heats κ=1.4, and
- standard atmosphere ISA (it defines temperature, Θ, pressure, p, and density, ρ, as functions of altitude h).

D.2 Aircraft Model for Boeing 767-300ER

The aircraft model of the Boeing 767-300ER considered in this thesis for the numerical applications has a wing surface area of 283.3 m^2, a maximum take-off mass of 186880 kg and a maximum fuel mass of 73635 kg.

The aerodynamic model defines the drag polar $C_D = C_D(M, C_L)$, that gives the drag coefficient as a function of Mach number, M, and lift coefficient, C_L. The lift and drag coefficients are defined by $L = \frac{1}{2}\rho V^2 S C_L$ and $D = \frac{1}{2}\rho V^2 S C_D$, respectively. The drag polar defined by Cavcar and Cavcar [Cavc 04] is considered; it is given by

$$\begin{aligned} C_D = &\left(C_{D_{0,i}} + \sum_{j=1}^{5} k_{0j} K^j (M) \right) + \left(C_{D_{1,i}} + \sum_{j=1}^{5} k_{1j} K^j (M) \right) C_L \\ &+ \left(C_{D_{2,i}} + \sum_{j=1}^{5} k_{2j} K^j (M) \right) C_L^2 \end{aligned} \tag{D.1}$$

where

$$K(M) = \frac{(M - 0.4)^2}{\sqrt{1 - M^2}} \tag{D.2}$$

The incompressible drag polar coefficients are $C_{D_{0,i}} = 0.01322$, $C_{D_{1,i}} = -0.00610$, $C_{D_{2,i}} = 0.06000$, and the compressible coefficients are given in Table D.1. This polar is valid for $M \geq 0.4$.

j	1	2	3	4	5
k_{0j}	0.0067	−0.1861	2.2420	−6.4350	6.3428
k_{1j}	0.0962	−0.7602	−1.2870	3.7925	−2.7672
k_{2j}	−0.1317	1.3427	−1.2839	5.0164	0.0000

Table D.1: Compressible drag-polar coefficients for the Boeing 767-300ER

For the available thrust the following general model is considered (see Torenbeek [Tore 97])

$$T = W_{TO}\delta C_T(M, N_c) \tag{D.3}$$

where W_{TO} is the reference take-off weight, $\delta = p/p_{SL}$ is the pressure ratio (p_{SL} being the reference sea-level pressure), and C_T is the thrust coefficient, which in general is a function of the Mach number and the engine control parameter N_c. For a given *engine rating* (maximum cruise or idle), the control parameter is a function of Mach number and altitude ($N_c(M, h)$), therefore one can also write the model as $T = T_{RATE}(M, h)$, that is, thrust dependent both on Mach number and altitude.

Although different functional dependencies should be used for the various engine ratings, in this thesis, for simplicity, the following single model is considered for the thrust coefficient (see Mattingly [Matt 02] and Barman and Erzberger [Barm 76])

$$C_T = \frac{T_{SL,RATE}}{W_{TO}} \left(1 + \frac{\kappa - 1}{2} M^2\right)^{\frac{\kappa}{\kappa-1}} \left(1 - 0.49\sqrt{M}\right) \frac{1}{\theta} \tag{D.4}$$

where $\theta = \Theta/\Theta_{SL}$ is the temperature ratio (Θ_{SL} being the reference sea-level temperature), and $T_{SL,RATE}$ is the thrust at sea level and for $M = 0$ for the given engine rating. The values used for this aircraft are T_{SL} =4.75×10^5 N for maximum cruise rating, and T_{SL} =7.3×10^3 N for idle rating.

For the specific fuel consumption the following general model is considered (see Torenbeek [Tore 97])

$$c = \frac{a_{SL}\sqrt{\theta}}{L_H} C_C(M) \tag{D.5}$$

where $a_{SL} = \sqrt{\kappa R_a \Theta_{SL}}$ is the speed of sound at sea level, L_H is the fuel latent heat, and C_C is the specific fuel consumption coefficient (in general C_C depends on C_T, but this dependence is neglected, since it is very weak in practice [Tore 97]). For the fuel latent heat, one can take $L_H = 43 \times 10^6$ J/kg. For the specific fuel consumption coefficient, the linear model defined by Mattingly [Matt 02] is considered; it is given by

$$C_C = c_{SL} \frac{L_H}{a_{SL}} (1.0 + 1.2M) \tag{D.6}$$

where c_{SL} is the specific fuel consumption at sea level and for $M = 0$. For this aircraft, c_{SL} =9.0×10^{-6} kg/(s N) is used.

D.3 Aircraft Models Based on BADA

For those aircraft different from Boeing 767-300ER we use aircraft models based on the information provided by BADA 3.6 [Nuic 04]. The wing surface area, operational weights and operational speeds are available in this database.

The drag polar considered for these aircraft is incompressible and parabolic, given by

$$C_D = C_{D_0} + C_{D_2} C_L^2 \tag{D.7}$$

where the coefficients C_{D_0} and C_{D_2} can be obtained from BADA for different aerodynamic configurations (clean, high-lift devices, and landing gear deployed).

The thrust and specific fuel consumption models considered are given by Eqs. (D.3), (D.4), (D.5), and (D.6), where the values of $T_{SL,RATE}$ and c_{SL} are obtained from BADA 3.6.

This page intentionally left blank

E Key Performance Indicators

In this Appendix the Key Performance Indicators (KPIs) used to evaluate the performance of the CR functions are defined.

KPI_1: Maximum deviation time

This is an efficiency indicator that measures the maximum absolute value of the difference between the ETA of the resolution trajectory and the STA. It is given by

$$KPI_1 = \max_i \left(|t_{ETA,i} - t_{STA,i}| \right) \tag{E.1}$$

KPI_2: Mean deviation time

This is also an efficiency indicator that is computed adding the absolute values of the differences between ETA given by the resolution trajectory and the STA and dividing the result by the number of unlocked aircraft. It is given by

$$KPI_2 = \frac{1}{N_u} \sum_{i=1}^{N_u} |t_{ETA,i} - t_{STA,i}| \tag{E.2}$$

KPI_3: Mean fuel cost

This is a cost-effectiveness indicator that is computed as the sum of the fuel costs for all aircraft, divided by the number of unlocked aircraft. It does not take into account how the costs are distributed among the aircraft.

Let C_k be the cost for aircraft k, defined as $C_k = c_{F,k} \cdot \Delta m_{F,k}$, where $c_{F,k}$ is a coefficient that can be different for each aircraft and $\Delta m_{F,k}$ is the extra fuel consumption due to the resolution trajectory of aircraft k. Then:

$$KPI_3 = \frac{1}{N_u} \sum_{k=1}^{N_u} C_k \tag{E.3}$$

KPI_4: Cost distribution

This is a participation indicator that measures the fairness of the solution. It is measured as the aggregated typical deviation of the costs for all unlocked aircraft. It is given by

$$KPI_4 = \sqrt{\frac{1}{N_u} \sum_{k=1}^{N_u} (C_k - KPI_3)^2} \tag{E.4}$$

KPI_5: Mean deviation from nominal trajectories

This is an efficiency indicator that is computed as the sum of the deviations from the nominal trajectories for all aircraft, divided by the number of unlocked aircraft. The deviation is measured as the mean of the distance between the nominal (intended) and the resolution trajectory at certain times, in the horizontal plane. Note that it does not take into account how the deviation is distributed.

Let $\mathbf{r}^{k,N}(t)$ and $\mathbf{r}^{k}(t)$ be the nominal and resolution trajectories at time t for aircraft k, respectively, $d(\mathbf{r}_1(t), \mathbf{r}_2(t))$ the distance (measured along Earth's surface) between $\mathbf{r}_1(t)$ and $\mathbf{r}_2(t)$ at time t, and $\mathcal{T}^k$ the set of time instants where the indicator is measured for aircraft k. The number of time instants in $\mathcal{T}^k$ is denoted as p_k. Thus,

$$KPI_5 = \frac{1}{N_u} \sum_{k=1}^{N_u} \left[\frac{1}{p_k} \sum_{t \in \mathcal{T}^k} d(\mathbf{r}^k(t), \mathbf{r}^{k,N}(t)) \right] \tag{E.5}$$

F Nominal Traffic and Resolution Trajectories

In this Appendix, the nominal traffic considered in Chapter 6 and the obtained resolution trajectories are presented.

F.1 Nominal Traffic

Aircraft No.	Aircraft (BADA code)	TMA entry time (s)	TMA entry point	Pressure altitude at entry point (ft)	Mass at entry point (kg)	M_c (-)	M_d (-)	CAS_d (kt)	STA (s)	ETA (s)	Estimated fuel consumption (kg)
1	CRJ1	260	RUSIK	30000	19628	0.74	0.739	290	2160	2152	281
2	A320	-50	TERTO	33000	58846	0.78	0.779	310	2280	2210	911
3	A320	510	RUSIK	33000	55098	0.78	0.779	310	2400	2396	654
4	CRJ1	870	WPT1	30000	21315	0.74	0.739	290	2520	2398	179
5	B734	300	TERTO	30000	51971	0.74	0.739	280	2640	2611	884
6	A320	490	TERTO	33000	58846	0.78	0.779	310	2760	2750	911
7	CRJ1	870	RUSIK	30000	19628	0.74	0.739	290	2880	2762	281
8	A320	1040	RUSIK	33000	55098	0.78	0.779	310	3000	2926	654
9	CRJ1	1570	WPT1	30000	21315	0.74	0.739	290	3120	3098	179
10	CRJ1	1200	RUSIK	30000	19628	0.74	0.739	290	3240	3092	281
11	A320	1400	RUSIK	33000	55098	0.78	0.779	310	3360	3286	654
12	A320	1160	TERTO	33000	58846	0.78	0.779	310	3480	3420	911
13	CRJ1	2060	WPT1	30000	21315	0.74	0.739	290	3600	3588	179
14	B734	1300	TERTO	30000	51971	0.74	0.739	280	3720	3611	884
15	CRJ1	2300	WPT1	30000	21315	0.74	0.739	290	3840	3828	179
16	A320	2000	RUSIK	33000	55098	0.78	0.779	310	3960	3886	654
17	CRJ1	2170	RUSIK	30000	19628	0.74	0.739	290	4080	4062	281
18	A320	1840	TERTO	33000	58846	0.78	0.779	310	4200	4100	911
19	B734	1980	TERTO	30000	51971	0.74	0.739	280	4320	4291	884
20	A320	2450	RUSIK	33000	55098	0.78	0.779	310	4440	4336	654
21	A320	2250	TERTO	33000	58846	0.78	0.779	310	4560	4510	911
22	CRJ1	2690	RUSIK	30000	19628	0.74	0.739	290	4680	4582	281
23	CRJ1	3260	WPT1	30000	21315	0.74	0.739	290	4800	4788	179
24	B734	2500	TERTO	30000	51971	0.74	0.739	280	4920	4811	884
25	CRJ1	3120	RUSIK	30000	19628	0.74	0.739	290	5040	5012	281
26	B734	2800	TERTO	30000	51971	0.74	0.739	280	5160	5111	884
27	A320	3370	RUSIK	33000	55098	0.78	0.779	310	5280	5256	654
28	A320	3000	TERTO	33000	58846	0.78	0.779	310	5400	5260	911
29	CRJ1	3970	WPT1	30000	21315	0.74	0.739	290	5520	5498	179
30	B734	3220	TERTO	30000	51971	0.74	0.739	280	5640	5531	884

Table F.1: Scenario 1: traffic data.

Aircraft No.	Aircraft (BADA code)	TMA entry time (s)	TMA entry point	Pressure altitude at entry point (ft)	Mass at entry point (kg)	M_c (-)	M_d (-)	CAS_d (kt)	STA (s)	ETA (s)	Estimated fuel consumption (kg)
1	CRJ1	610	WPT1	30000	21000	0.74	0.74	290	2160	2139	180
2	A320	-50	TERTO	32000	64000	0.78	0.78	310	2280	2196	958
3	B734	200	WPT2	32000	58000	0.74	0.74	280	2400	2360	787
4	CRJ1	550	RUSIK	30000	21000	0.74	0.74	290	2520	2437	280
5	A320	400	WPT2	32000	64000	0.78	0.78	310	2640	2505	858
6	A320	1200	WPT1	32000	64000	0.78	0.78	310	2760	2724	444
7	A320	900	RUSIK	32000	64000	0.78	0.78	310	2880	2766	688
8	CRJ1	650	TERTO	30000	21000	0.74	0.74	290	3000	2933	391
9	CRJ1	800	WPT2	30000	21000	0.74	0.74	290	3120	2936	350
10	B734	1400	WPT1	32000	58000	0.74	0.74	280	3240	2947	399
11	B734	1400	RUSIK	32000	58000	0.74	0.74	280	3360	3308	627
12	B773	1200	WPT2	34000	240000	0.84	0.84	310	3480	3281	3360
13	B734	1050	TERTO	32000	58000	0.74	0.74	280	3600	3358	880
14	B773	1750	RUSIK	34000	240000	0.84	0.84	310	3720	3607	2551
15	B734	1450	WPT2	32000	58000	0.74	0.74	280	3840	3610	787
16	CRJ1	1400	TERTO	30000	21000	0.74	0.74	290	3960	3683	391
17	CRJ1	2400	WPT1	30000	21000	0.74	0.74	290	4080	3929	180
18	B773	2100	RUSIK	34000	240000	0.84	0.84	310	4200	3957	2551
19	B773	1900	WPT2	34000	240000	0.84	0.84	310	4320	3981	3360
20	B734	1900	TERTO	32000	58000	0.74	0.74	280	4440	4208	880
21	B773	2700	WPT1	34000	240000	0.84	0.84	310	4560	4236	1388
22	A320	2400	RUSIK	32000	64000	0.78	0.78	310	4680	4266	688
23	B773	2250	TERTO	34000	240000	0.84	0.84	310	4800	4463	3835
24	A320	2500	WPT2	32000	64000	0.78	0.78	310	4920	4605	858
25	B734	3100	WPT1	32000	58000	0.74	0.74	280	5040	4647	399
26	B773	2450	TERTO	34000	240000	0.84	0.84	310	5160	4663	3835
27	B734	3100	RUSIK	32000	58000	0.74	0.74	280	5280	5008	627
28	CRJ1	2750	TERTO	30000	21000	0.74	0.74	290	5400	5033	391
29	B773	3400	WPT1	34000	240000	0.84	0.84	310	5520	4936	1388
30	B773	3300	RUSIK	34000	240000	0.84	0.84	310	5640	5157	2551
31	CRJ1	3600	WPT1	30000	21000	0.74	0.74	290	5760	5129	180
32	B734	3400	WPT2	32000	58000	0.74	0.74	280	5880	5560	787
33	CRJ1	3600	RUSIK	30000	21000	0.74	0.74	290	6000	5487	280
34	A320	3400	TERTO	32000	64000	0.78	0.78	310	6120	5646	958
35	A320	3600	WPT2	32000	64000	0.78	0.78	310	6240	5705	858

Table F.2: Scenario 2: traffic data.

F.2 Resolution Trajectories

Aircraft No.	Aircraft (BADA code)	ΔM_c (-)	ΔM_d (-)	ΔCAS_d (kt)	$t_{ETA} - t_{STA}$ (s)	Estimated m_F (kg)	Δm_F (kg)
1	CRJ1	0.002	-0.010	-7.27	0.03	281	-3
2	A320	-0.026	-0.076	-16.83	-0.08	911	-42
3	A320	-0.003	-0.008	0.00	0.00	654	-2
4	CRJ1	-0.074	-0.074	10.68	0.00	179	4
5	B734	-0.017	-0.040	-0.15	0.05	884	-7
6	A320	-0.005	-0.024	-0.05	0.09	911	-6
7	CRJ1	-0.074	-0.074	-2.36	0.04	281	-23
8	A320	-0.060	-0.072	0.54	-0.04	654	-35
9	CRJ1	-0.029	-0.031	0.00	-0.03	179	-6
10	CRJ1	-0.074	-0.074	-4.89	0.02	281	-17
11	A320	-0.071	-0.075	26.96	-0.01	654	-26
12	A320	-0.036	-0.043	-0.59	0.06	911	-26
13	CRJ1	-0.017	-0.017	0.08	-0.01	179	-3
14	B734	-0.055	-0.055	-7.53	0.02	884	-23
15	CRJ1	-0.015	-0.025	0.00	-0.07	179	-3
16	A320	-0.067	-0.066	11.04	-0.01	654	-30
17	CRJ1	-0.014	-0.017	0.07	-0.02	281	-5
18	A320	-0.045	-0.055	-21.33	-0.01	911	-51
19	B734	-0.014	-0.060	-2.38	0.10	884	-9
20	A320	-0.078	-0.078	15.35	-0.07	654	-25
21	A320	-0.034	-0.062	16.98	-0.08	911	-19
22	CRJ1	-0.068	-0.071	-3.58	0.09	281	-24
23	CRJ1	-0.016	-0.023	0.02	-0.07	179	-3
24	B734	-0.062	-0.064	4.28	-0.05	884	-16
25	CRJ1	-0.021	-0.029	-0.41	0.08	281	-8
26	B734	-0.026	-0.043	-3.12	-0.10	884	-13
27	A320	-0.030	-0.038	14.58	-0.01	654	-8
28	A320	-0.075	-0.076	-10.66	0.00	911	-56
29	CRJ1	-0.035	-0.037	4.58	0.05	179	-5
30	B734	-0.066	-0.072	12.50	0.00	884	-12

Table F.3: 2-step CR: resolution speeds and arrival times (Scenario 1).

Aircraft No.	Aircraft (BADA code)	ΔM_c (-)	ΔM_d (-)	ΔCAS_d (kt)	$t_{ETA} - t_{STA}$ (s)	Estimated m_F (kg)	Δm_F (kg)
1	CRJ1	0.008	0.003	-0.15	0.01	180	9
2	A320	0.075	0.073	21.26	-0.01	958	250
3	B734	-0.016	-0.074	22.21	0.09	787	26
4	CRJ1	0.073	0.012	-3.13	0.09	280	72
5	A320	0.067	-0.046	23.56	-0.03	858	227
6	A320	0.064	0.058	-3.63	0.07	444	57
7	A320	0.073	0.073	14.91	0.05	688	214
8	CRJ1	-0.000	-0.002	13.21	0.03	391	29
9	CRJ1	-0.005	-0.021	7.57	-0.08	350	52
10	B734	-0.028	-0.045	23.08	0.06	399	195
11	B734	-0.049	-0.068	-3.75	0.06	627	-12
12	B773	-0.047	-0.062	6.32	0.05	3360	567
13	B734	-0.037	-0.058	-7.19	16.77	880	103
14	B773	0.082	-0.035	-9.60	0.02	2551	444
15	B734	-0.058	-0.058	27.99	16.85	787	125
16	CRJ1	0.038	0.006	-0.53	0.02	391	121
17	CRJ1	0.074	0.032	4.70	-0.03	180	82
18	B773	0.068	-0.046	-1.12	0.07	2551	1037
19	B773	0.030	-0.065	6.27	-0.00	3360	1367
20	B734	-0.052	-0.052	4.01	16.56	880	100
21	B773	-0.028	-0.061	13.53	-0.09	1388	1207
22	A320	-0.056	-0.071	-15.61	37.94	688	196
23	B773	0.067	0.035	-2.25	-0.07	3835	1566
24	A320	-0.022	-0.023	8.42	37.67	858	219
25	B734	-0.051	-0.067	4.76	0.00	399	215
26	B773	0.029	-0.007	18.96	-0.04	3835	2196
27	B734	-0.065	-0.072	-2.75	16.35	627	118
28	CRJ1	0.055	-0.069	7.92	0.08	391	169
29	B773	-0.027	-0.060	2.37	-0.03	1388	2009
30	B773	0.029	0.013	-2.40	0.00	2551	1840
31	CRJ1	-0.022	-0.033	9.89	19.91	180	169
32	B734	0.074	0.020	-4.82	0.09	787	292
33	CRJ1	-0.014	-0.016	3.64	-0.02	280	131
34	A320	0.075	0.040	-9.69	0.02	958	497
35	A320	0.038	-0.017	-6.86	-0.01	858	446

Table F.4: 2-step CR: resolution speeds and arrival times (Scenario 2).

Aircraft No.	Aircraft (BADA code)	ΔM_c (-)	ΔM_d (-)	ΔCAS_d (kt)	$t_{ETA} - t_{STA}$ (s)	Estimated m_F (kg)	Δm_F (kg)
1	CRJ1	-0.008	-0.074	-0.31	-0.01	180	-4
2	A320	-0.055	-0.061	7.75	0.10	958	-29
3	B734	-0.019	-0.065	-4.43	0.06	787	-7
4	CRJ1	0.010	-0.014	-8.95	-0.11	280	22
5	A320	-0.078	-0.078	16.47	0.21	858	-14
6	A320	0.012	-0.017	-12.82	0.14	444	3
7	A320	-0.063	-0.067	-13.22	0.19	688	-22
8	CRJ1	-0.035	-0.063	0.62	0.40	391	-17
9	CRJ1	-0.074	-0.074	-2.88	-0.20	350	-17
10	B734	-0.074	-0.074	7.81	0.35	399	148
11	B734	0.009	-0.017	-19.34	0.34	627	1
12	B773	-0.014	-0.033	-13.19	0.08	3360	481
13	B734	-0.074	-0.074	22.51	16.96	880	101
14	B773	-0.084	-0.084	9.26	0.20	2551	251
15	B734	-0.074	-0.074	6.71	17.12	787	87
16	CRJ1	-0.072	-0.072	-11.32	-0.27	391	-6
17	CRJ1	-0.010	-0.063	-14.16	0.02	180	22
18	B773	0.050	0.050	6.61	0.31	2551	1142
19	B773	-0.035	-0.038	-30.67	0.44	3360	663
20	B734	-0.074	-0.074	-22.51	17.17	880	38
21	B773	-0.083	-0.083	10.32	0.04	1388	1063
22	A320	-0.078	-0.078	0.80	38.47	688	189
23	B773	0.014	-0.026	19.71	-0.13	3835	1490
24	A320	-0.078	-0.078	9.42	37.55	858	113
25	B734	-0.074	-0.074	-7.49	0.08	399	186
26	B773	-0.077	-0.077	-1.31	-0.31	3835	1325
27	B734	-0.024	-0.024	-12.61	16.20	627	136
28	CRJ1	-0.074	-0.074	3.92	-0.50	391	21
29	B773	0.010	-0.052	-12.69	0.47	1388	1948
30	B773	-0.084	-0.084	-3.47	-0.05	2551	1349
31	CRJ1	-0.074	-0.074	18.82	19.83	180	129
32	B734	-0.074	-0.074	21.38	-0.02	787	144
33	CRJ1	-0.074	-0.074	-15.12	-0.52	280	63
34	A320	-0.078	-0.078	-16.38	0.09	958	142
35	A320	-0.078	-0.078	-14.85	0.35	858	195

Table F.5: 3-step CR: resolution speeds and arrival times (Scenario 2).